5-1-1995

Investigation of inertia controlled bubble departure mechanism in subcooled flow boiling using high speed photography

Viktor R. Mizo

"Investigation of Inertia Controlled Bubble Departure Mechanism in Subcooled Flow Boiling Using High Speed Photography"

by

Viktor R. Mizo

A Thesis Submitted
in
Partial Fulfillment
of the
Requirements for the

MASTER OF SCIENCE

in

Mechanical Engineering

Approved by:

Professor Satish Kandlikar
Thesis Advisor

Professor R. J. Hefner

Professor Alan Nye

Professor Charles W. Harris
Department Head

DEPARTMENT OF MECHANICAL ENGINEERING
COLLEGE OF ENGINEERING
ROCHESTER INSTITUTE OF TECHNOLOGY
MAY 1995

Permission To Reproduce:

Thesis title: "Investigation of Inertia Controlled Bubble Departure Mechanism in iii Subcooled Flow Boiling Using High Speed Photography"

I, Viktor Mizo, hereby grant permission to the Wallace Memorial Library, of the Rochester Institute of Technology to reproduce my thesis in whole or part. Any reproduction can not be used for commercial use or profit.

May 31, 1995

I would like to express my appreciation to the following individuals:

Dr. Satish Kandlikar for all of his creative ideas, guidance and support;

Tom Locke for his patience, help and understanding in the test section refinement process;

Michael Cartwright for his cooperation in this endeavor;

Andy Hayes for the interesting conversations and the camera operation lessons;

Todd Geib and Joe Scippo for their help with the ThermoNet analysis.

A special thank to my parents for their support and encouragement over the last five years. And to everyone else that I haven't mentioned, thank you for everything.

Table of Contents

A summary of important theoretical models available for bubble growth and departure behavior in flow boiling is presented. Experimental bubble growth rate curves under subcooled flow boiling conditions are obtained in the Thermal Analysis Laboratory in the Mechanical Engineering Department at the Rochester Institute of Technology utilizing high-speed photography. The effects of flow rate, subcooling, heater surface temperature, and cavity size are investigated, and specific trends observed in the bubble growth rate behavior are discussed. The growth rates in flow boiling are compared with the ones for pool boiling, and a need for an improved model for predicting bubble growth rates in flow boiling is established.

The new model based on a control volume approach for the front and rear halves of a bubble developed earlier in the Thermal Analysis Lab at RIT is extended to include the inertia forces acting on a growing bubble. The predictions from the model are compared to the experimental data and are found to agree within an average absolute error of 7.45 %. The mechanism of the actual bubble departure from the heater surface is discussed, and suggestions for future work in the area are outlined.

List of Figures

List of Tables

1. INTRODUCTION:

The mechanism of nucleate flow boiling and the understanding of the principles behind it are of great importance in a number of applications. They can be used to predict the flow behavior in a nuclear reactor based on the conditions of initial bubble departure and net vapor generation. The correct prediction of the actual conditions leading to bubble departure could be used to optimize the design of enhanced heat transfer surfaces for flow boiling application.

The process of subcooled internal flow boiling is of interest in a variety of applications as well. Subcooled liquid is frequently used in boilers and vapor generators. The phenomenon of subcooled boiling has been extensively utilized as a source for high heat flux cooling in specialized thermally controlled applications like cooling of microelectronic chips.

In order to accurately predict the heat transfer characteristics of a heated (nucleating) surface, it is essential to understand the heat transfer processes associated with the phenomenon. The most important aspect of this process requires a thorough comprehension of the various forces that a vapor bubble is subjected to under dynamic flow conditions.

Considering the difficulties in experimental measurements and analytical modeling, the analysis of vapor bubble behavior and detachment from a heated surface in flow boiling has received very little attention in the past, and has been almost neglected compared to the work done in pool boiling. This has been the case despite its significance

and relevance in the understanding and the study of the microconvection component of heat transfer. Initial study of the bubble behavior under static conditions and a good understanding of the mechanisms involved are essential before considering the thermal effects and performing a dynamic force analysis .

2. OBJECTIVES OF CURRENT STUDY:

The scope of the work presented here is to establish the factors influencing bubble growth mechanisms in subcooled flow boiling. An existing control volume approach developed by Kandlikar and Stumm (1995) to predict the bubble departure in a thermally controlled region is modified to cover the inertia controlled region. Experimental data collected by utilizing a high-speed flow visualization system will be used to verify the proposed theory and to quantify the applicable forces acting on the bubble. As a supplement, an in-depth literature review of the processes responsible for bubble formation, and the recently conducted relevant studies reported in literature will precede the analysis.

3. LITERATURE REVIEW:

The objective of the literature review reported here is to develop an understanding of bubble nucleation in pool and flow boiling, and review literature on the proposed models to predict the departure bubble diameters under subcooled flow boiling conditions.

3.1. Bubble Nucleation

Before discussing the relevant research in the area of nucleate boiling, several concepts which form the basis for the bubble growth theory will be presented. These include the homogeneous and heterogeneous nucleation, and the thermodynamic aspects leading to their occurrence.

Vapor can be generated by three different processes that correspond to the departure from a stable, metastable, or unstable equilibrium rate. Bubble formation in a superheated liquid usually occurs over a wide range of temperatures within the metastable region. The same is valid for droplet formation in superheated vapor. Metastable state is a non-equilibrium condition at which a superheated liquid exists above its corresponding saturation temperature, or a subcooled vapor exists below its saturation temperature. Homogeneous nucleation is the process of bubble nucleation that occurs entirely in a superheated liquid. Heterogeneous nucleation, on the other hand, is a process of bubble nucleation initiated at the interface between a metastable liquid phase and a different phase (in most cases solid) that it is in contact with it.

In order to determine the stability of an embryo bubble in a liquid at or near the saturation line, and whether it collapses or grows if stable, a system as shown on Figure 3.1 needs to be considered. At the equilibrium condition, the chemical potential in both liquid and vapor phases, and the corresponding temperatures are equal.

$$\mu_l = \mu_{ve} \tag{3.1}$$

The vapor pressure in the bubble differs from the liquid pressure due to the curvature of the interface, caused by the surface tension, and is given by the Young-Laplace equation:

$$P_v = P_l + \frac{2\sigma}{r_e} \tag{3.2}$$

A thermodynamic analysis of the system yields an equation for the critical bubble radius r_e that will support a bubble that is at equilibrium with the surrounding superheated liquid at temperature T_l and pressure P_l:

$$r_e = \frac{2\sigma}{P_{sat}(T_l)\exp\{v_l[P_l - P_{sat}(T_l)]/RT_l\} - P_l} \tag{3.3}$$

The resulting equilibrium vapor pressure can be approximated by:

$$P_{ve} = P_{sat}(T_l)\exp\left(\frac{-2v_l\sigma}{r_e RT_l}\right) \tag{3.4}$$

by neglecting $P_{ve} - P_{sat}(T_l)$ which is negligible compared to $2v_l\sigma$. The liquid superheat $(T_g - T_{sat})$ corresponding to the pressure difference is given by:

$$(T_g - T_{sat}) = \Delta T_{sat} = \frac{RT_{sat}^2}{Jh_{fg}M}\frac{2\sigma}{P_l r_e} \tag{3.5}$$

This condition implies that $P_{ve} < P_{sat}$, which is true if both the liquid and the vapor phases are superheated relative to the normal saturation state for that interface. Figure 3.2 clearly indicates the steepness of the slope of the superheated vapor line which forces P_{ve}

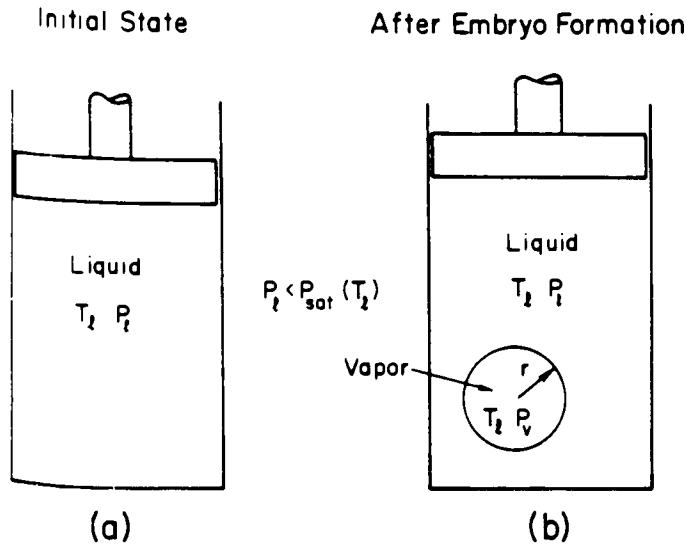

Figure 3.1 System model considered in the thermodynamic analysis of formation of an embryo vapor bubble by homogeneous nucleation

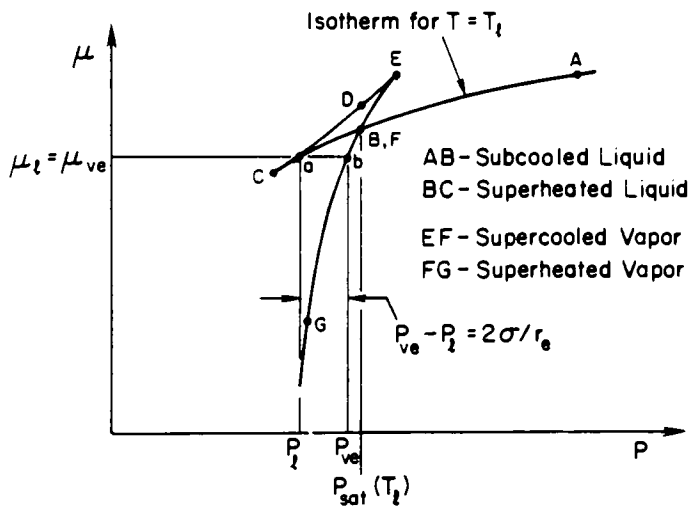

Figure 3.2 The liquid and vapor states for a vapor bubble in equilibrium with the surrounding liquid

to be much closer to $P_{sat}(T_l)$ than to P_l, therefore justifying the assumption that the term $(P_{sat}(T_l)-P_{ve})$ is negligible in deriving Eq. 3.4.

Once a bubble achieves equilibrium with the surrounding superheated liquid, its stability can be determined through basic thermodynamic considerations. The resulting relationship expressing available free energy ($\Delta\Psi$) as a function of r is given by:

$$\Delta\Psi = \frac{4}{3}\pi r_e^2\sigma - \frac{4\pi\sigma}{3}\left[2+\frac{P_l}{P_v}\right](r-r_e)^2+... \tag{3.6}$$

which achieves a local maximum at $r = r_e$. For stable equilibrium to be achieved $\Delta\Psi$ has to be at a minimum leading to the conclusion that $r = r_e$ is an unstable condition. For $r > r_e$, the free energy increases and the embryo will grow. For $r < r_e$, the embryo collapses.

Similar analysis for a subcooled region results in a critical equilibrium radius given as follows:

$$r_e = \frac{2\sigma}{RT_v \ln[P_v / P_{sat}(T_v)]} \quad \text{for} \quad P_v - P_{sat}(T_v) << \frac{2\sigma}{r_e} \tag{3.7}$$

at a condition where

$$P_v = P_{sat}(T_v)\exp\left(\frac{2v_l\sigma}{r_e RT_v}\right) \tag{3.8}$$

The corresponding availability relationship in this case is the same as in the superheated region (Eq. 3.6) , and the same stability conditions apply.

The third process of bubble formation and vapor generation that is centered around foreign bodies and container surfaces is heterogeneous nucleation. In this case, non-condensable gas bubbles suspended in the liquid, and gas or vapor filled cracks and cavities on the liquid container surface act as pre-existing nuclei.

The analysis of this phenomenon takes into consideration the partial pressure of the gas in the cavities. Eq. 3.2 can therefore be modified to:

$$P_g + P_a - P_l = \frac{2\sigma}{r_e} \tag{3.9}$$

and Eq. 3.5 to:

$$T_g - T_{sat} = \frac{RT_{sat}T_g}{h_{fg}} \ln\left[1 + \left(\frac{2\sigma}{P_l r_e}\right)\left(1 + \frac{v_l}{v_g}\right) - \frac{P_a}{P_l}\right] \tag{3.10}$$

The presence of dissolved gas in the process decreases the superheat required to maintain a bubble radius r_e in unstable equilibrium. The embryo vapor bubble formed at a surface is given in Figure 3.3. A thermodynamic analysis of this condition for the equilibrium state at which $r = r_e$ yields a free energy value given by:

$$\Delta\Psi = \frac{4}{3}\pi r_e^2 \sigma_{lv} F - \left(\frac{4\pi\sigma_{lv}F}{3}\right)\left(2 + \frac{P_l}{P_{ve}}\right)(r - r_e)^2 + \ldots \tag{3.11}$$

where

$$F = F(\theta) = \frac{2 + 3\cos\theta - \cos^3\theta}{4} \tag{3.12}$$

Equation 3.11 is the same as Eq. 3.6 corresponding to the homogeneous state, except for σ being replaced by σF. The dependence of the free energy $\Delta\Psi$ on the bubble radius r is identical as for homogeneous nucleation, with the embryos having radii smaller than r_e spontaneously collapsing, and the ones having a radii greater than r_e spontaneously growing. The reduction factor F which is a function of the contact angle θ between the surface and the liquid (Figure 3.4) is also given as:

$$F = \frac{2 + 2\cos\theta + \cos\theta\sin^2\theta}{4} \tag{3.13}$$

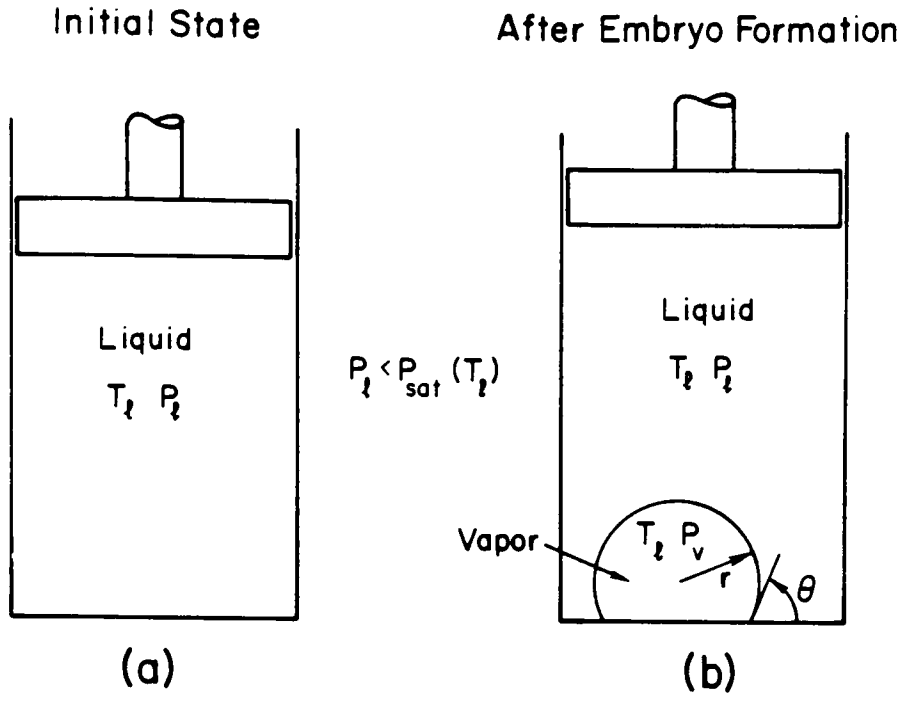

Figure 3.3 System model considered in the thermodynamic analysis of formation of an embryo vapor bubble by heterogeneous nucleation

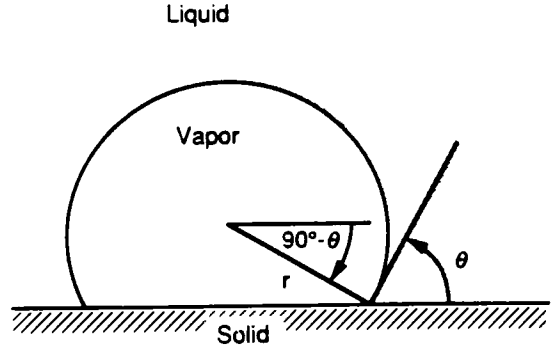

Figure 3.4 An embryo vapor bubble formed at an idealized liquid-solid interface

by Kast (1964) and Bankoff (1957). For completely wetting surfaces where $\theta = 0°$ and $F = 1$, the free energy of formation of the embryo is not reduced. For completely non-wetting surfaces ($\theta = 180°$) the corresponding reduction factor $F = 0$, and therefore the free energy $\Delta\Psi = 0$, leading to the conclusion that no superheat is required for nucleation at the surface.

The reduction of the free energy as a function of the contact angle does not entirely address the considerably lower superheats required to initiate heterogeneous nucleation than those needed for homogeneous nucleation. The solution of this paradox is attributed to the presence of trapped gas in narrow cavities which act as nucleation sites and cause inception of the heterogeneous nucleation under such conditions.

3.2. Bubble Growth Theory

The bubble growth mechanism from a superheated wall occurs in stages as shown in Figure 3.5. The time, t_w, that elapses after the bubble departure, when liquid at a bulk temperature, T_∞, is brought over the cavity at $T_w > T_{sat}(P_\infty)$, and during which transient conduction into the liquid, but no bubble growth occurs, is the waiting time or waiting period.

The rapid growth following the bubble embryo formation, when the bubble grows in an almost hemispherical shape, is the inertia controlled stage. During this period, the thin liquid microlayer remaining below the bottom portion of the bubble interface that stays in contact with the heater surface is the evaporation microlayer. The thickness of the microlayer varies from a finite value corresponding to the bubble radius, to zero at the mouth of the cavity. The microlayer is the medium that transfers heat from the wall to the interface, therefore vaporizing the liquid in contact with the interface. The thin area occupied by liquid at the bubble interface is the relaxation microlayer. The temperature of the interface corresponds to the saturation temperature of the liquid at ambient pressure. Away from the interface, the liquid temperature increases, and after reaching a peak, it declines toward the liquid bulk temperature. The temperature increase away from the liquid-vapor interface is attributed to the liquid rotation. Liquid initially present at the interface, reaches a high temperature, and moves away from it, while it is replaced with a lower temperature bulk liquid. This continuous liquid replacement keeps the liquid at the interface at a constant $T_{sat}(P_\infty)$ temperature.

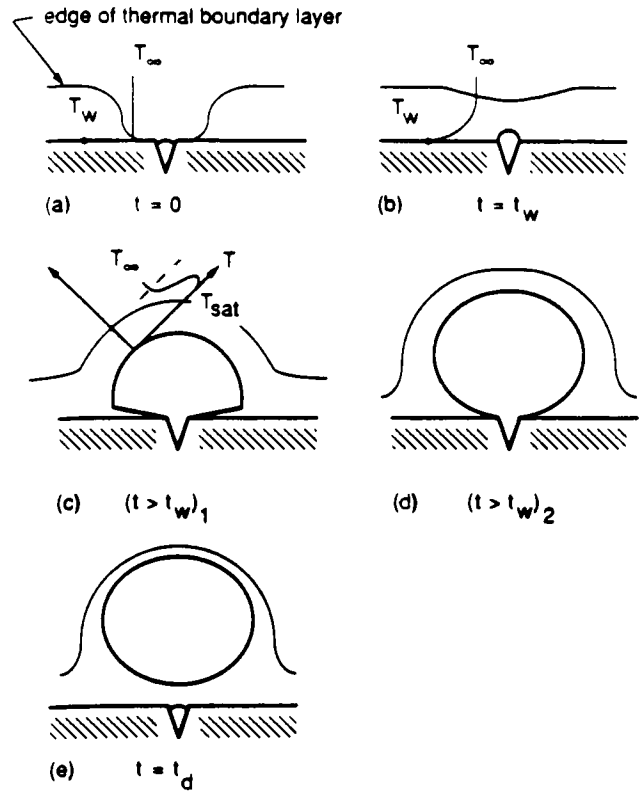

Figure 3.5 The waiting period and subsequent growth of a vapor bubble at an active cavity site

For small diameter bubbles (actual diameter depends on surface tension magnitude), the bubble shape is spherical rather than hemispherical shape. This is a result of the predominant surface tension forces acting on the liquid-vapor interface. When the combined effect of the buoyancy, lift, drag, and inertia forces, that tend to pull the bubble away, overcome the retaining effect of surface tension force, the bubble detaches from the surface.

Rapid, inertia controlled growth is usually applicable to systems subjected to the following conditions:

- High wall superheat
- High heat flux
- Very smoothly polished surface with only small cavities present
- Low contact angle corresponding to highly wetting liquids
- Low latent heat of vaporization
- Low system pressure which leads to low vapor density.

These conditions generally imply that the flow is at high Jakob number Ja (a dimensionless number given as $Ja = (\Delta T c_l/h_{fg})(\rho_v/\rho_l)$), and the bubble would usually assume hemispherical shape.

Heat transfer controlled growth, on the other hand, is most likely to apply to systems that satisfy the following conditions:

- Low wall superheat
- Low heat flux
- Rough surface with larger size cavities

- Moderate contact angle corresponding to less wetting liquids

- High latent heat of vaporization

- Relatively high system pressure.

The aforementioned conditions yield a slower bubble growth with diminished inertia effects where the governing factor is the heat transfer across the liquid-vapor interface.

3.3 Pool and Flow Boiling Bubble Growth Models

Bubble growth rates and models to analyze their behavior have been extensively researched over the last few decades. Two different main regions for the growth mechanism could be established by examining the work done by a bubble in pushing the surrounding liquid. One focuses on the growth rates controlled by the inertia forces, applicable in the range of relatively low pressure and high Jakob numbers, and the other on growth rates for the thermally controlled (heat diffusion) region. This leads to two types of growth rate predictions applicable in the respective regions. The transition between the regions is not distinctly defined, and depends on the given set of parameters at which the bubble growth occurs, e.g. type of fluid, liquid and wall superheat, pressure, etc. A correct prediction for the type of growth can be made only based on previously conducted experiments in similar conditions, for which a controlling mechanism for the bubble behavior has already been determined.

Mikic, Rohsenow, and Griffith (1970) established a general relationship for bubble growth rates in uniformly superheated liquid valid in both inertia controlled and heat diffusion controlled regions. The Rayleigh (1917) solution which accounts for inertia is given by:

$$(\frac{dR}{dt})^2 = b\frac{P_v - P_\infty}{\rho_l} \tag{3.14}$$

where b = 2/3 for bubble growth in an infinite mass, and b = π/7 for a spherical bubble growing attached to a surface. Equation 3.14 is combined with the Clausius-Clapeyron equation

$$\frac{P_v - P_\infty}{\rho_l} = \frac{T_v - T_{sat}}{\rho_l T_{sat}} \rho_v h_{fg} \tag{3.15}$$

to obtain

$$(\frac{dR}{dt})^2 = A^2 \frac{T_v - T_{sat}}{\Delta T} \tag{3.16}$$

where $\Delta T = T_\infty - T_{sat}(P_\infty)$; $A = (b \frac{h_{fg} \rho_l \Delta T}{\rho_l T_{sat}})$

Equation 3.16 was then solved simultaneously with the heat diffusion solution for asymptotic growth previously presented by Plesset and Zwick (1954), Forster and Zuber (1955), and Scraven (1959):

$$\frac{dR}{dt} = \frac{1}{2} \frac{B}{\sqrt{t}} (1 - \frac{T_v - T_{sat}}{\Delta T}) \tag{3.17}$$

where $B = (\frac{12}{\pi} \alpha)^{1/2} Ja$; $Ja = \frac{\Delta T c_l \rho_l}{h_{fg} \rho_v} = \frac{[T_\infty - T_{sat}(P_\infty)] c_l \rho_l}{h_{fg} \rho_v}$

and the following equation was obtained

$$\frac{1}{A^2} (\frac{dR}{dt})^2 + \frac{2\sqrt{t}}{B} \frac{dR}{dt} - 1 = 0 \tag{3.18}$$

After integrating and transforming the equation in a dimensionless form, setting $R^+ = 0$ at $t^+ = 0$, the general bubble growth relation obtained was the following

$$R^+ = \frac{2}{3}[(t^+ + 1)^{3/2} - (t^+)^{3/2} - 1] \tag{3.19}$$

where $R^+ = \frac{AR}{B^2}$; $t^+ = \frac{A^2 t}{B^2}$

For $t^+ \ll 1$, Eq. 3.19 simplifies to the Rayleigh solution

$$R^+ = t^+ \quad (R = At) \tag{3.20}$$

and for $t^+ \gg 1$, to the Plesset and Zwick solution

$$R^+ = \sqrt{(t^+)} \qquad (R = B\sqrt{t}) \tag{3.21}$$

Mikic and Rohsenow (1969) extended this solution to account for non-uniform temperature of the liquid. A one dimensional mathematical model was developed, corrected to allow for the three-dimensional effects, and a relationship was obtained to predict the growth in saturated or subcooled liquid. They considered the heat transfer at the interface rather than the surface tension and the liquid inertia forces to be the controlling factors governing the flow. The transient heat diffusion equation in the liquid adjacent to the wall, given by:

$$\frac{\partial T}{\partial t} = \alpha \frac{\partial^2 T}{\partial x^2} \tag{3.22}$$

was solved considering the following boundary conditions

$$\begin{aligned} &T(x,-t_w) - T_\infty = 0 \qquad \text{for } t > -t_w \\ &T(0,t) - T_\infty = T_w - T_\infty \\ &\\ &T(x,0) - T_\infty = 0 \qquad \text{for } t > 0 \\ &T(0,t) - T_\infty = -(T_w - T_{sat}) \end{aligned} \tag{3.23}$$

that take into account the waiting time. Waiting time is the time that passes from the instant of liquid at uniform temperature T_∞ comes in contact with the superheated surface, T_w, till the time of bubble formation, t = 0, when the liquid surface temperature drops to T_{sat} corresponding to the vapor pressure inside the bubble. The vapor temperature inside the bubble T_v is constant. The resulting expression is:

$$\rho_v h_{fg} \frac{dR}{dt} = k_l \sqrt{3}\left[\frac{T_w - T_v}{(\pi\alpha t)^{1/2}} - \frac{T_w - T_\infty}{[(\pi\alpha(t + t_w)]^{1/2}} \right] \tag{3.24}$$

where t is the time measured from the bubble inception. The waiting time, t_w, is given through a simplified expression based on a thermodynamic analysis of a hemispherical bubble of radius r_c located over a cavity of the same radius as:

$$t_w = \frac{1}{\pi\alpha}\left\{\frac{(T_w - T_\infty)r_c}{T_w - T_{sat}[1+(2\sigma V_{fg}/r_c h_{fg})]}\right\}^2 \tag{3.25}$$

Using

$$\theta = \frac{T_w - T_\infty}{T_w - T_{sat}} \tag{3.26}$$

and expressing the solution of Eq. 3.24 in dimensionless form, the following result was obtained for the bubble growth rate:

$$\frac{dR^+}{dt^+} = \left[t^+ + 1 + \theta\left(\frac{t^+}{t^+ + t_w^+}\right)^{1/2}\right]^{1/2} - (t^+)^{1/2} \tag{3.27}$$

For a case where $t \Rightarrow \infty$, corresponding to growth in a uniformly superheated liquid, Eq. 3.27 reduces to the derivative of Eq. 3.19. Integration of the above expression yields a relationship between bubble radius and time given as:

$$R^+ = (t^+)^{1/2}\left\{1 - \theta\left[\left(1+\frac{t_w^+}{t^+}\right)^{1/2} - \left(\frac{t_w^+}{t^+}\right)^{1/2}\right]\right\} \tag{3.28}$$

The result was compared with experimental data reported by Han and Griffith (1965) and was found to be in a satisfactory agreement.

An expression for the maximum bubble radius (R_{max}) that can be achieved for a bubble growing in a subcooled liquid over time t_m (time necessary to achieve the maximum radius) was also reported. Solving Eq. 3.28 for t_w/t_m, and using $t_m = t$ for $dR/dt = 0$, the following solution was obtained:

$$t_w = t_m\left[\left(\frac{\Delta T_{sub}}{\Delta T}\right)^2 - 1\right] \tag{3.29}$$

where $$\Delta T_{sub} = T_w - T_\infty \tag{3.30}$$

The dimensionless form of the bubble growth equation in this case is given as:

$$Y_m = \frac{2}{\pi}\sqrt{3}Ja\{1 - \delta[\delta - (\delta^2 - 1)^{1/2}]\} \tag{3.31}$$

$$Y_m = \frac{R_{\max}}{\sqrt{\pi\alpha t_m}} \qquad \delta = \frac{\Delta T_{sub}}{\Delta T}$$

The expression compared with experimental data by Elliot presented in Zuber (1969) with a fair agreement.

Van Stralen et al. (1975) extensively reviewed all the existing models predicting bubble growth rates in pure and binary mixtures. They also identified three governing mechanisms for bubble growth.

Evaporation Microlayer model involves a thin liquid microlayer under a hemispherical bubble occurring just after the initial equilibrium radius formation. As heat flows through the microlayer, its thickness decreases as a result of evaporation which finally leads to dry spots being formed around the nucleation sites that grow with time. This model assumes only conductive heat transfer in the microlayer therefore neglecting laminar liquid flow in it. Local surface temperature fluctuations in the vicinity of the bubble are attributed to this phenomenon.

Relaxation Microlayer model which is attributed to the evaporation occurring over the entire liquid vapor interface at the bubble dome. This contribution to the rate of bubble growth in non-uniform temperature field is a result of the excess enthalpy of the superheated relaxation microlayer. As the initial thermal boundary layer is displaced by the rapid bubble growth, the microlayer fills the void.

The heat flux density at the heater surface using a transient conduction analysis for semi-infinite bodies is given by:

$$q_w = \frac{F_w}{F_w + F} \frac{F}{(\pi t)^{1/2}} \theta_o^* \tag{3.32}$$

for

$$T_w^* = \frac{F}{F_w + F} \theta_o \tag{3.33}$$

Combination of evaporation and relaxation microlayer poses a significant complication due to the different stages of bubble growth - hydrodynamic and diffusion controlled. Van Stralen et al. presented a solution incorporating the vapor production at the interface of the evaporation microlayer at the base of a hemispherical bubble.

Pohlausen (1921) presented a laminar forced convection boundary layer heat transfer solution to determine the initial thickness of the microlayer formed around the bubble during the initial growth. The local boundary layer thickness at this condition is given by:

$$\frac{\delta}{x} = 3.012\left(\frac{Ux}{\nu}\right)^{-1/2} \mathrm{Pr}^{-1/} \tag{3.34}$$

where U is the free stream liquid velocity. Van Stralen replaced U with $\dot{R}$ = dR/dt, δ by δ_{lo}, and x with r for analyzing growth of a bubble attached to the heated surface, and obtained the following relationship:

$$\delta_{lo} = 3.012\left(\frac{\nu_l r}{\dot{R}}\right)^{1/2} \mathrm{Pr}_l^{-1/3} \tag{3.35}$$

approximating the microlayer underneath a growing hemispherical bubble assuming that it is initially formed as a laminar boundary layer in parallel flow along a horizontal and uniformly heated plate. The bubble radius R can be expressed as a power-law function of the time as:

$$R = \gamma t^m \tag{3.36}$$

which leads to

$$\dot{R} = m\gamma t^{m-1} \tag{3.37}$$

Since R in Eq. 3.35 is evaluated at r = R

$$\frac{r}{\dot{R}} = \frac{t}{m} \tag{3.38}$$

and Eq. 35 can be expressed as:

$$\delta_{lo} = 3.012\left(\frac{\nu_l t}{m}\right)^{1/2} \mathrm{Pr}_l^{-1/3} \tag{3.39}$$

Since Eq. 39 is applicable at $r = R = \gamma t^m$,

$$t = \left(\frac{r}{\gamma}\right)^{1/m} \tag{3.40}$$

and substituting in Eq. 39, the following result is obtained

$$\delta_{lo} = 3.012\,\mathrm{Pr}_l^{-1/3}\left(\frac{\nu_l}{m\gamma^{1/m}}\right)^{1/2} r^{1/2m} \tag{3.41}$$

For asymptotic bubble growth of a hemispherical bubble, where Reynolds number is independent of time, based only on evaporation of the microlayer under its base, the energy-balance relationship that governs the phenomenon is given as:

$$\rho_v h_{lv}(2\pi R)\dot{R} = \int_0^R \frac{k_l(T_w - T_{sat})(2\pi R)}{\delta_{lo}}\,dr \tag{3.42}$$

Substituting Eq. 3.40 into Eq. 3.41, and using Eq. 3.35, the prediction of the bubble growth rate in the inertia controlled region is defined as:

$$\dot{R} = \left[\frac{\alpha_l Ja\,\mathrm{Pr}_l^{1/3}}{3.012(2-1/2m)}\right]\left(\frac{m}{\nu_l}\right)^{1/2} t^{-1/2} \tag{3.43}$$

The dependence of the bubble radius with time is then given as:

$$R(t) = 0.470\,Ja\,\mathrm{Pr}_l^{-1/6}(\alpha_l t)^{1/2} \tag{3.44}$$

In both the inertia controlled growth due to the evaporation of the microlayer, and the heat transfer controlled growth occurring as a result of the latent heat supplied to the bubble interface from the relaxation microlayer, the variation of the bubble radius with

time is proportional to $t^{1/2}$. Due to this similarity, the distinction between the controlling mechanisms is quite difficult.

Van Stralen proposed the following correlation for bubble growth rate in either inertia controlled or heat transfer controlled regime for pure and binary systems:

$$R(t) = \frac{R_1(t)R_2(t)}{R_1(t) + R_2(t)} \tag{3.45}$$

where the modified Raleigh (1917) solution for inertia controlled region is given by:

$$R_1(t) = 0.8165\sqrt{\frac{\rho_v h_{lv}(T_w - T_{at})\exp[-(t/t_d)^{1/2}]}{\rho_l T_{sat}}t} \tag{3.46}$$

and the combined relaxation and microlayer evaporation solution is given by:

$$R_2(t) = 1.9544\left\{b^* \exp\left[-\left(\frac{t}{t_d}\right)^{1/2}\right] + \frac{T_\infty - T_{sat}}{T_w - T_{sat}}\right\}Ja(\alpha_l t)^{1/2} \tag{3.47}$$

$$+0.3730\,\mathrm{Pr}_l^{-1/6}\left\{\exp\left[-\left(\frac{t}{t_d}\right)^{1/2}\right]\right\}^{1/2} Ja(\alpha_l t)^{1/2}$$

where b* is a factor accounting for the fact that only a portion of the vapor bubble dome may be in contact with superheated liquid, and is determined by the following expression:

$$b^* = 1.3908\frac{R_2(t_d)}{Ja(\alpha_l t)^{1/2}} - 0.1908\,\mathrm{Pr}_l^{-1/6} \tag{3.48}$$

t_d in the above equations is defined as the time of departure of the bubble from the surface. Equations 3.44 - 3.47 are the pure liquid forms of the solution. Van Stralen et al.(1975) in a parallel study reported quite good agreement of the bubble growth prediction with experimentally obtained data.

Beer et al. (1977) presented a survey of the bubble growth models in pool boiling in the two existing growth regimes. The equations developed by him apply only for bubble growth on solid heating surfaces without including any information on bubble departure. The first bubble departure studies, like the one conducted by Fritz (1935), were based only on the static bubble growth. This growth is governed by buoyancy forces F_b and surface tension forces F_S only (as shown on Figure 3.6), and the departure condition occurs when the upward forces exceed the retaining forces acting on the bubble

$$F_b = F_S \tag{3.49}$$

The first available relation for determining the bubble departure radius was given by Fritz as:

$$R_d = 0.0104\Phi\sqrt{\frac{\sigma}{g(\rho_l - \rho_v)}} \tag{3.50}$$

All these models predict bubble departure sizes smaller than the actual ones, especially for conditions applicable in the high growth rate (inertia controlled) region, since the buoyancy and the surface tension forces dominate only in quasistatic bubble growth.

Beer et al. investigated the rapid growth region, where dynamic forces (inertia, drag, and pressure), are included in the governing growth relation. They considered a bubble in a shape of truncated sphere attached to and growing on a heating surface, with forces as shown on Figure 3.7 acting on it. The pressure force F_p and the buoyancy force F_b which act normal to the bubble base contribute toward bubble detachment. The surface tension force F_s and the drag force F_d oppose bubble detachment, trying to retain the bubble on the surface, or retard its growth respectively. The inertia force F_i may either oppose or aid the detachment depending on the bubble growth trend. At the instance of

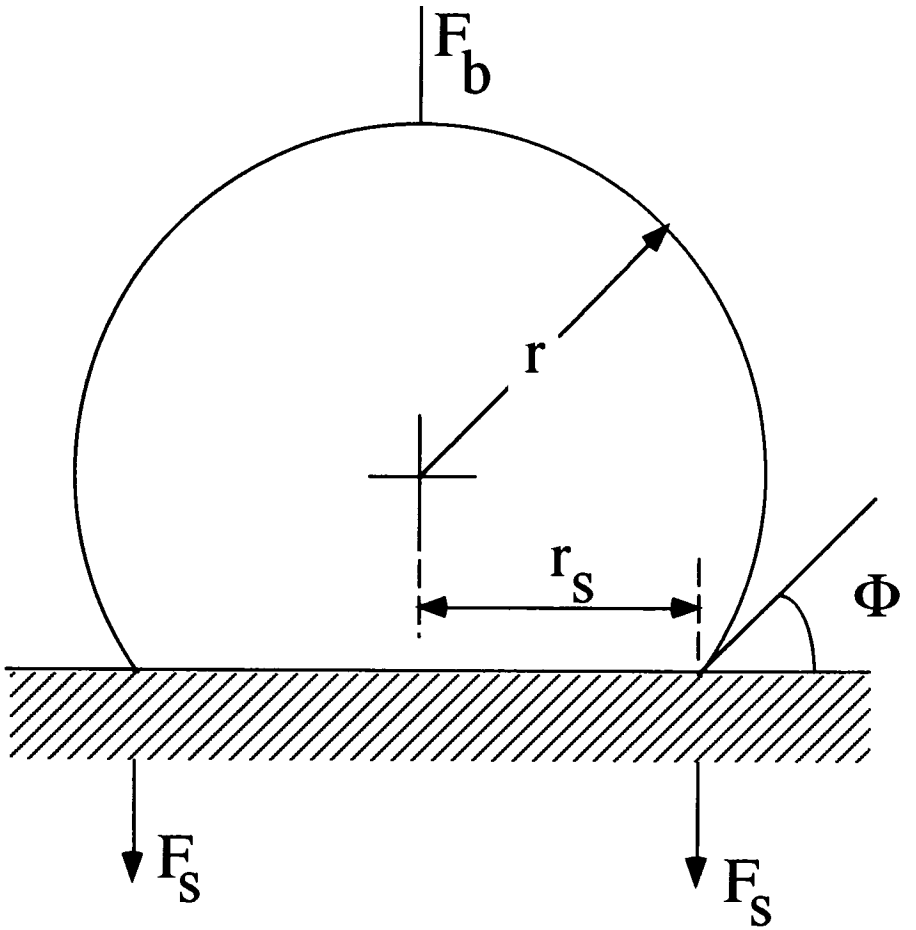

Figure 3.6 Static Force Balance - Beer et al. (1977)

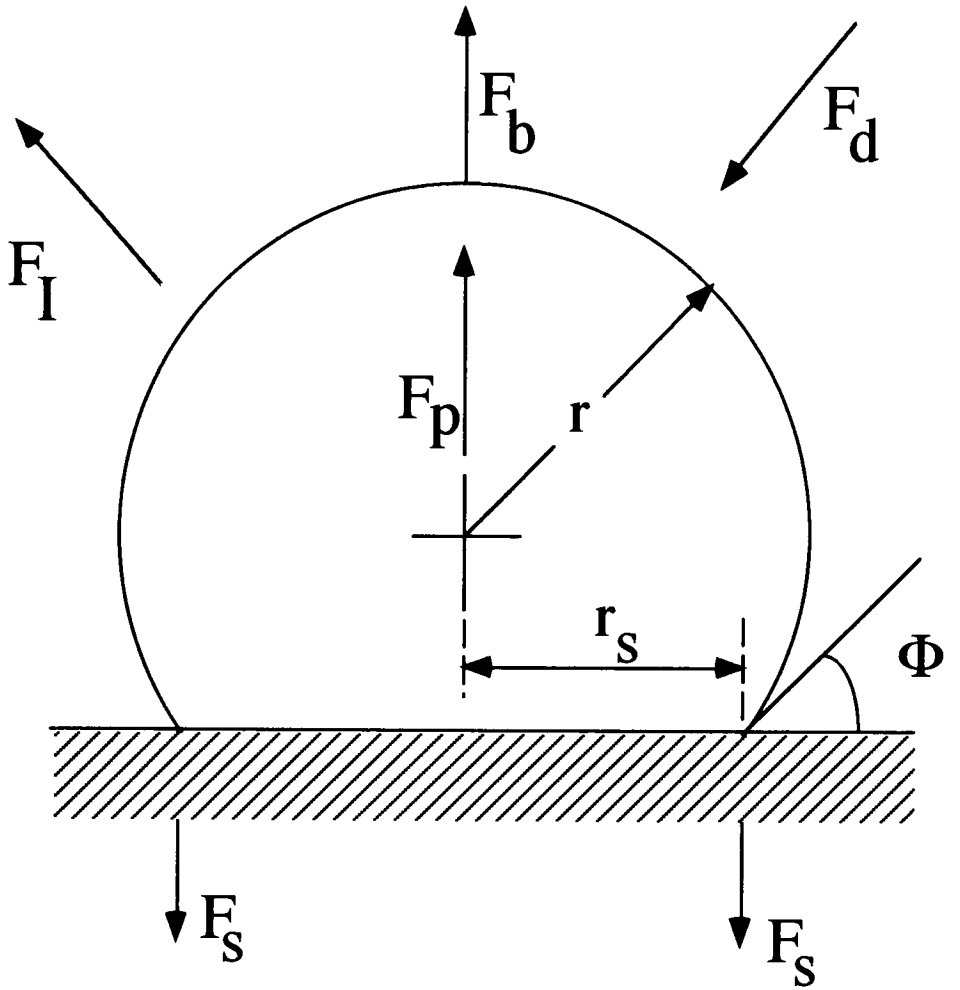

Figure 3.7 Dynamic Force Balance - Beer et al. (1977)

bubble detachment from the surface, the force balance on the bubble can be written as follows:

$$F_d + F_s = F_p + F_b + F_i \tag{3.51}$$

Assuming spherical bubble, using the drag force coefficient c_w, and evaluating the pressure inside the bubble as a sum of the capillary pressure $2\sigma/R$ and the dynamic excess pressure ΔP_v, the above equation can be written as:

$$c_w \frac{\rho_l}{2}\left(\frac{dR}{dt}\right)^2 \pi R_s^2 + 2\pi R_s \sigma \sin\Phi = -\frac{4}{3}\pi R_d^3 \rho_l \frac{d^2R}{dt^2} + \left(\frac{2\sigma}{R_d}\right)\pi R_s^2 + \Delta P_v \pi R_s^2 + \frac{4}{3}\pi R_d^3 \rho_l g \tag{3.52}$$

The inertia, surface tension, and buoyancy forces were determined from experimental data. In order to evaluate the drag and pressure forces, the bubble growth process before departure was considered to obtain values for the drag coefficient c_w and the excess dynamic pressure ΔP_v. By performing an energy balance (first law of thermodynamics), assuming that the spherical bubble grows unattached to the surface, the following expression was obtained:

$$dE_{\Delta P} = dE_i + dE_d \tag{3.53}$$

$$\Delta P_v 4\pi R^2 dR = \frac{4}{3}\pi R^3 \rho_l \frac{d^2R}{dt^2} dR + c_w \frac{\rho_l}{2}\pi R^2 \left(\frac{dR}{dt}\right)^2 dR \tag{3.54}$$

From Equations 3.52 and 3.54, the values for c_w and ΔP_v were determined, and c_w was plotted and correlated as a function of Reynolds number Re (defined by the bubble growth velocity and the departure diameter) for laminar and turbulent flow.

Klausner et al. (1993) studied the bubble departure in forced convection boiling of R113. A growing bubble attached to a heating surface (nichrome heater used in this

particular study) is shown on Figure 3.8. The force analysis on the bubble included the effects of the surface tension force F_s, quasi-steady drag F_{qs}, unsteady drag due to assymptotical bubble growth F_{du}, shear lift force F_{sl}, buoyancy force F_b, hydrodynamic pressure force F_h, and contact pressure force F_{cp},

The force balance in the flow (horizontal) direction is given as:

$$\sum F_x = F_{sx} + F_{qs} + F_{dux} \tag{3.55}$$

and in the vertical direction as:

$$\sum F_y = F_{sy} + F_{duy} + F_{sl} + F_b + F_h + F_{cp} \tag{3.56}$$

A typical bubble was used to estimate the forces acting on it, with characteristic parameters such as d (mean bubble diameter) = 260 μm, d_w (surface contact bubble diameter) = 90 μm, $\alpha \approx \pi/4$ and $\beta \approx \pi/5$ (advancing and receding contact angles), fluid velocity u = 0.52 m/s, liquid film thickness δ = 6.5 mm, wall heat flux q_w = 23.6 kW/m^2, and wall superheat ΔT_{sat} = 15.8°C. The bubble diameters were determined using probability density analysis of sets of approximately 200 bubbles over range of flow conditions with G = 133 kg/m^{2}s. The reported comparison between the measured and predicted departure diameter was quite satisfactory.

The authors observed sliding of the bubble along the heating surface prior to departure, and lift off at some final distance. Strong dependence of the mean departure diameter on the heat flux was reported, which shows the importance of the quasi-steady drag force. Influence of heat transfer on the mean bubble diameter was also reported, which expresses the importance of steady drag force due to asymmetrical bubble growth.

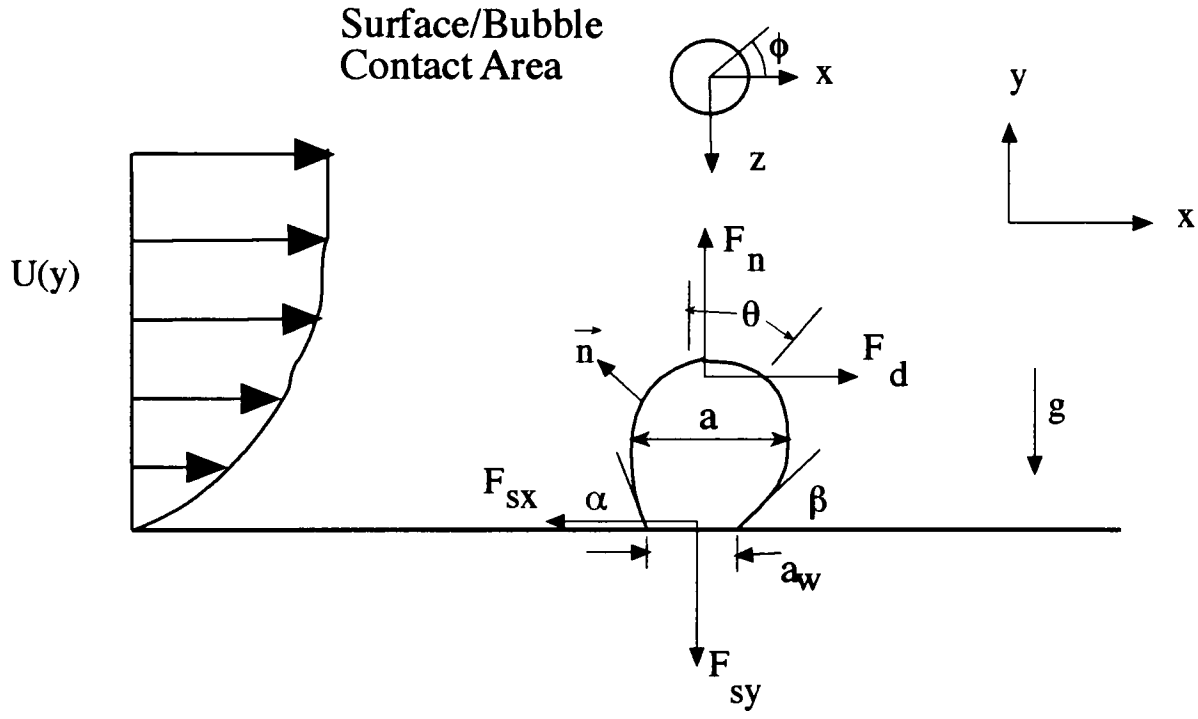

Figure 3.8 Growing vapor bubble attached to a heating surface in shear flow (Klausner et al. 1993)

The significant standard deviation of the departure diameter from the mean was reported to be indicative of the stochastic nature of the bubble departure process.

Zeng et al. (1993) used the same experimental set up utilizing R113 in a Pyrex square channel. The wall superheat range of the analyzed system was 5.5°C - 12°C, and the mean liquid velocity 0.35 - 1 m/s. The model proposed for bubble departure and lift-off neglects surface tension, therefore simplifying the departure and lift-off diameter prediction, since no knowledge of the advancing and the receding contact angle is required.

The model proposed by Klausner et al. (1993) has been improved by determining the inclination angle on a dynamic basis which means that it is not required as an input parameter. With this modification, the force balance of the bubble is given as:

$$\sum F_x = F_{sx} + F_{qs} + F_{dux} = \rho_v V_b \frac{du_{bcx}}{dt} \tag{3.57}$$

$$\sum F_y = F_{sy} + F_{duy} + F_{sl} + F_b + F_h + F_{cp} = \rho_v V_b \frac{du_{bcy}}{dt} \tag{3.58}$$

where V_b is the bubble volume, u_{bc} the velocity of the center of mass (as specified on Figure 3.9), and ρ_v the vapor density.

The vapor bubble lift-off process was analyzed through probability density functions, and was indicated that it is strongly dependent on wall superheat and weakly dependent on liquid velocity. This finding was in contradiction with the bubble departure process described by Klausner which suggested strong dependence on both wall superheat and liquid velocity.

Kandlikar and Stumm (1995) presented a unique and new approach for predicting the forces acting on a departing bubble in flow boiling. A control volume approach was employed to study the departure mechanism. In order to approximate the phenomena, four basic forces acting on the bubble - Pressure force, surface tension acting on the interface between the two control volumes, surface tension acting along the heater surface wall, and buoyancy force were used in the model. Momentum equations for each control volume were also included in the analysis.

The assumptions made in development of the proposed model were as follows:

- Bubble was assumed to be spherical in momentum equation derivation.

- Velocity vectors impacting the liquid-vapor interface deflect off tangentially at the point of contact with the bubble.

- The deflected velocities in the lower hemisphere of the bubble were treated differently than in the upper hemisphere.

- The front and the rear control volumes were analyzed separately for the force balance.

- Contact angle was assumed to vary linearly from the front to the rear edge of the bubble.

- A fully developed velocity profile was assumed.

- The bubble shape was assumed to be truncated sphere.

Based on this assumption, the forces acting on the bubble in the front and the rear control volumes were determined. Figure 3.10 shows the front and the rear control volumes that were used in order to perform the force balance on the bubble.

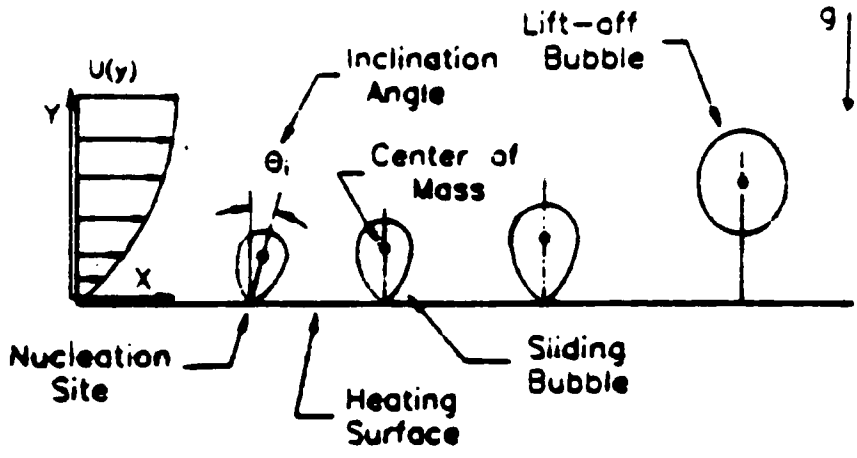

Figure 3.9 Vapor bubble departure and lift off (Zeng et al. 1993)

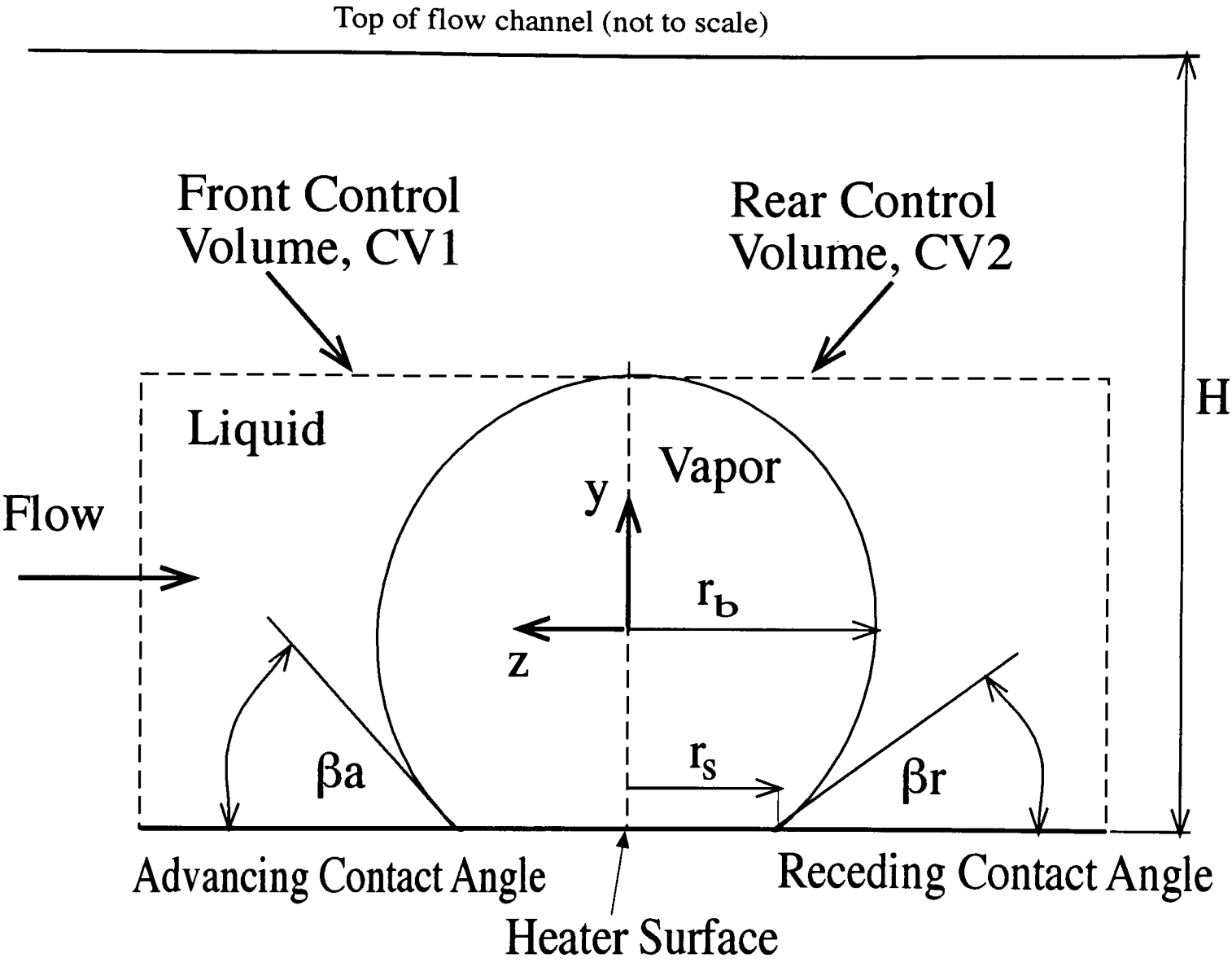

Figure 3.10 Front and Rear Control Volumes for Force Balance on a Bubble - Kandlikar and Stumm (1995)

Front Control Volume, CV1

Figure 3.11 shows the front control volume of the bubble with the forces acting on it. In the front control volume CV1, the two surface tension forces act: along the edge at the base of the bubble (at the heater surface) and along the diametric plane separating the two control volumes. The pressure force acts in the y and z directions as shown. The inlet velocity vector u is in the negative z direction, and is a function of y alone.

Front Control Volume, CV1, z-direction

A force balance in the z direction for the front control volume yields the following relation:

$$F_{\sigma,1,z}+F_{\sigma,2,z}+F_{B,CV1,z}+F_{D,CV1,z}+F_{P,CV1,z}=\dot{M}_{out,z}-\dot{M}_{in,z} \qquad (3.59)$$

The forces and the equations used to approximate their action are defined in the following pages.

The contact angle was assumed to vary from the advancing angle β_a to the receding angle β. as a linear function. For $\gamma<\pi/2$,

$$\beta(\gamma) = \beta_a - (\beta_a - \beta_m)\frac{\gamma}{(\pi/2)} \qquad (3.60)$$

and for $\pi/2<\gamma<\pi$,

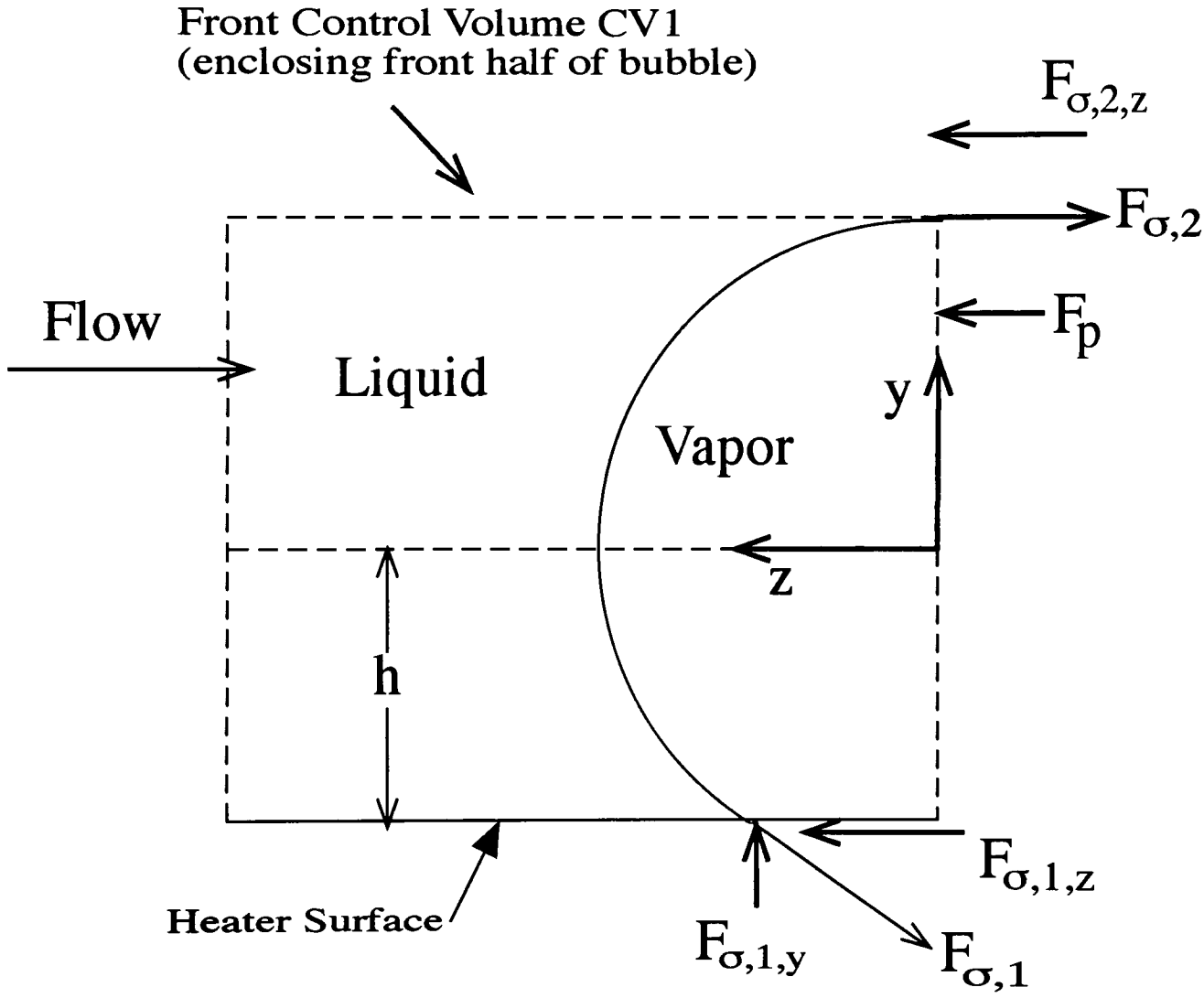

Figure 3.11 Force Balance on Front Control Volume, Side View - Kandlikar and Stumm (1995)

$$\beta(\gamma) = \beta_m - (\beta_m - \beta_r)\frac{(\gamma - \pi/2)}{\pi/2} \qquad (3.61)$$

where $\beta_m = (\beta_a + \beta_r)/2$, and γ is the angle between the radial lines, one joining the front edge of the bubble to the center of the bubble base, and the other line joining a given location on the base periphery to the center in radians.

The surface tension force, $F_{\sigma,1,z}$, acting in the z direction in the plane of the heated wall along the edge of the bubble in the front control volume is given by:

$$F_{\sigma,1,z} = -2\sigma r_s \int_0^{\pi/2} \cos(\beta(\gamma))\cos(\gamma)d\gamma \qquad (3.62)$$

where r_s is the radius of the bubble base (assumed to be circular).

The surface tension force, $F_{\sigma,2,z}$, acting along the interface separating the two control volumes is given by:

$$(F_{\sigma,2})_z = -2\sigma\pi r_b\left(1-\frac{\beta_m}{\pi}\right) \qquad (3.63)$$

The net pressure force, $F_{P,CV1,z}$ acting on the front control volume in the z direction is given by:

$$F_{p,CV1,z} = A_p(p_b - p_L) \qquad (3.64)$$

The static pressure variation across the height of the bubble due to flow was assumed to be neglegibly small (estimated to be less than 1 Pa for the bubbles investigated in the

study).

The buoyancy force $F_{B,CV1,z}$ in the z direction was not used since its action is only present in the y direction.

The drag force $F_{D,CV1,z}$ was estimated by comparing a pure vapor sphere in a liquid flow. The total drag force on the entire bubble was calculated from a relation proposed by Clift, et. al (1978) for a pure vapor bubble subjected to a uniform liquid flow around it.

$$F_{D,b,z} = \left[\frac{8}{Re_b}\left(\frac{2+3\kappa}{1+\kappa}\right)\frac{\rho u^2}{2}\right]A_p \qquad (3.65)$$

where κ is the viscosity ratio, μ_v/μ_f, u is the flow velocity, and A_p is the projected area of the bubble normal to the flow direction.

The value of the drag force was neglected since the excess pressure that was generated as a result of its action was less that 0.1% of the excess pressure for a typical bubble.The excess pressure, ΔP, is the difference between the vapor pressure, P_v, present inside the bubble, and the liquid pressure, P_l, in the bulk of the liquid. The excess pressure is given by:

The rate of entering momentum in the z-direction was calculated by taking a dx dy element at a location (x, y) on the front face of CV1. The resulting equation was given by:

$$\dot{M}_{in,CV1,z} = -2\int_{-h}^{r_b}\int_{0}^{\sqrt{r_b^2-y^2}} \rho u^2 dx dy \qquad (3.66)$$

The fluid velocity, u, was assumed to have parabolic profile, and was modeled as a second order (quadratic) function.

The momentum going out in the z direction was calculated by dividing the bubble in two regions, one below the center plane, and the other above the center plane. For the lower region, the deflected velocity vector was assumed to be parallel to the heated wall and tangential to the bubble profile in the plane parallel to the heated wall with no y direction vectors for the deflected velocity in this region. For the upper region, the deflected velocity was assumed to be tangential to the spherical bubble surface and could propagate in x, y, and z directions..

The rate of exiting momentum in the z direction was given by:

$$\dot{M}_{out,CV1,z} = -2\int_{-h}^{0}\int_{0}^{\sqrt{r_b^2-y^2}} \rho u^2 \left[\frac{u'^3_z}{(u'^2_x+u'^2_z)^{3/2}}\right]dxdy - 2\int_{0}^{r_b}\int_{0}^{\sqrt{r_b^2-y^2}} \rho u^2 \left[\frac{u'^3_z}{(u'^2_x+u'^2_z+u'^2_z)^{3/2}}\right]dxdy \qquad (3.67)$$

The excess pressure in the bubble was then obtained from equations 3.59 and 3.64, and was given by

$$\Delta p_{CV1,z} = \frac{\dot{M}_{out,z} - \dot{M}_{in,z} - F_{\sigma,1,z} - F_{\sigma,2,z} - F_{B,CV1,z}}{A_p} \qquad (3.68)$$

Front Control Volume, CV1, y-direction

A similar force balance in the y-direction was performed to yield:

$$F_{\sigma,1,y}+F_{\sigma,2,y}+F_{p,cv1,y}+F_{B,CV1,y}=\dot{M}_{out,y}-\dot{M}_{in,y} \qquad (3.69)$$

The surface tension force $F_{\sigma,1}$ was obtained as

$$F_{\sigma,1,y} = 2\sigma r_s \int_0^{\pi/2} \sin(\beta(\gamma))d\gamma \qquad (3.70)$$

The surface tension force $F_{\sigma,2}$ has no component in the y-direction. The net pressure force on the CV1 in the y-direction was then given by:

$$F_{p,CV1,y} = \frac{1}{2}\pi r_s^2(p_b - p_L) \qquad (3.71)$$

and the buoyancy force in the y-direction is given by

$$F_{B,CV1,y} = \frac{1}{2}V_b(\rho_L-\rho_V)g \qquad (3.72)$$

The inlet velocity in the y-direction was assumed to be zero, resulting in no entering momentum. The deflected velocity vector in the y-direction was divided into two regions, similar to the z-direction analysis presented above.

For the region below the center plane, the deflected velocity was assumed to have no component in the y-direction. The rate of exiting momentum in the y-direction for the region above the center was then given by:

$$\dot{M}_{out,CV1y} = -2 \int_0^{r_b} \int_0^{\sqrt{r_b^2 - y^2}} \rho u^2 \left[\frac{u'^3_y}{(u'^2_x + u'^2_z + u'^2_z)^{3/2}} \right] dx dy \qquad (3.73)$$

The excess pressure calculated from the equilibrium of forces in the y direction for the front control volume was finally obtained from equations 3.70 and 3.72 and was given by:

$$\Delta p_{CV1y} = \frac{\dot{M}_{out,y} - \dot{M}_{in,y} - F_{\sigma,1,y} - F_{\sigma,2,y} - F_{B,CV1,y}}{(\pi r_s^2/2)} \qquad (3.74)$$

REAR CONTROL VOLUME, CV2

The rear control volume analysis was performed in similar fashion as the one for the front control volume.

4. EXPERIMENTAL INVESTIGATION:

4.1. Experimental Setup

The experimental setup shown in Figure 4.1 consisted of a constant temperature bath, flow meter, horizontal rectangular flow channel with attached aluminum heater, microscope, video recorder system, and temperature data acquisition unit.

The horizontal flow channel, made of 6061-T6 aluminum, had a 3x50 mm cross section, with a circular heater 9.4 mm in diameter placed in the center of the lower (50 mm side) wall. The heater was machined from aluminum 2024-T3 stock. The surface of the heater which is in contact with the flowing liquid (water) was polished on a cloth covered metallographic polishing wheel using 1μ particle size alumina in a water suspension resulting in a 1 μm surface finish. Despite the fine surface finish, the natural cavities of approximately 2-15 μm were still present at the heater surface and acted as nucleation sites for vapor bubbles. Four E-type thermocouples, with an accuracy of 0.1 °C, were placed along the length of the heater rod as shown in Figure 4.2. They were bonded to the heater using Omega® CC High Temperature Cement which resists temperatures of up to 843°C, and is water, oil, and electrically resistant. The thermocouples were connected to a Keithley 740 System Scanning Thermometer which digitally displayed the temperature at each of the four thermocouples. A fifth thermocouple was attached to the thermometer to obtain the ambient air temperature in the vicinity of the test loop. The heater was insulated using a multi-layer fiberglass insulation and separated from the flow channel by a Torlon® bushing as shown in Figure 4.3. In order to prevent leakage, the bushing was press fitted into the flow chamber as

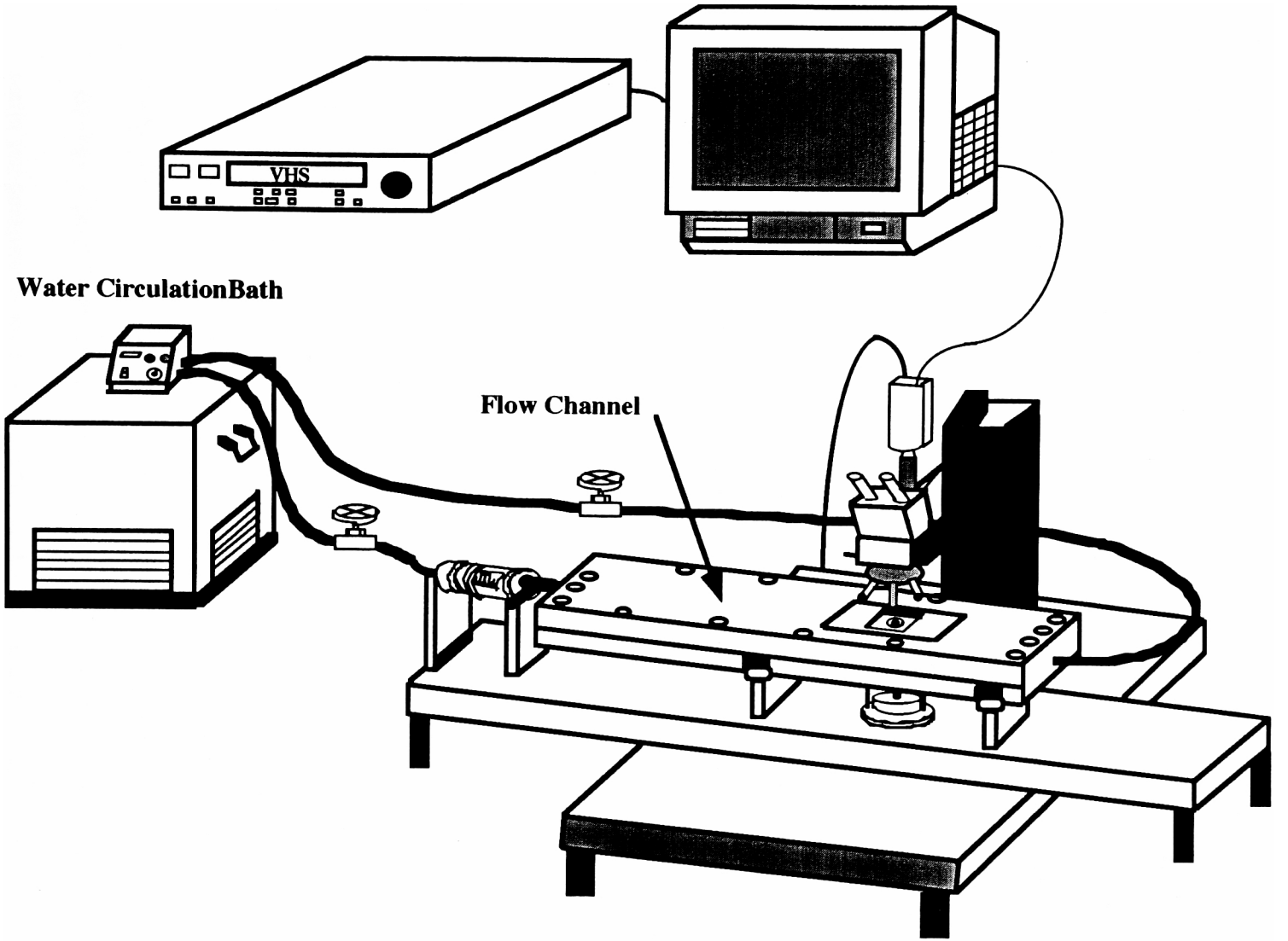

Figure 4.1 Experimental Flow Loop Setup

was the heater into the bushing. Both the top surface of the bushing and heater surface were flush with the lower face of the flow channel in an attempt to reduce flow instabilities. To ensure the two top thermocouples would not be pulled out of the heater when press fit into the bushing, a small channel was machined on the periphery of the heater rod to allow for adequate wire clearance between the heater and bushing.

The aluminum rod was heated using a Watlow circumferencial electrical resistance heater wrapped around its based as shown in Figure 4.3. The heater was connected to a voltage adjustable power supply capable of a maximum power output of 1500W.

The flow channel had a 1/4" thick 50x50 mm polycarbonate window located directly above the heater surface to allow for viewing (Figure 4.2). A front surface silicon polished mirror was placed at 45° adjacent to the heater surface and parallel to the flow in order to allow for side viewing capabilities. To ensure viewing access to the base of nucleating bubbles, the mirror was embedded 1 mm into the bottom of the channel. The mirror was placed at a distance from the heated surface sufficient enough so as not to disrupt the flow field over the heater surface.

The length of the channel was 400 mm and the heater was placed 300 mm from the inlet in order to achieve a fully developed flow regime. The transition from the 1/2" inlet diameter to the 3x50 mm rectangular flow channel was smooth and gradual to achieve fully developed flow conditions.

The flow chamber was only one of many parts that made up the entire experimental test loop shown in Figure 4.1. A MGW Lauda RC20 constant temperature bath was utilized to ensure a uniform inlet water temperature. The bath could control the water temperature to within 0.1°C and had a total capacity of approximately four gallons.

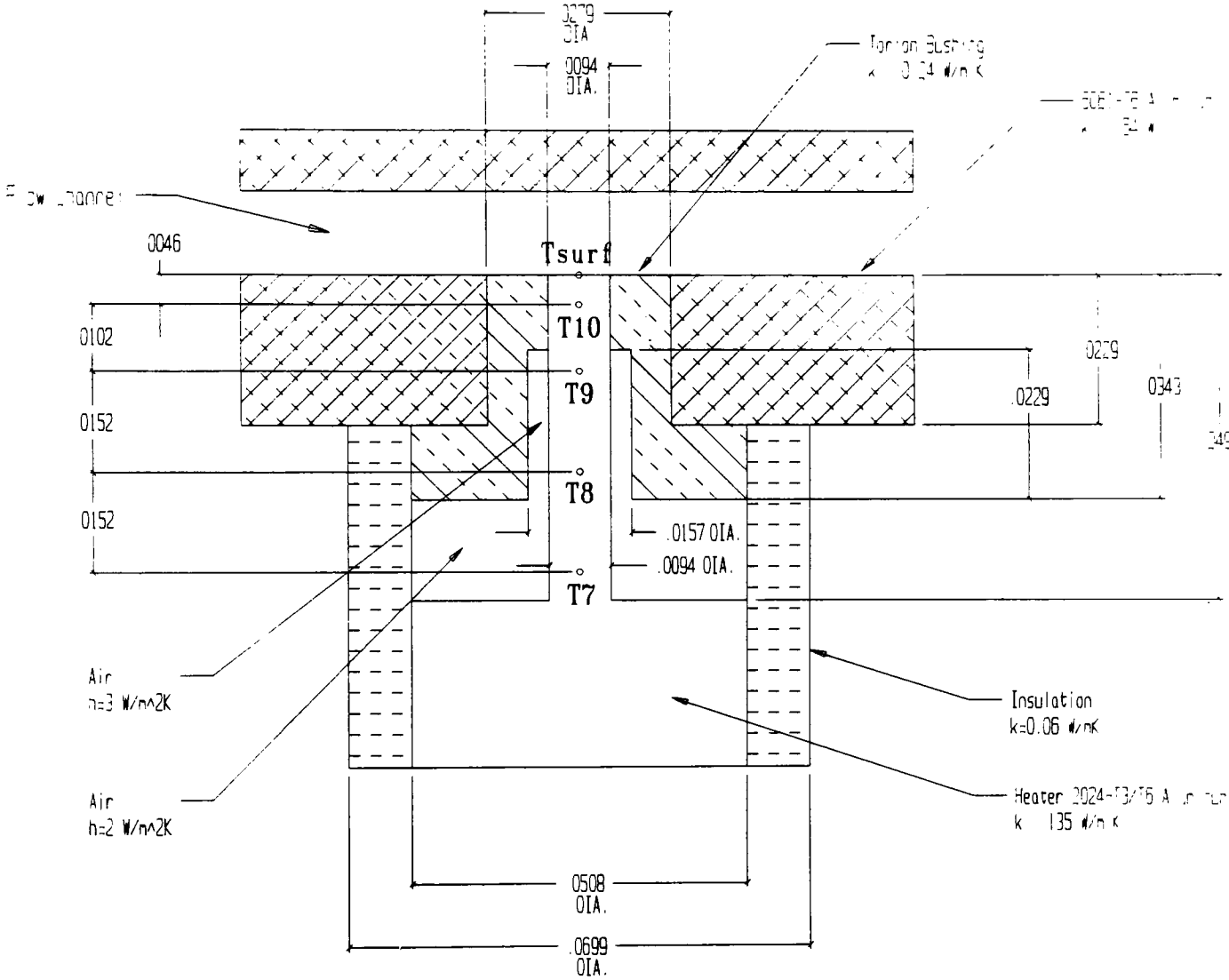

Figure 4.2 Heater cross section

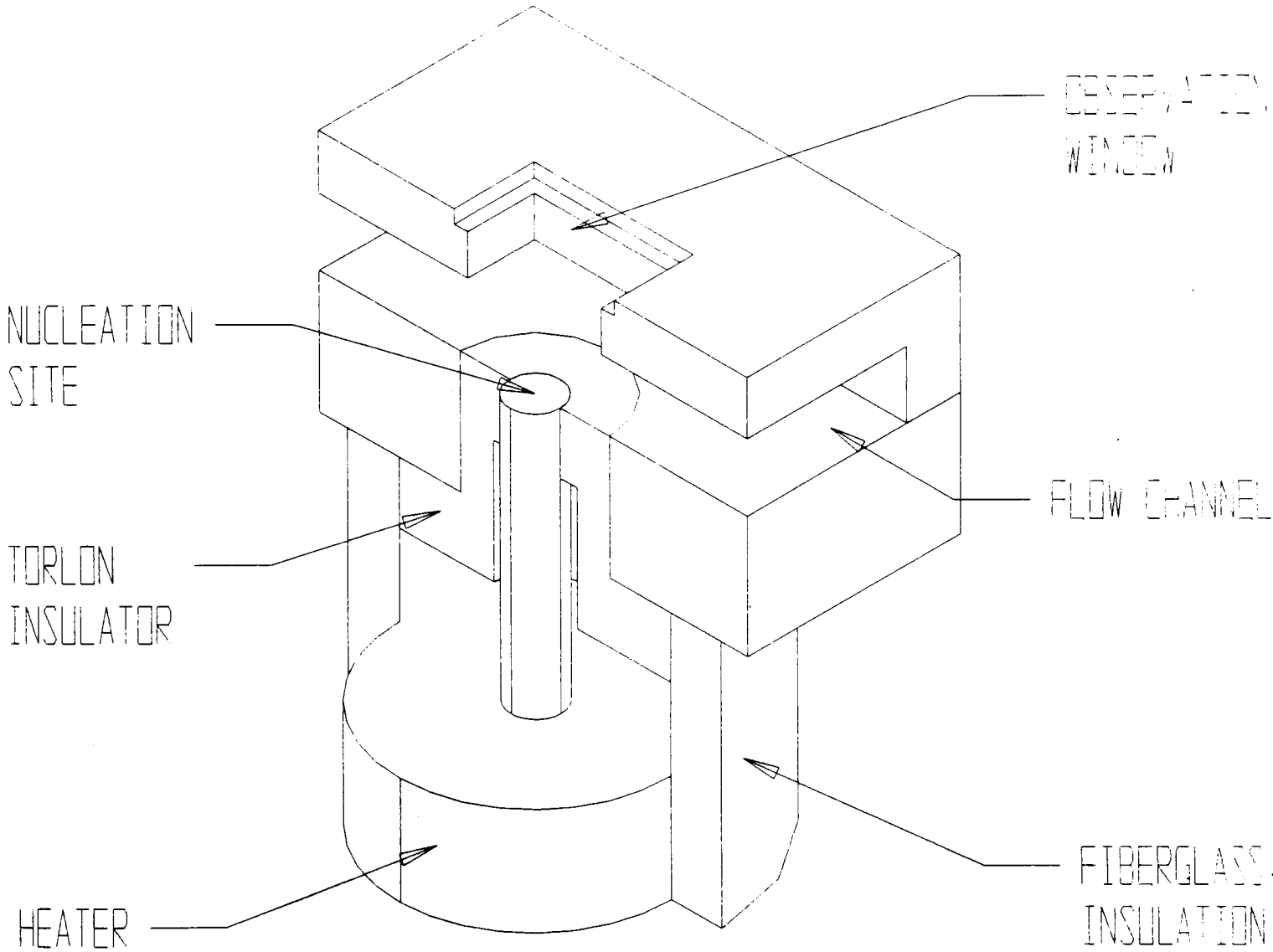

Figure 4.3 3-D View of the heater section

A variable flow pump was integrated into the constant temperature bath, and had a maximum pumping capacity in the range of 2 GPM for the experimental test loop configuration. The flow rate was measured using an Omega® FL-1503A rotameter calibrated for a maximum flow of 2.53 GPM. The meter measured percentage of the maximum flow in 2% increments which yielded an accuracy of ± 0.023 GPM. The constant temperature bath, the rotameter and flow chamber were connected by a 1/2" inside diameter high temperature hose.

The visual setup consisted of a Micromanipulator® HSDS-1 microscope equipped with a variable magnification eye piece and three Bausch & Lomb lenses. The microscope was also equipped with a special mount for video cameras. This allowed for simultaneous viewing of the surface by both the attached eye piece as well as a Sony Trinitron GVM 1300, 20" Monitor. All cavity and bubble size measurements were taken from the monitor. Since the image magnification was dependent on both the lens and the camera used. The resulting magnification for different combinations is listed in Table 4.1.

The first of the two cameras used was a Hitachi KP-C501, all Solid State color camera which had a recording speed of 30 frames per second (fps). This camera was used mostly to record slower growing bubbles, or when a higher quality picture was required. For viewing bubbles with fast growth rates, a high speed Kodak Ektapro 1000 Image Intensifying system was used. This camera had the capability to capture images at a rate as high as 6000 fps. The high speed camera had no mechanical shutter, rather an image intensifying system which electronically controlled aperture setting depending on the available lighting. This allowed for images to be captured without the use of a flash, like many other high speed cameras. The high speed image could be played back at 30 fps

Color Camera

Lens	Eyepiece	Magnification
2.25*0.04	1	60
	2	120
8*0.15	1	210
	2	420
25*0.31	1	675
	2	1350

High Speed Camera

Lens	Eyepiece	Magnification
2.25*0.04	1	20
	2	40
8*0.15	1	70
	2	140
25*0.31	1	215
	2	430

Table 4.1 Microscope Lens/Camera Combined Magnification

and transfer to a normal VHS through a Panasonic AG-6300 video cassette recorder. This VCR had the capability to advance one frame at a time which is required when accurately deterring the location of bubble nucleation sites and bubble growth rates.

4.2. Experimental Procedure

The fluid used in the experiments was distilled water. In order to clean the test loop from any impurities that may affect the results, water at or above 90°C was circulated through the system over a period of several hours and then drained. After draining the system, the inside of the tank of the constant temperature bath was thoroughly cleaned by physical means (wiping the inside with paper towels). Chemical additives for cleaning the system were not utilized since even slight traces of their presence would cause significant change in the physical properties of the water (especially in the surface tension values).

The system was then filled with new distilled water, which was circulated at temperatures in the range of 85-90°C for over five hours. This was done in order to remove any dissolved gasses from the water, otherwise known as degassing. Through this procedure, it was ensured that the observed bubbles are product of heterogeneous boiling at the heater surface, rather than from the degassing.

The surface tension values of the water used in the testing at temperatures between 20°C and 60°C were verified through the use of three basic experimental techniques: capillary rise test, a drainage technique method, and by method of direct pull. Refer to the results of the capillary rise test in the Appendix A. All tests resulted in surface tension values within 5% of the published values for pure water at the corresponding

temperatures. This finding led to the conclusion that the published surface tension values could be used in the analysis supporting the current work.

Once the system was flushed and degassing was completed, the actual experimental procedure began. The first step was to set the constant temperature bath to a specified value within the range of 60-90°C and adjust the flow to a constant value in the range on 0.25-1.00 GPM. The system was allowed time to reach a steady state condition (approximately 1 hour). Once steady state was achieved, the heater power was turned on. The voltage and current were gradually increased based on the reading of the thermocouples until a temperature slightly lower than the water saturation temperature was achieved near the heater surface.

At this point the voltage was incrementally increased, each time allowing the thermocouple temperature readings to stabilize between the voltage increases. The constant temperature values were recorded and later processed using ThermoNet™ to find the surface temperature and the heat transfer from the heater surface to the water (see ThermoNet™ Analysis section). The voltage was increased by equal amounts until a wall superheat of approximately 14-16°C was achieved.

As the surface temperature approached the saturation temperature, the Hitachi color camera was employed to closely observe the heater surface and detect the onset of nucleation. Once active cavities were observed, the high speed Kodak camera was utilized to record the bubble nucleation, growth, and departure phenomena. Before the image could be recorded, the high speed Image Intensifying system required the tape to be conditioned through the Intensified Imager Controller for proper operation when capturing images at high frame rates. The captured images were then transferred from the

high speed tape to a normal VHS tape through a Panasonic AG-6300 VCR. This procedure was repeated often because when recording at frame rates of 1000 fps the tape could only store 30 seconds of images, and only 5 seconds when using 6000 fps.

Each recorded series had a unique session number which was used for matching it with a corresponding temperature distribution during later analysis. This information was recorded on a data sheet (Table 4.2) which also contains information on liquid conditions (flow rate and temperature), lens magnification, and power supply output. The data sheets were sequentially numbered, and dated. A log of over 40 data sheets with more than 200 data sets was collected over the course of the experimental testing. The flow rate for each corresponding water temperature was varied between 10% and 40% of the maximum flow rate (0.25-1.00 GPM).

Since only a small portion of the heated surface could be observed in the field of view, the microscope was translated to numerous locations for each flow condition in order to scan the entire heater surface.

Experiment Data Sheet #

Date:

Velocity:

Water Temperature:

Voltage (V):							
Current (A):							
T7 (°C)							
T8 (°C)							
T9 (°C)							
T10 (°C)							
Tsurf (°C)							
Heat Flux (W)							
Magnification:							
Departure Diameter:							
Cavity Diameter (in):							
Tape Location:							

Table 4.2 Experimental Data Sheet

4.3. ThermoNet™ Analysis

4.3.1 ThermoNet™ Model

The temperature measurement obtained from the thermocouples gave a temperature distribution along the length of the aluminum heater rod, unfortunately the surface temperature was not known. In order to determine this temperature, ThermoNet™, a thermal network analysis software, was utilized.

The heater assembly system consisting of aluminum rod, Torlon bushing, and installation wrapping was discretisized into the network of 66 nodes as well as numerous convection and conduction resistances as shown in Figures 4.4 and 4.5. The values for the thermal resistances in the heater were calculated using the following equations

$$R_{COND} = L/kA_C \text{ (Axial)} \tag{4.1}$$

$$R_{COND} = \ln(r_2/r_1)/2kL \text{ (Radial)} \tag{4.2}$$

$$R_{CONV} = 1/hA_S \tag{4.3}$$

where A_C is the cross sectional area, A_S is the surface area and r_1 and r_2 are the inner and outer radius of a cylinder respectively.

A spread-sheet was formulated to calculate all the resistance values used in the model (Appendix B). VisualNet™ was used to create a visual nodal/resistance model as shown in Figure 4.5. The node and resistance information created in VisualNet™ was transferred to ThermoNet™ where a steady state analysis was performed on the model.

The nodes 1, 6, 12, and 18 in Figure 4.5 correspond to the four thermocouples with node 1 being the thermocouple (T7) located nearest to the base and node 18 being the thermocouple nearest to the surface. Other important nodes and resistances are node

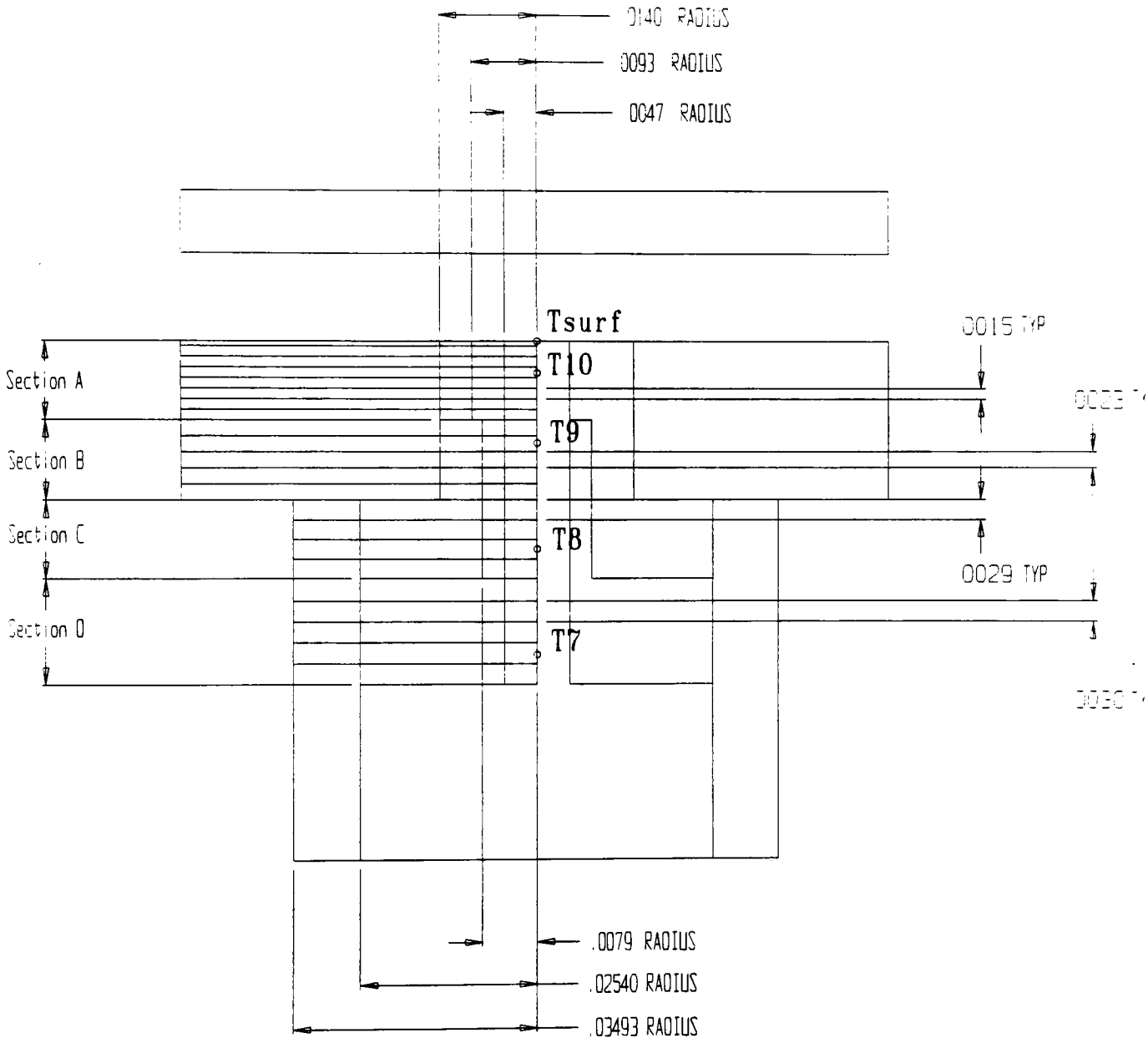

Figure 4.4 Discretisized heater

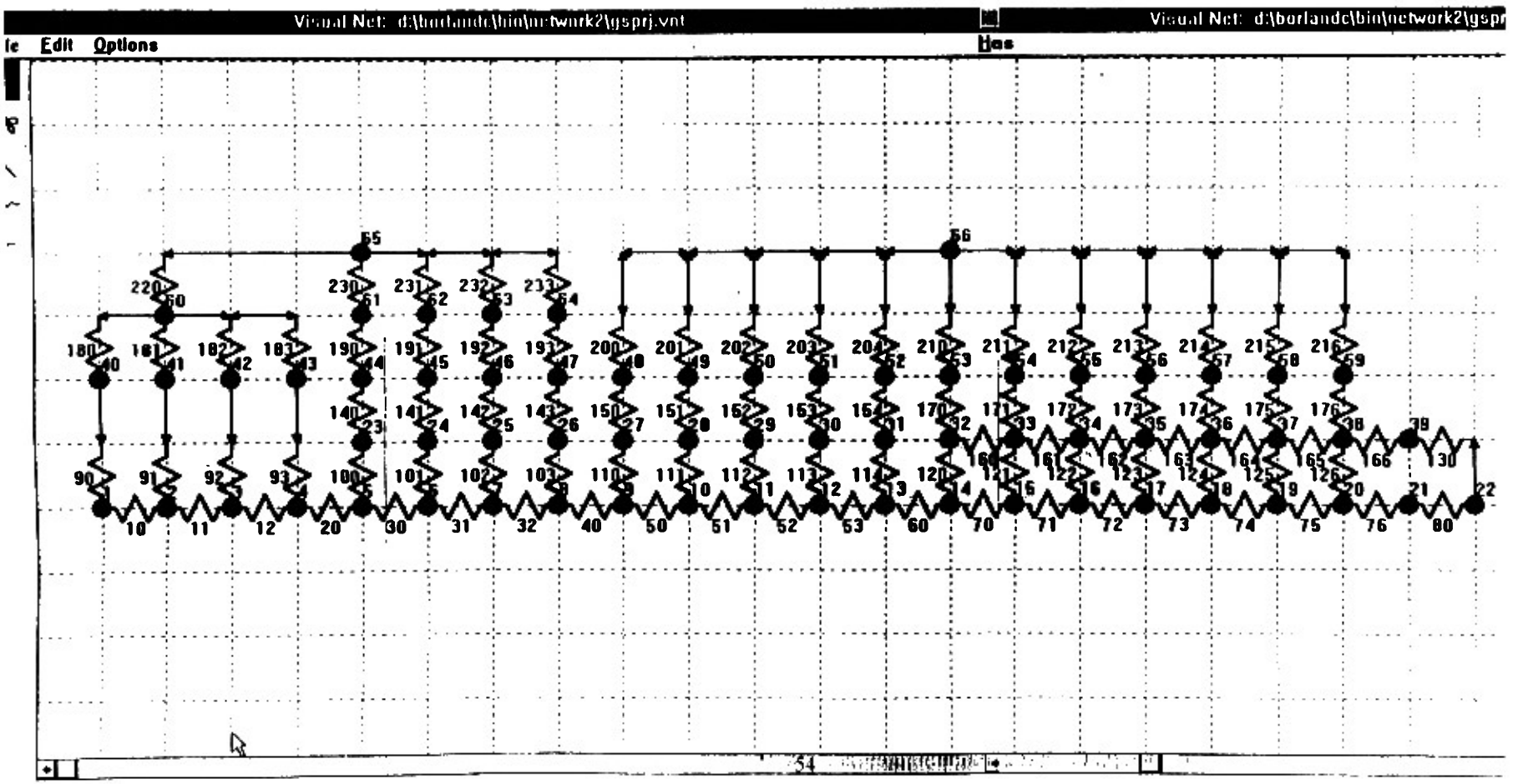

Figure 4.5 VisualNet Node/Resistor Setup

21 which represented the heater surface, node 22 which represented the temperature of the flowing water and resistance 80 which was the combined boiling and convective resistance between the surface(21) and the flowing water (22). Node 39 represented the surface of the Torlon® bushing. Since no boiling occurred on the Torlon® surface, the resistance (130) between it and the flowing water (22) was purely a single phase convective resistance having no boiling component.

4.3.2 Analysis Procedure

In order to accurately calculate the heater surface temperature and heat transfer from the surface to the water, the temperature reading from T7 was entered into node 1 for heater temperature distribution at sub-boiling conditions, and the specified water temperature was entered into node 22. An initial guess for the convective heat transfer coefficient (h) was calculated using Gnielinski's correlation (1976)

$$Nu_D = \frac{(f/8)(\mathrm{Re}_D - 1000)\,\mathrm{Pr}}{1 + 12.7(f/8)^{1/2}(\mathrm{Pr}^{2/3} - 1)} \tag{4.4}$$

where

$$f = (0.79 \ln \mathrm{Re}_D - 1.64)^{-2} \tag{4.5}$$

for a single-phase flow across a flat plate. This h value was then used to calculate resistances 80 and 130. At this point the steady state model was ready for analysis. After running the model, the calculated temperatures for nodes 6, 12, and 18 were compared with the corresponding thermocouple readings T8, T9, and T10. Adjusting resistance 80 by a small increment, a better match of the model temperatures to the thermocouple

readings could be achieved. This process was continued until a satisfactory match was found between the calculated values and the thermocouple readings. Once a suitable match (less then 0.1°C error for each of the three temperature readings) was found for a given flow condition, the single-phase convective resistance was found. For subsequent heater temperature distributions at the same flow conditions the convective resistance was held constant for resistance 130, while resistance 80 was changed to take into account for the effects of additional heat transfer due to the onset of nucleate boiling. An iterative process was again employed to match the calculated node temperatures with the thermocouple readings, this time only changing the value of resistance 80. Appendix C shows a comparison of the actual thermocouple temperature readings and the two ThermoNet models used to approximate the heater surface temperature.

4.4 Determination of Experimental Error

There were several sources of error associated with the experimental setup and the data collection techniques utilized.

- The bulk temperature of the liquid, T_∞, could be controlled within 0.1°C in the constant temperature bath.

- The flow rate and the flow velocity were measured within accuracy of 1 % of the rotameter range which yielded an error of 0.025 GPM.

- The heater surface temperature, obtained from the ThermoNet model was accurate within 0.1°C.

- The thermocouple temperature readings, used in the ThermoNet analysis were accurate within 0.1°C.

- The bubble size visual measurements were accurate within 2 μm as a result of the monitor resolution.

5. THEORETICAL MODEL DEVELOPMENT

The control volume approach for analyzing the forces acting on a departing bubble introduced by Kandlikar and Stumm (1995) was developed for thermally controlled region. It did not account for small, fast growing bubbles in the inertia dominated region. The experiments performed in the present investigation involved subcooled flow boiling of water at near atmospheric pressure, where the influence of the inertia forces on a growing bubble is significant. In order to model this effect, the Kandlikar and Stumm's work was extended further, to include the inertia force.

The inertia force, acting on a truncated bubble attached to a heating surface was approximated as:

$$F_i = V_d \rho_l \frac{d^2 R}{dt^2} \tag{5.1}$$

where V_d is the volume of the vapor bubble and d^2R/dt^2 is the acceleration of the liquid-vapor interface.

The d^2R/dt^2 interface acceleration values were determined from the experimental data. Growth rate curves for bubbles growing from different cavity sizes, under variable fluid velocity, subcooled water temperatures, and heater surface temperatures were obtained. A power law fit

$$R = R_o + \gamma t^m \tag{5.2}$$

was used to capture the bubble growth behavior near the departure from the heated surface ($0.7t_d \leq t \leq t_d$). The interface acceleration was obtained from the second derivative of the bubble growth rate curve given as:

$$\frac{d^2R}{dt^2} = \gamma m(m-1)t_d^{m-2} \tag{5.3}$$

where t_d is the departure time.

5.1 Front Control Volume Analysis

In the z direction (parallel to the flow) the volume of the entire bubble in the front control volume - CV1 (which represents one half of the entire bubble volume) was used.

A force balance in the z direction yields the following relation:

$$F_{\sigma,1,z} + F_{\sigma,2,z} + F_{B,CV1,z} + F_{D,CV1,z} + F_{P,CV1,z} - F_{i,1,z} = \dot{M}_{out,z} - \dot{M}_{in,z} \tag{5.4}$$

All the forces are evaluated in a similar fashion as discussed in section 3, Eq. 3.59 - 3.67.

Figure 5.2 shows the resulting excess pressure relation for the z direction on the front control volume is:

$$\Delta P_{CV1,z} = \frac{\dot{M}_{out,z} - \dot{M}_{in,z} - F_{\sigma,1,z} - F_{\sigma,2,z} - F_{B,CV1,z} + F_{i,1,z}}{A_P} \tag{5.5}$$

In the y direction, the volume used is as shown on Figure 5.1. It is assumed that the work done by the vapor pushing the liquid in the top hemisphere of the bubble, below the horizontal dash line, would be the same as the work done by the vapor in the bottom hemisphere. However, since there is no room for expansion at the bottom, the surface reaction force would act in such a manner that the work done by the adjacent top and bottom hemisphere vapor domes would cancel out. The only portion of the bubble that

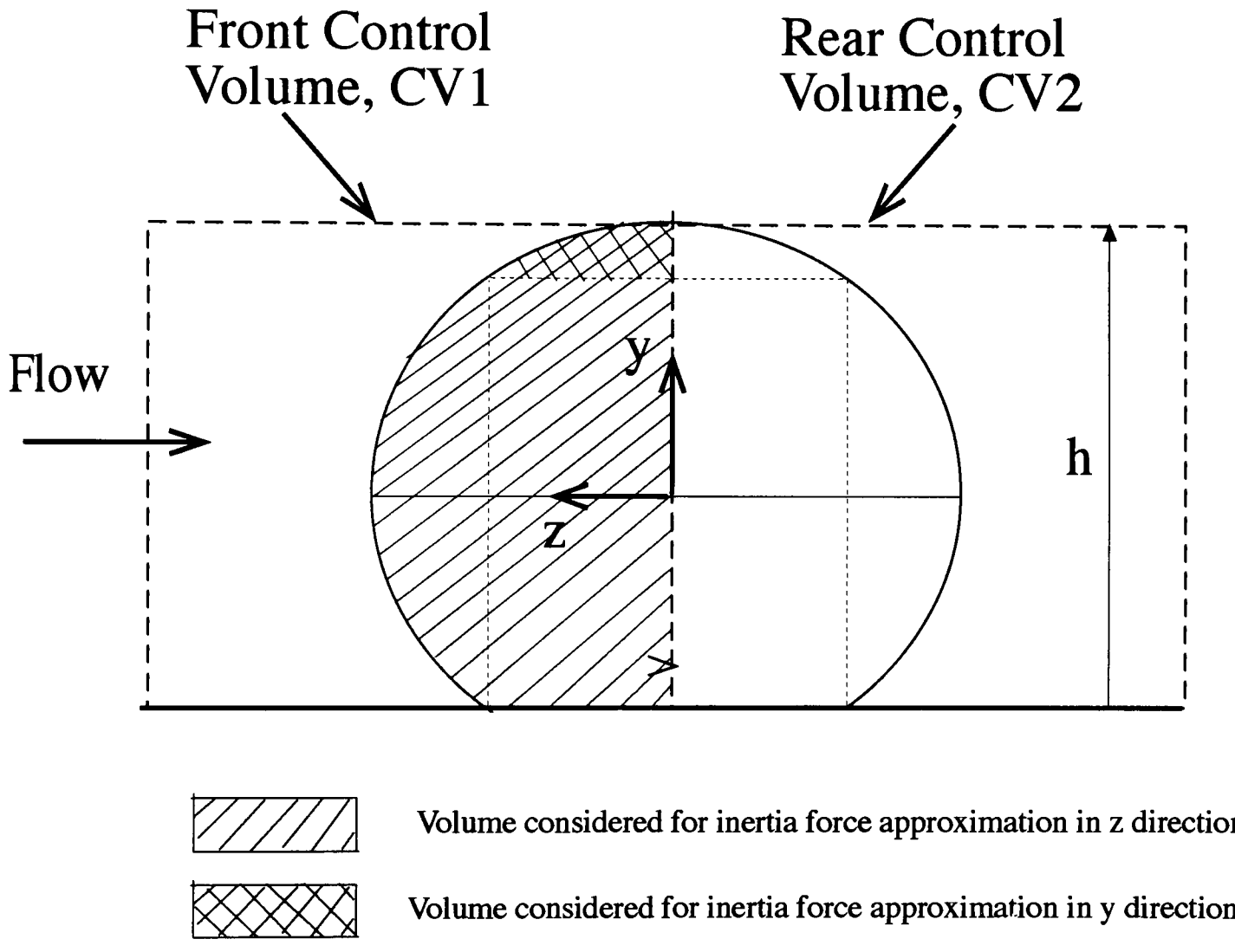

Figure 5.1 Volumes Considered for Inertia Force Approximation in y and z Directions

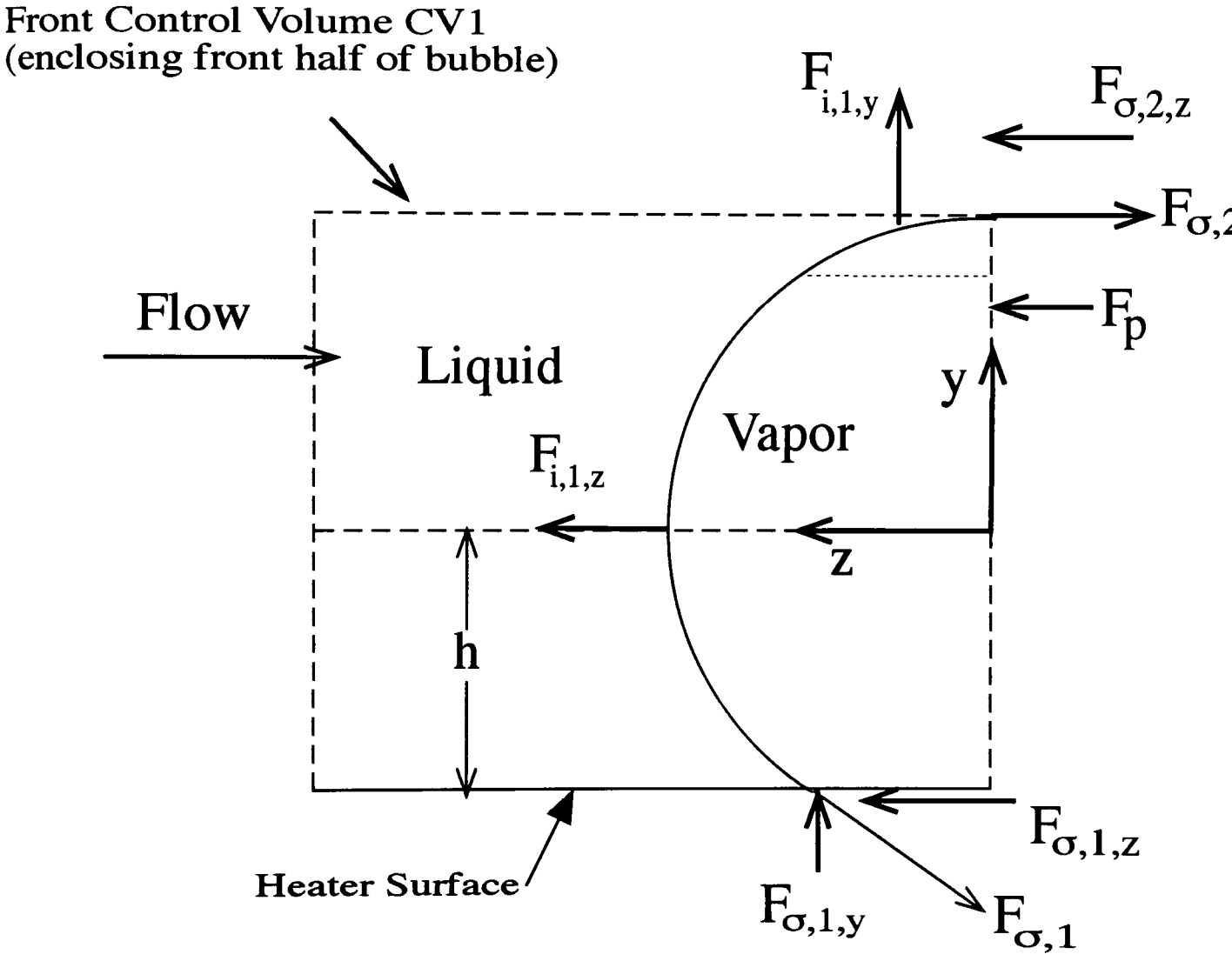

Figure 5.2 Force Balance on Front Control Volume (side view)

would perform "positive" work is the vapor above the horizontal dash line in the top hemisphere of the bubble.

A force balance in the y direction yields the following relation:

$$F_{\sigma,1,y} + F_{\sigma,2,y} + F_{B,CV1,z} - F_{i,1,y} = \dot{M}_{out,y} - \dot{M}_{in,y} \tag{5.6}$$

All the forces are evaluated in a similar fashion as discussed in section 3, Eq. 3.70 - 3.73.

The resulting excess pressure relation for the y direction on the front control volume is:

$$\Delta P_{CV1,y} = \frac{\dot{M}_{out,y} - \dot{M}_{in,y} - F_{\sigma,1,y} - F_{\sigma,2,y} - F_{B,CV1,y} + F_{i,1,y}}{(\pi r_s^2 / 2)} \tag{5.7}$$

5.2 Rear Control Volume Analysis

The rear control analysis was performed similarly, except for the reversed direction of the inertia force F_i in the z direction.

The excess pressure in the y direction was determined using Eq. 5.7 where the only difference were the values of the rate of the momentum going in and out of the rear control volume CV2.

The excess pressure in the z direction was determined by:

$$\Delta P_{CV2,z} = \frac{\dot{M}_{out,z} - \dot{M}_{in,z} - F_{\sigma,1,z} - F_{\sigma,2,z} - F_{B,CV1,z} - F_{i,1,z}}{A_P} \tag{5.8}$$

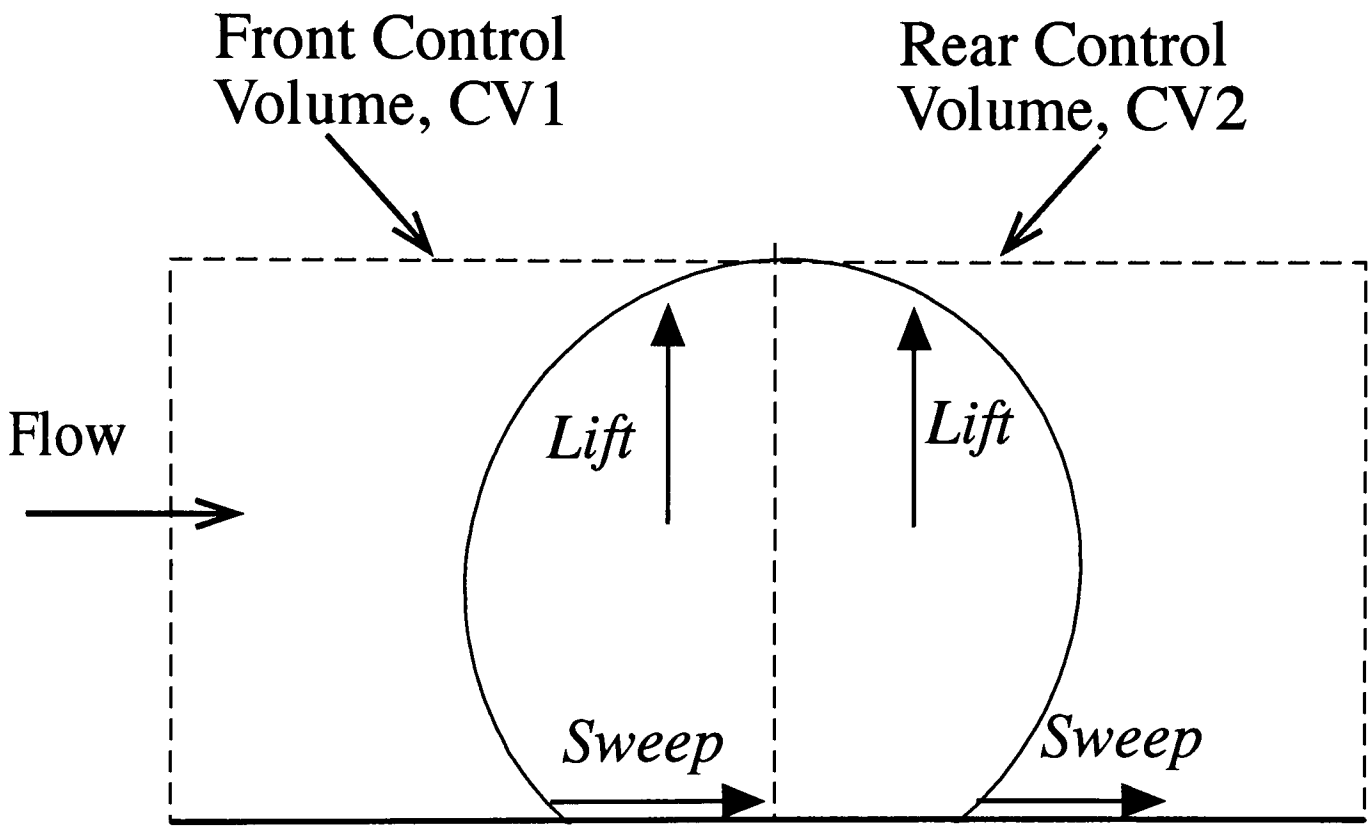

Figure 5.3 Bubble Removal Mechanism

6. COMPUTER PROGRAM FOR THEORETICAL MODEL PREDICTION

In order to quantify the forces acting on each observed bubble at departure, a FORTRAN program was developed. The code is listed in Appendix D with a brief explanation of the task performed by each of its components in the corresponding heading.

One notable feature of the program is the ability to obtain inertia force values for bubbles whose growth can be approximated by either power, logarithmic, or polynomial equations. The power equation of the form

$$\dot{R} = R_o + \gamma t^m \tag{6.1}$$

requires only the values of the γ and m constants as input. A logarithmic equation of the form

$$R = A \ln t \tag{6.2}$$

requires only the values of A as input. A polynomial equation of up to fifth order could be used where only the values of the constants corresponding to the fifth through the second terms are needed.

The information supplied to the code to perform the analysis consisted of: departure radius, flow velocity, front and rear contact angles, fluid density at the interface (evaluated at the mean temperature between the heated surface and the saturation temperature), departure time, type of growth curve fit, and the constants that quantify the fit.

The code output (Appendix E) consists of information about the analyzed bubble (departure radius, flow velocity, front and rear contact angles for easy identification and

match to the corresponding bubble), the values of the estimated excess pressure in y and z directions, and the force values due to surface tension at the control volume interface (F_{s1}), surface tension in y and z directions (F_{s2z}, F_{s2y}), the buoyancy force (F_b), the momentum in y and z direction (Mom_y, Mom_z), and the inertia forces in y and z directions ($Finer_y$, $Finer_z$). The same information was calculated and displayed for both the front an the rear control volumes.

7. EXPERIMENTAL RESULTS AND DISCUSSION

7.1 Experimental Results

The experimental results are presented for the following ranges of parameters: bulk temperature: 60°C to 90°C; Reynolds number: 1267 to 5643; saturation temperature of water: 100°C; and heater surface temperature: 100°C to 120°C.

Before reviewing the experimental data, it would be useful to see the theoretically predicted growth curve for pool boiling case using Mikic and Rohsenow's (1969) model. Figure 7.1 shows one such plot drawn for T_b=80°C, T_w=112.3°C, and a cavity radius r_c=5.53 μm. These conditions are comparable to those employed in the flow boiling experiments.

The growth rate curve shown in Figure 7.1 is based on the bubble radius prediction proposed by Mikic and Rohsenow in Eq. 3.28. The figure indicates that for the stated conditions under pool boiling, a bubble growing on this cavity grows to a size of 130 μm in about 70 μsec. The bubble growth is extremely rapid and in order to visually observe say 10 frames during the bubble growth, a frame rate of 140,000 fps is needed. It may be noted that in pool boiling, nucleation is obtained over much larger cavity sizes which corresponds to a somewhat slower bubble growth. Small cavities of the size used in Figure 7.1 will generally not be activated as they may be covered by larger bubbles. These cavities therefore may not play an important role in pool boiling.

Figure 7.2 presents bubble growth for the same conditions as previously stated (T_b =80°C, T_w = 112.3°C, r_c = 5.53 μm) using two different models for pool boiling proposed

by van Stralen (1975). When the model incorporating the inertia and the heat transfer controlled growth is employed (proposed in Eq 3.45), a bubble growing from this cavity reaches a size of 5000 μm in only 5 msec. For a growth in the inertia region only (proposed by Eq. 3.44), the growth is slower, and a size of 2000 μm is reached in approximately 35 msec. Once again, as in Figure 7.1, an extremely rapid bubble growth occurs, which requires very fast frame rate for visual observation. The same conclusions as the ones drawn for the previous pool boiling model apply here.

In the following paragraphs the bubble growth data obtained in the present investigation under flow boiling conditions is presented.

Figure 7.3 shows the bubble growth curves for r_c=3.23 μm, T_W=80°C, and Re = 1664 for three different wall temperatures of 107.2, 108.3 and 108.7°C. A change of 0.5°C in wall temperature causes significant changes in the bubble growth curves. The growth time reduces from 130 msec to 22 msec, and further down to 5 msec with increasing wall temperatures. Note however that the departure bubble radius remains approximately the same around 40 to 45 μm. This data was obtained using high speed camera at 1000 fps.

With further increase in wall temperature, the growth rate becomes even faster. Figure 7.4 corresponds to the same conditions as for Figure 7.3, except the wall temperature being higher at 109.6 and 110.4°C. The bubble growth time is reduced drastically to about 1.7 and 1.5 msec respectively, while the departure bubble radius became only slightly smaller to about 34 μm. Data in Figure 7.4 was obtained using the

Missing Page

curves are essentially parallel with the one corresponding to the bubble that originated from the larger cavity being shifted up.

The effect of flow rate on bubble growth rate could also be seen on this figure. As the Reynolds number is increased to 5068 (Figure 7.7), smaller cavities of 2.77 and 3.7 μm became active. The growth rates for the bubbles growing over these cavities were much faster. The larger cavity yielded a larger bubble, although the departure bubble sizes were also considerably reduced to 18 and 22 μm respectively.

Figure 7.8 presents two sets of conditions at the same flow rate yielding identical bubble growth rate curves. In the first case, a lower wall superheat combined with larger cavity size yielded the same curve as that for a higher wall superheat with lower cavity size. Again note that the departing bubbles are extremely small, reaching only 12 μm radius.

Effect of flow velocity is seen in Figure 7.9. Here same cavity yields larger bubbles at smaller flow velocities under identical set of conditions; at Re = 2280, departure radius is 27 μm, while at Re = 1267, the departure radius increases to 38 μm. The bubble growth curves in the two cases are very similar, and almost identical in their initial stages.

Figure 7.10 shows a similar plot as Figure 7.9, however here the flow velocities are quite different. At Re = 1568, the bubble growth rate curve is much slower and yields a departure bubble radius of 89 μm. For the case of Re = 5643, the growth rate is much faster with the departure radius being only 15 μm. The cavity radii in the two cases are somewhat different, 5.53 and 5.08 μm respectively, with a difference of 0.7°C in the wall superheat.

Missing Page

7.4 Effect of Subcooling

The effect of Subcooling is quite interesting. At lower bulk temperatures (high subcooling), bubble growth was slow and was essentially in the thermally controlled region due to rapid condensation occurring at the top of the bubble exposed to the bulk flow. With higher bulk temperatures, the bubble growth was rapid, departure bubble radii became smaller, and bubble frequency increased. The bubble growth was so strongly dependent on the bulk temperature that at and above 90°C, no bubble activity could be traced in spite of careful monitoring of the surface temperatures in small steps up to 116° C. It is possible that bubbles smaller than 5 μm are ejected at high speeds (in excess of 6000 bubbles/second) and go undetected with the present imaging capabilities.

7.5 Comparison with Pool Boiling Bubble Growth Rates

The data presented in Figures 7.3-7.10 can be compared with the pool boiling growth rates presented in Figures 7.1 and 7.2. From this comparison, following observations can be made.

(i) The bubble growth rate curves are significantly slowed down with increasing flow velocity under flow boiling.

(ii) The sizes of cavities nucleating in flow boiling are much smaller as compared to pool boiling (compared to data presented by Mikic, Rohsenow and Griffith, 1969).

Missing Page

(i). Sweep-removal initiated at the front edge of the bubble;

(ii). Lift-removal initiated at the front edge of the bubble;

(iii). Sweep-removal initiated at the rear edge of the bubble;

(iv). Lift-removal initiated at the rear edge of the bubble.

Comparison of the excess pressure values displayed in Table 7.1 leads to a conclusion that in the majority of the cases, sweep-removal at the front edge of the bubble is responsible for bubble departure from the heated surface. The equilibrium excess pressure generated inside the bubble can not be supported by the surface tension forces, and the bubble is removed, or "swept", from the surface.

The three cases where lift-off at the front edge of the bubble is responsible for bubble departure correspond to the extremely fast, inertia controlled growth region. The bubbles that depart due to this mechanism reach the departure size extremely fast. (From Figures 7.3 and 7.4 it can be seen that they grow to approximately 33, 33, and 43 μm in 1.5, 1.7, and 5 msec respectively). The values of the inertia forces acting on this bubbles at departure are of the same order of magnitude as the surface tension force (Appendix D). This means that departure in the vertical direction, rather than in the horizontal flow direction occurs under inertia controlled conditions of bubble growth.

On Figure 7.11 the comparison between the estimated (Eq. 5.5 and 5.7) and the actual excess pressure

$$\Delta p_{eq} = \frac{2\sigma}{R} \tag{7.1}$$

is displayed. The average absolute error of the excess pressure estimation was found to be 7.45 %. All the points lie within the ±10 % error band, expect the ones where extremely

fast inertia growth is present. For these fast growing bubbles, the entire bubble growth was captured in 3-5 frames. The error associated in time estimation (time between two consecutive frames) is of the same order of magnitude as the total growth time. This is probably the main reason for a somewhat larger scatter of data points in this region.

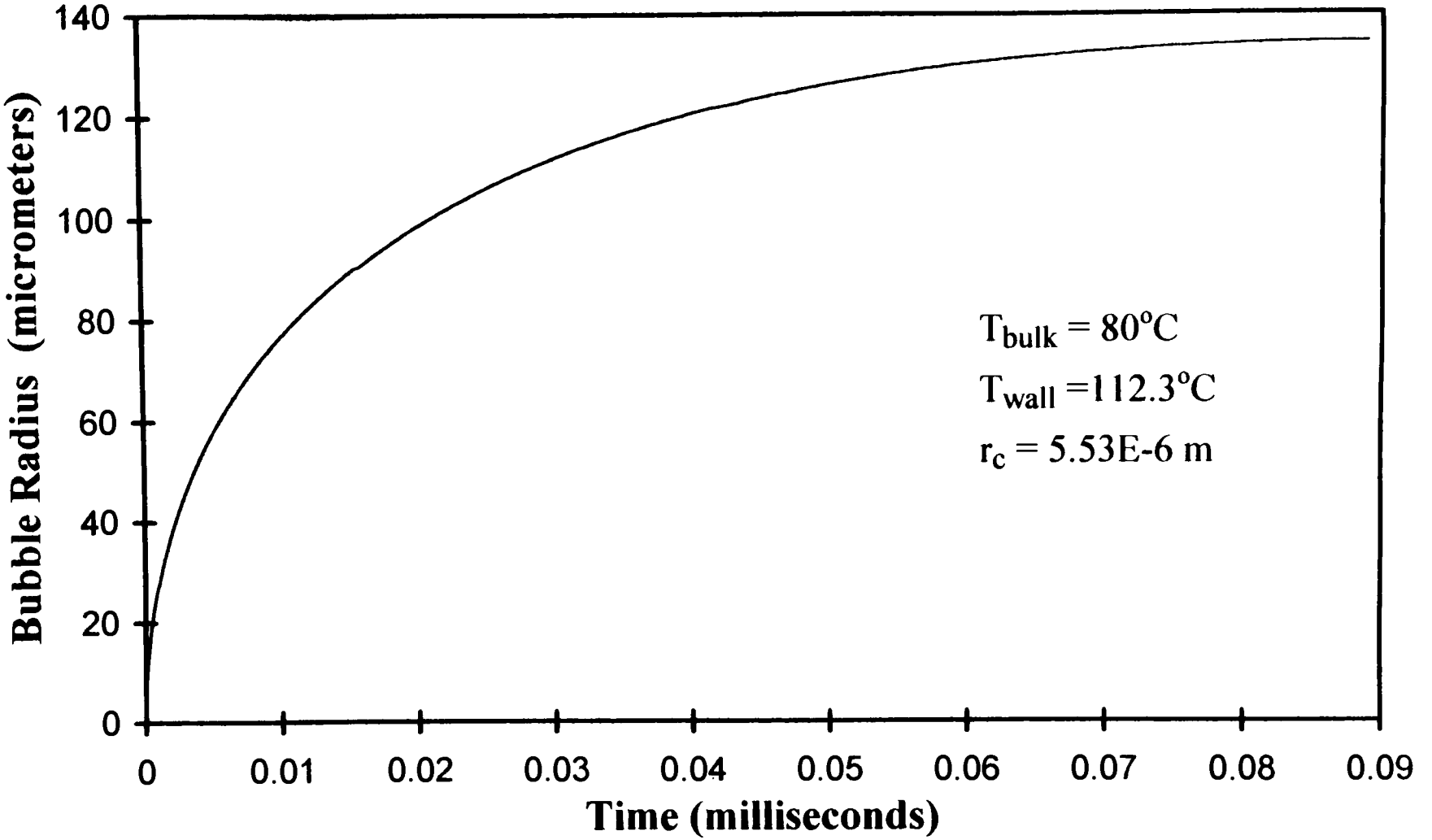

Figure 7.1 Mikic and Rohsenow (1969) Pool Boiling Bubble Growth Model

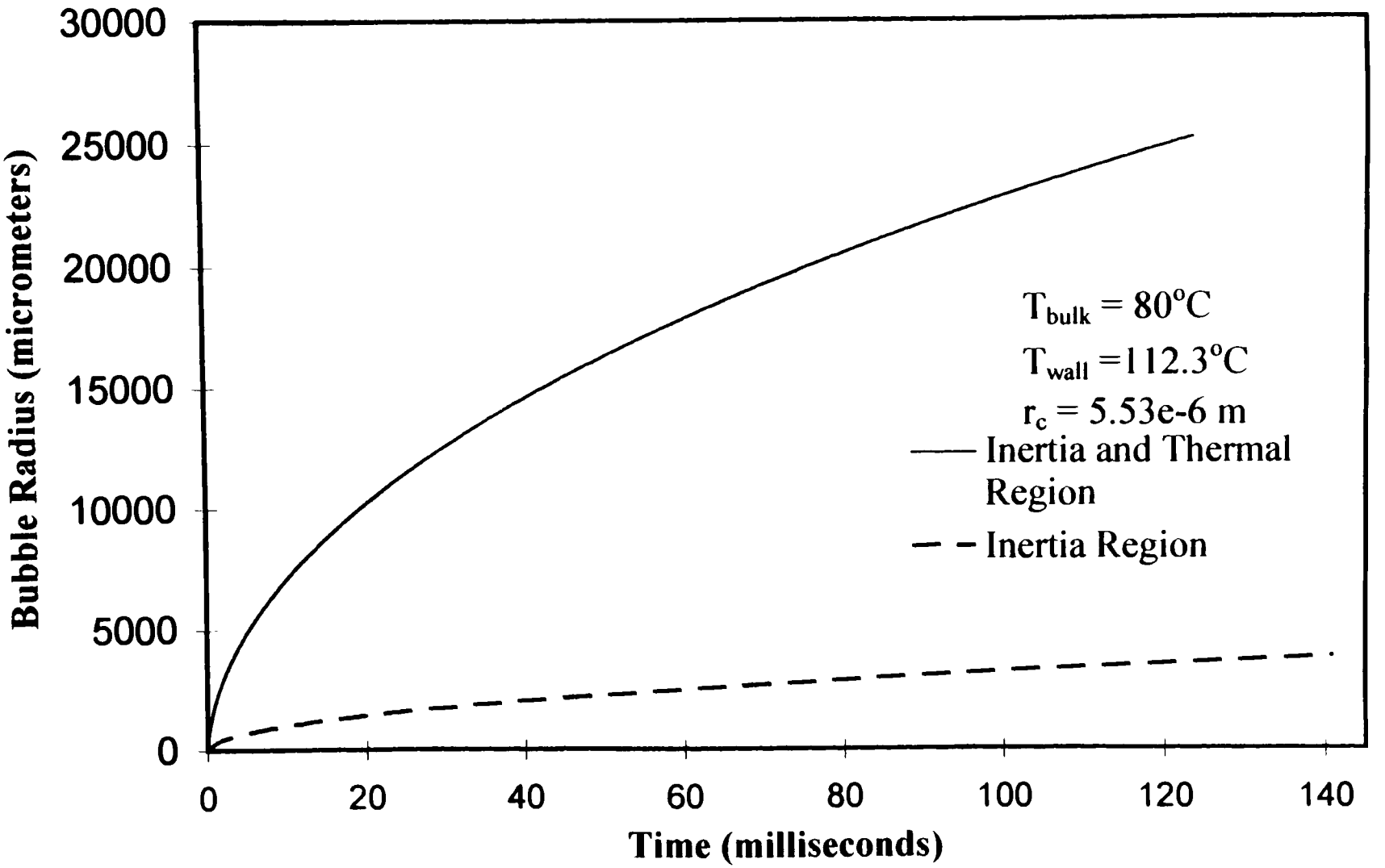

Figure 7.2 van Stralen et al. (1975) Pool Boiling Bubble Growth Model

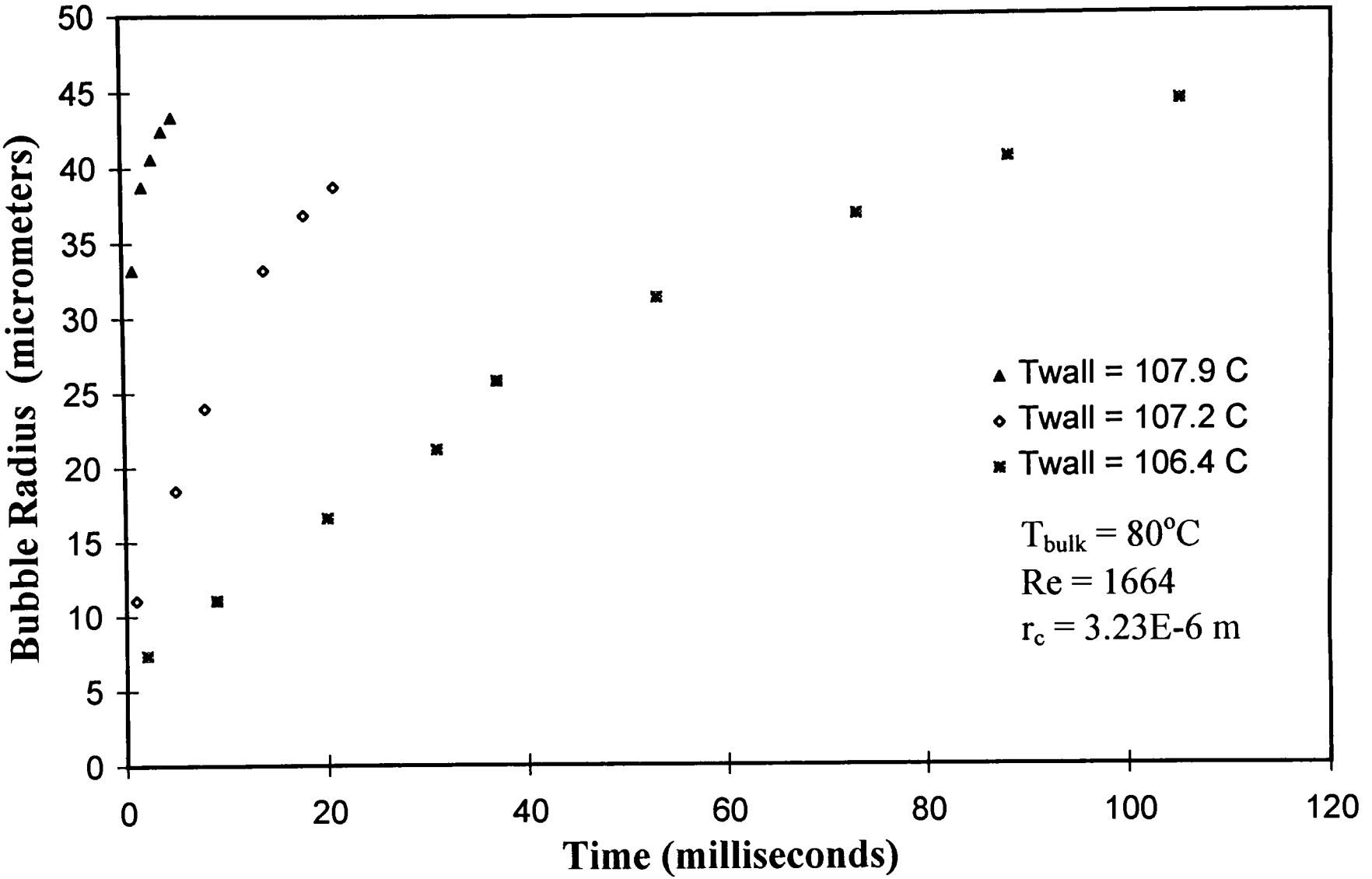

Figure 7.3 Effect of Wall Superheat on Bubble Growth

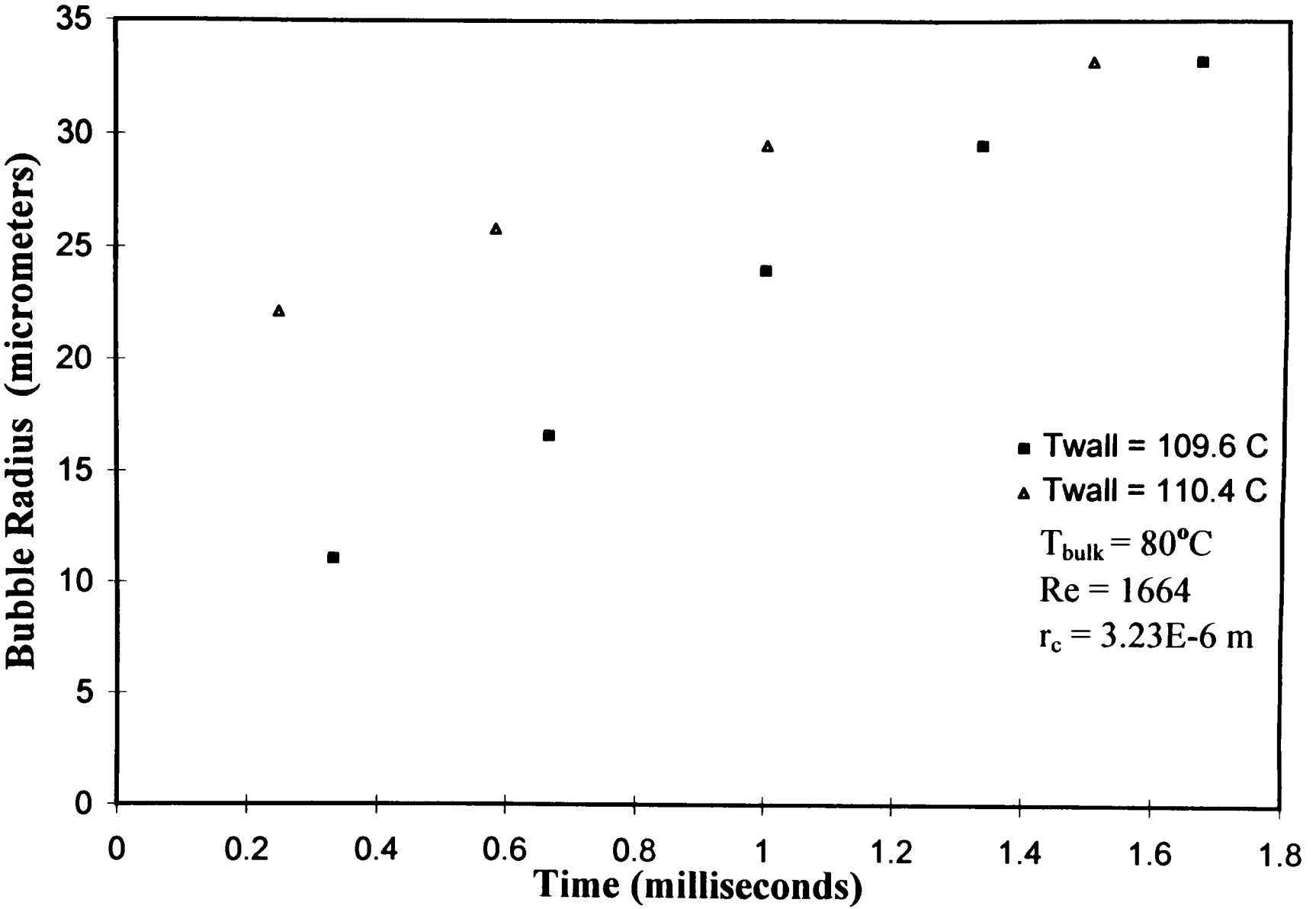

Figure 7.4 Effect of Wall Superheat on Bubble Growth

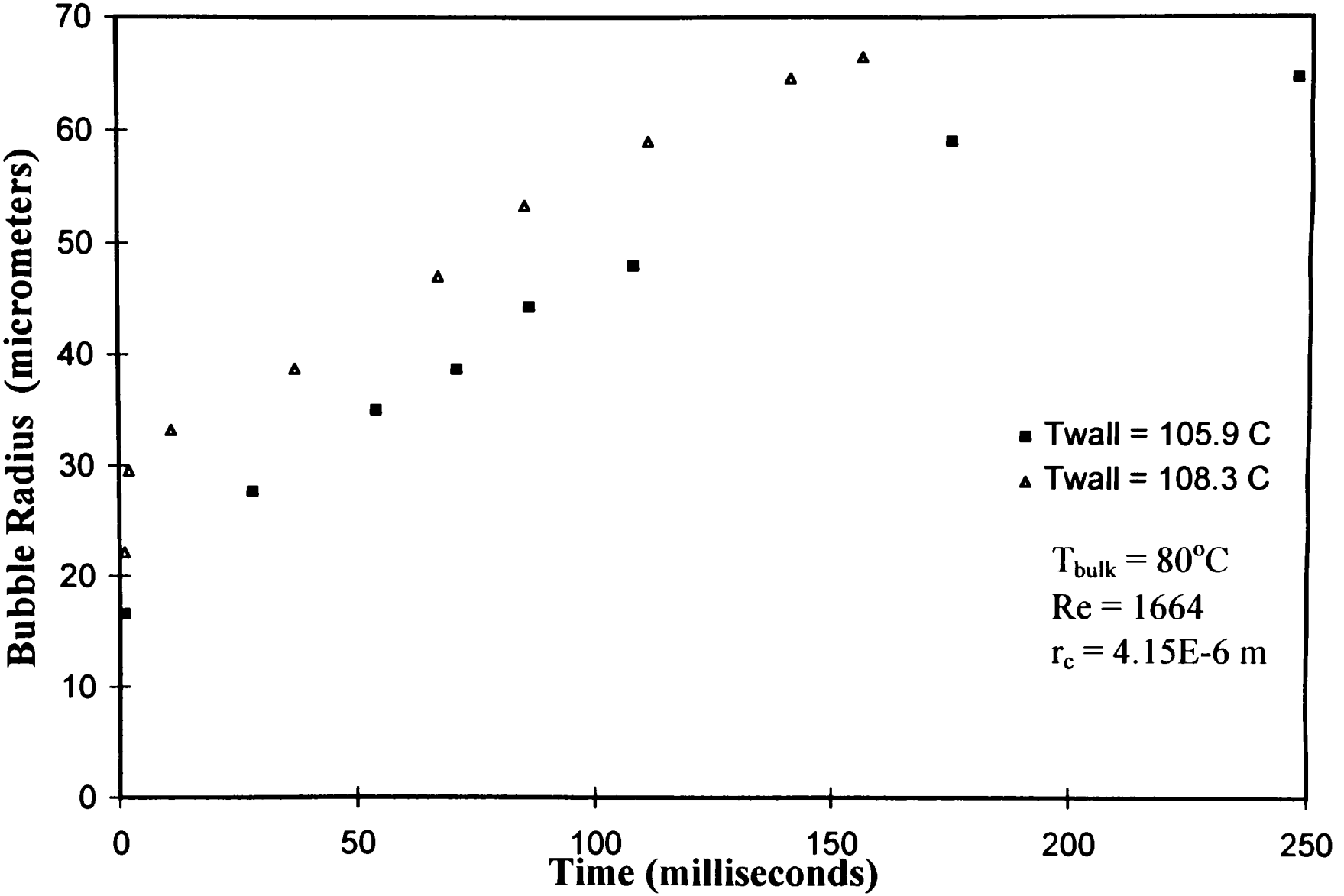

Figure 7.5 Effect of Wall Superheat on Bubble Growth

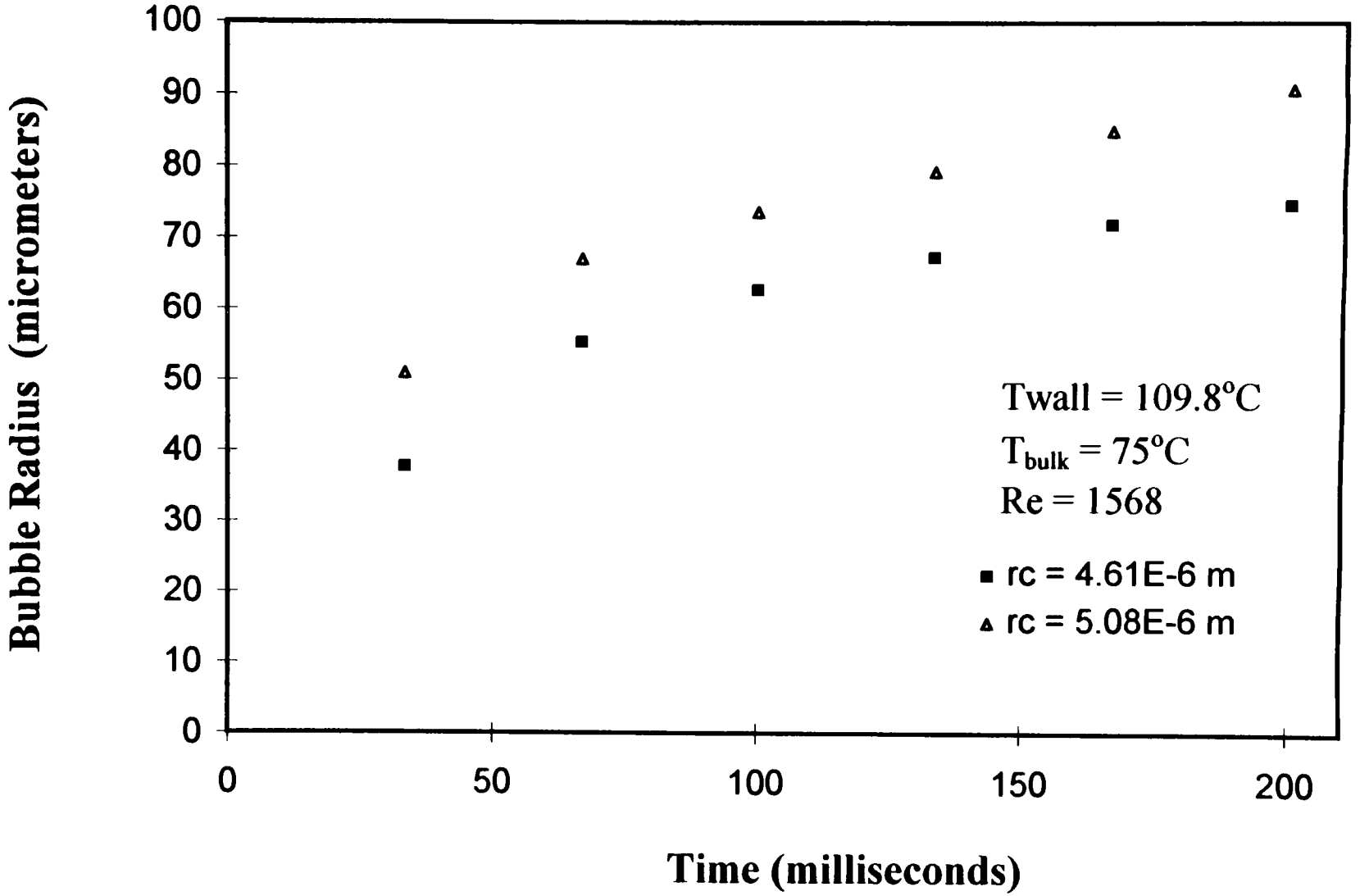

Figure 7.6 Effect of Cavity Size on Bubble Growth

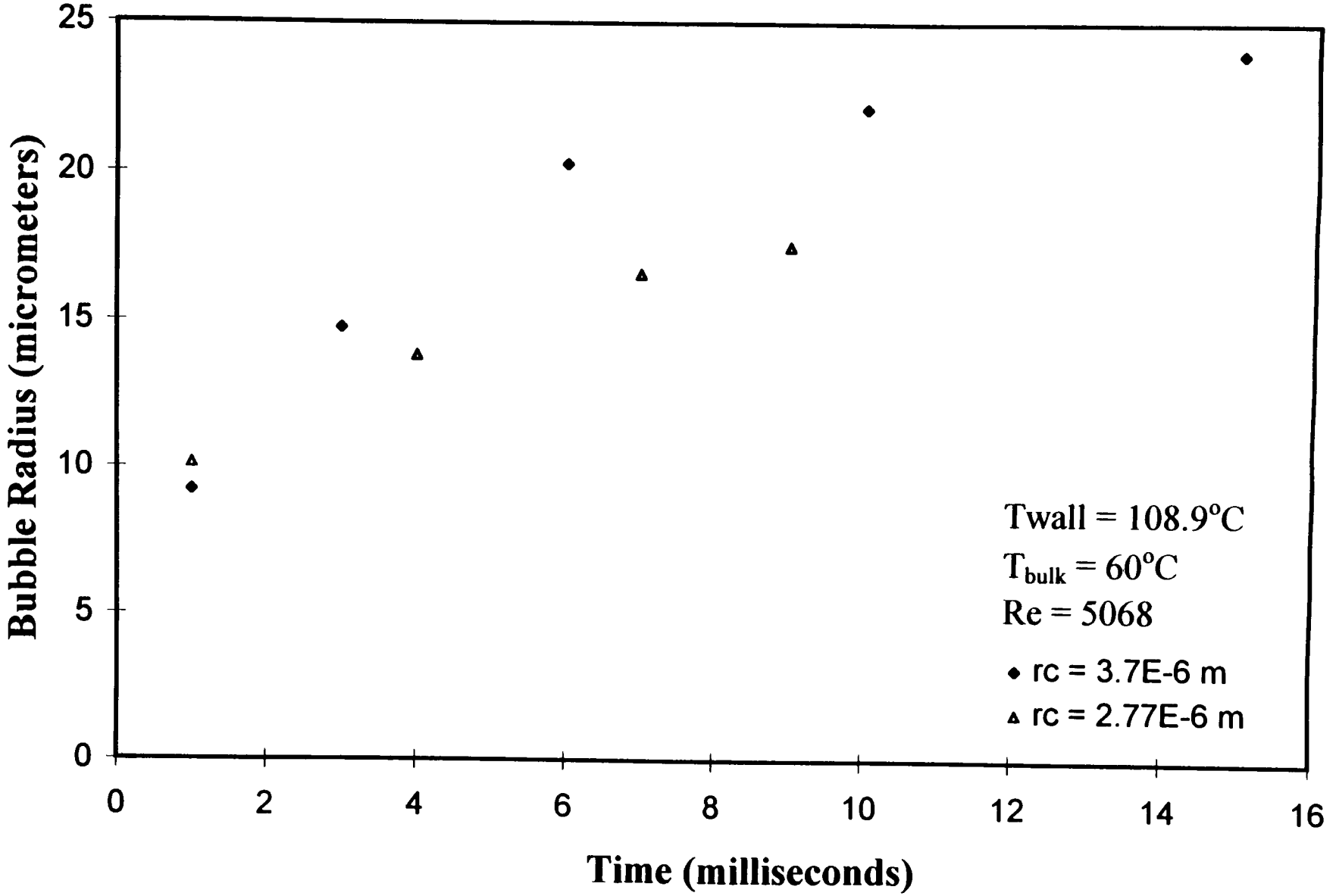

Figure 7.7 Effect of Cavity Size on Bubble Growth

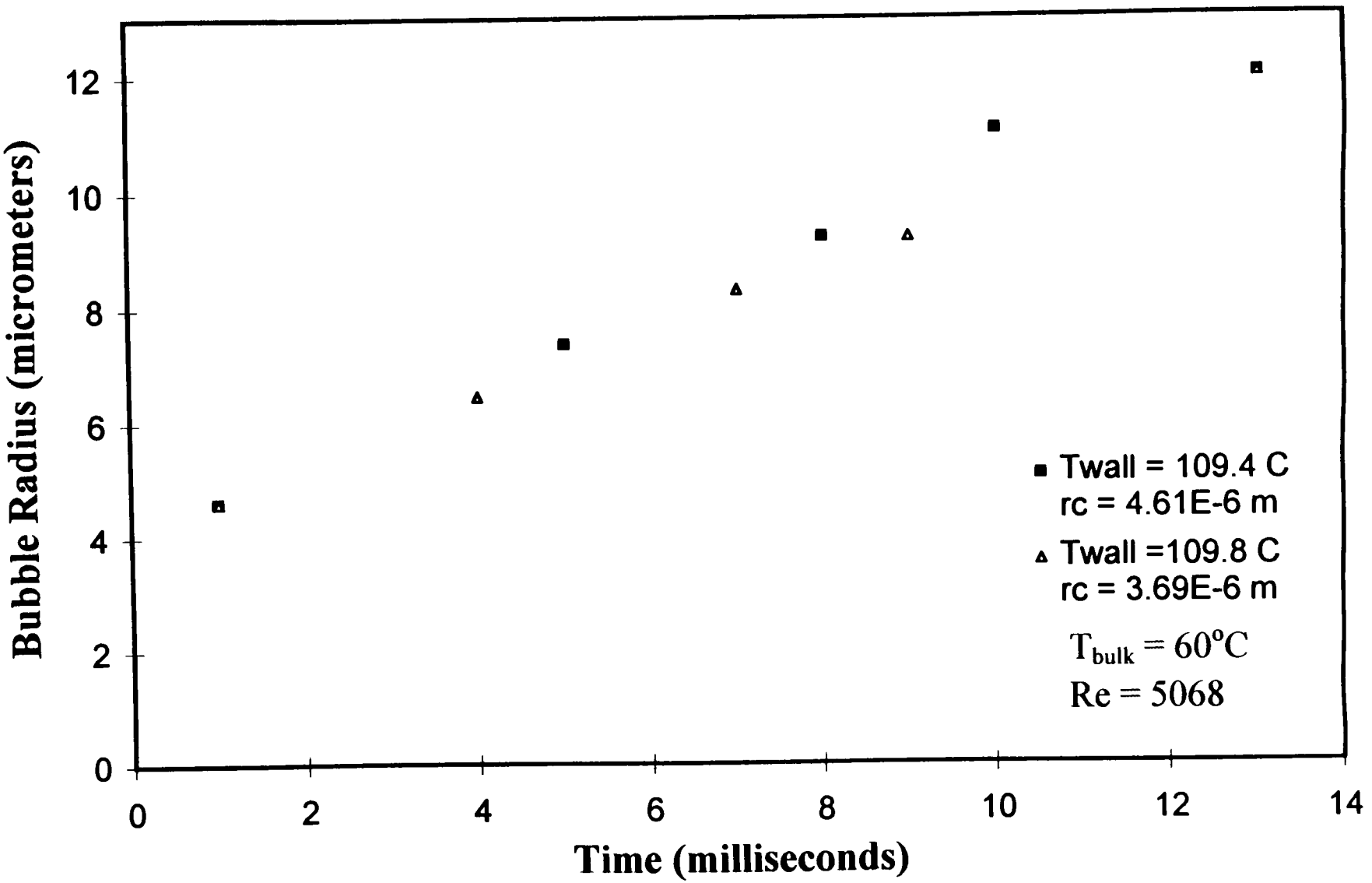

Figure 7.8 Combined Effect of Wall Superheat and Cavity Size on Bubble Growth

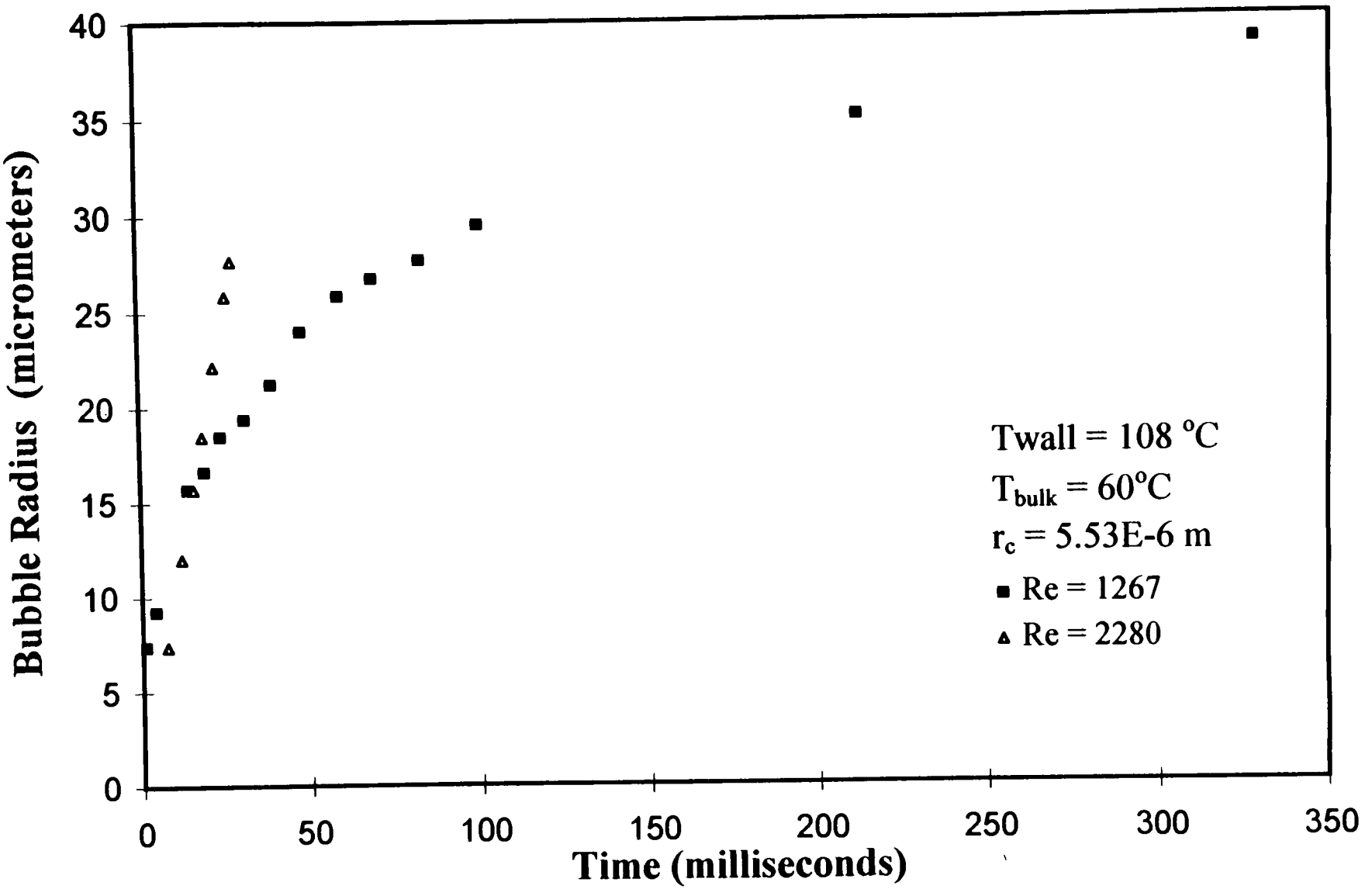

Figure 7.9 Effect of Flow Velocity on Bubble Growth

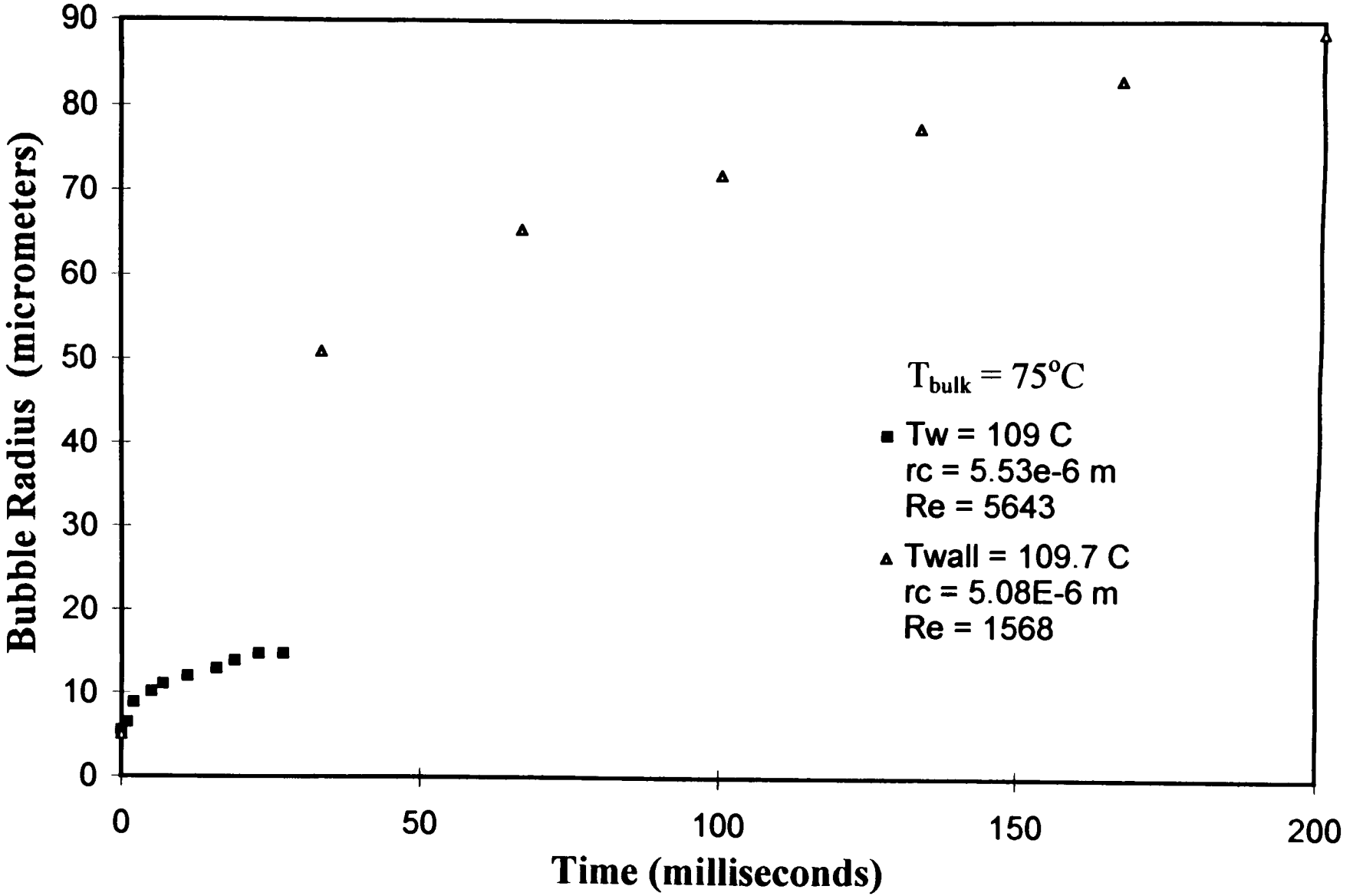

Figure 7.10 Effect of Flow Velocity on Bubble Growth

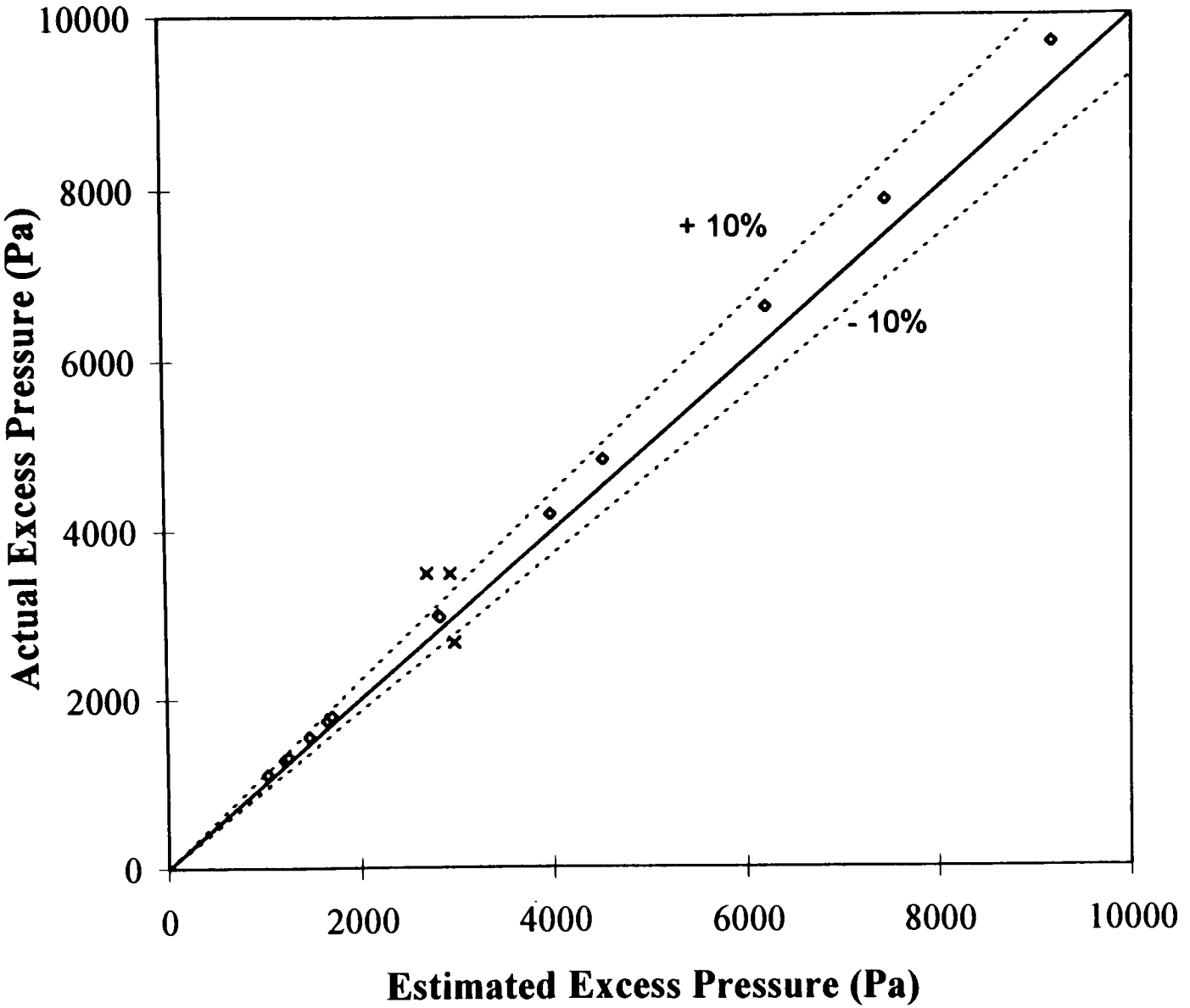

Figure 7.11 Comparison of the Proposed Model with Experimental Data

8. REFERENCES

Al-Hayes, R.A., and Winterton, R.H.S., 1981, "Bubble Diameter on Detachment in Flowing Liquids," *International Journal of Heat and Mass Transfer*, Vol. 24, pp. 223-230.

Bankoff, S.G., 1957, Ebullition from solid surfaces in the absence of pre-existing gaseous phase, *Trans. ASME*, vol. 79, pp. 735-740.

Bergles, A.E, and Rohsenow, W.M., 1964, "The Determination of Forced-Convection Surface Boiling Heat Transfer," Journal of Heat Transfer, Vol. 86, pp. 365-372.

Blasius, H., 1913, "Das Ahnlichkeitsgesetz bei Reibungsvorgangen in Flussigkeiten", Forschg. Arb. Ing.-Wes., 131, Berlin.

Brock, J.R. and Baird, R.B., Surface Tension and the Principle of Corresponding States, *AIChE J.*, vol. 1 pp 174-184, 1955.

Carey, V.P., 1992, Liquid-Vapor Phase Change Phenomen, Taylor & Francis, Bristol, PA.

Clift, R., Grace, J.R. and Weber, M.E., 1978, *Bubbles, Drops and Particles*, Academic Press, New York, p. 33.

Cooper, M.G., and Chandratilleke, T.T., 1981, "Growth of Diffusion-Controlled Vapor Bubbles at a Wall in a Known Temperature Gradient," *International Journal of Heat and Mass Transfer*, Vol. 24, No. 9, pp. 1475-1492.

Cooper, M.G., Mori, K., and Stone, C.R., 1983, "Behavior of Vapor Bubbles Growing at a Wall with Forced Flow," *International Journal of Heat and Mass Transfer*, Vol. 26, No. 10, pp. 1489-1507.

Forster, H.K., and Zuber, N., 1955, Dynamics of vapor bubbles and boiling heat trnafer, *AIChE J.*, vol. 1, pp 531-535.

Hsu, Y.Y., 1962, "On the Size Range of Active Nucleation Cavities on a Heating Surface," Journal of Heat Transfer, Vol. 84, pp. 207-216.

Incropera, F.P., and Dewitt, D.P., 1990, Fundamentals of Heat and Mass Transfer, Third Edition, John Wiley and Sons, New York.

Jasper, J.J., The surface tension of pure liquid components, *J.Phys. Chem. Ref. Data.* vol. 4, pp 841-1010, 1972.

Kandlikar, S.G., 1994, "Measurement of Departure Bubble Diameter and Advancing and Receding Contact Angles in Subcooled Flow Boiling of Water," Paper presented at the joint ASME and ISME Conference, BARC, Bombay.

Kandlikar, S.G., 1992, "Bubble Behavior and Departure Bubble Diameter of Bubbles Generated over Nucleating Cavities in Flow Boiling," Paper presented at the Conference on Pool and External Flow Boiling, Santa Barbara.

Kandlikar, S.G., Mizo, V.R., and Cartwright, M.D., "Investigation of Bubble Departure Mechanism in Flow Boiling using High-speed Photography," Proceedings of International Conference on Convective Flow Boiling, ASME Foundation Conference, Banff, Canada, April 30-May 5.

Kandlikar, S.G., 1990, "A Mechanistic Model for Flow Boiling Heat Transfer," Paper presented at the 1990 ASME Winter Annual Meeting, Dallas, Nov., 1990.

Kandlikar, S.G., 1992,"Bubble Behavior and Departure Bubble Diameter of Bubbles Generated Over Nucleating Cavities in Flow Boiling," Pool and External Flow Boiling, Proceedings of The Engineering Foundation Conference on Pool and External Flow Boiling, March 22-27, ASME.

Kandlikar, S.G., Cartwright, M.D., and Mizo V.C., 1995, "A Photographic Study of Nucleation Characteristics of Cavities in Flow Boiling," Proceedings of International Conference on

Convective Flow Boiling, ASME Foundation Conference, Banff, Canada, April 30-May 5.

Kandlikar, S.G., and Stumm B.J., 1993, "A Control Volume Approach for Investigating Forces on a Departing Bubble under Subcooled Flow Boiling," ASME National Heat Transfer Conference, Colorado Springs. Also accepted for publication in Journal of Heat Transfer.

Kedzierski, M.A., 1993, "Simultaneous Visual and Calorimetric Measurements of R11, R123, and R123/Alkylbenzene Nucleate Flow Boiling," HTD-Vol. 243, Heat Transfer with Alternate Refrigerants, Eds. Sour, H.J., Jr., and Kuehn, T.H., ASME.

Klausner,J.F., Mei, R., Bernhard, D.M., and Zeng, L.Z., 1993, "Vapor Bubble Departure in Forced Convection," International Journal of Heat and Mass Transfer, Vol.36, No.3, pp. 651-662.

Levy, S., 1967, "Forced Convection Subcooled Boiling Prediction of Vapor Volumetric Fraction," *Inetrnational Journal of Heat and Mass Transfer*, Vol. 10, pp. 951-965.

Mikic, B.B., Rohsenow, W.M., abd Griffith, P., 1970, "On Bubble Growth Rates," International Journal of Heat and Mass Transfer, Vol. 13, pp. 667.

Mikic, B.B., and Rohsenow, W.M., 1969, "Bubble Growth Rates in Non-uniform Temperature Field," Progress in Heat and Mass Transfer, Vol. II, pp. 283-293.

Miller, D.G., On the reduced Frost-Kalkwarf vapor pressure equation, *Ind. Eng. Chem. Fundamentals*, vol. 2, pp 78-99, 1963.

Nukiyama, S., 1934, "The Maximum and Minimum Values of Heat q Transmitted from Metal Surface to Boiling Water under Atmospheric Pressure," Journal of Society of Mechanical Engineers (Japan), Vol. 37, pp. 367-374, 553-554.

Plateau. Static experimentale et therorique des Liquides soumis aux seules Forces moleculaires. 1873.

Plesset, M.S., and Zwick, S.A., 1954, The growth of vapor bubbles in superheated liquids, *J.*

Appl. Phys., vol 25, pp. 493-500.

Pohlhausen, E., 1921, Der Warmeaustauch Zwishen Festen Korpern und Flussigkeiten mit kleiner Treibung und Warmeleitung, *Z. Angew. Math. Mech.*, vol 1, pp. 115-121.

Rayleigh, Lord, 1917, On the pressure developed in a liquid during the collapse of a spherical cavity, *Phil. Mag.*, vol. 34, pp. 94-98.

Rodgers, J.T., and Salucha, M., 1987, "Onset of Significant Void in Up-Flow of Water at Low Pressure and Velocity," *International Journal of Heat and Mass Transfer*, Vol. 30, pp. 2247.

Scriven, L.E., 1959, On the dynamics of phase growth, Chem. Eng. Sci., vol. 90, pp. 1-13.

Staub, F.W., 1968, "The Void Fraction in Subcooled Boiling - Prediction of the Initial Point of Net Vapor Generation,"*Journal of Heat Transfer*, Vol. 90, pp. 151-157.

Van Stralen, S.D.J., 1968, "The growth rate of vapor bubbles in superheated pure liquids and binary mixtures," *International Journal of Heat and Mass Transfer*, Vol. 11, pp. 1467-1489.

Van Stralen, S.D.J., Sohar, M.S., Cole, R., Sluyter, W.M, 1975, "Bubble Growth rates in Pure and Binary Systems: Combined Effect of Relaxation and Evaporation Microlayers," *International Journal of Heat and Mass Transfer*, Vol. 18, pp. 453-467.

Zeng, L.Z., Klausner, J.F., Bernhard, D.M., and Mei, R., 1993, "A Unified Model for the Prediction of Bubble Detachment Diameters in Boiling Systems - II Flow Boiling," *International Journal of Heat and Mass Transfer*, Vol. 36, No. 9, pp. 2271-2279.

APPENDIX A

A.1 Surface Tension - Definition and Experimental Results

The fundamental of liquid surfaces is that they tend to contract to the smallest possible area. This tendency is shown in the spherical form of small drops of liquid, in the tension exerted by soap films as they tend to become lass extended, and in many other properties of liquid surfaces. Plateau (1873) had undertaken a prolonged study of the forms assumed by the liquid surfaces, under conditions when the disturbing effect of gravity is absent; he showed that the surfaces always assume a curvature such that, if R_1 and R_2 are the principal radii of curvature at any point,

$$1/R_1 + 1/R_2 = \text{constant.} \qquad (A.1)$$

It is a geometrical fact that surfaces for which the relation (A.1) holds are surfaces of minimum area.

The simplest properties of molecules in liquids suffice to account for this tendency of the surface to contract. Molecules are small objects, possessing definite size and shape, in all states of matter; in all fluids they are free to move relative to one another, and in liquids they are kept close to each other by the cohesion forces between them. Liquids are thus distinguished from solids by their fluidity, that is, the freedom of the molecules to move. They are distinguished from gases by the fact that the attraction between the molecules restrains the motion sufficiently to prevent more than a small portion of the molecules escaping into vapor. Translatory and rotary motions go on within the liquid with considerable freedom.

In the interior each molecule is surrounded by others on every side. Therefore, it is subject to attraction in all directions. On the average, over period of time, long compared to the molecular vibrations, the attraction on any molecule is uniform in all directions. At the surface, however, conditions are entirely different. Molecules at the surface are attracted inwards, and to each side by its neighbors, but there is no outward attraction to balance the inward pull, because there are very few molecules outside. Hence, every surface molecule is subject to a strong inward attraction, perpendicular to the surface.

This inward attraction causes the surface to diminish in area, because the surface molecules are continually moving inwards more rapidly than the others move outwards to take their places. the number of molecules in the surface is therefore continually diminishing and the contraction of the surface continues until the maximum possible number of molecules are in the interior, i.e. until the surface is the smallest possible for a given volume, subject to the external conditions or forces acting on the drop.

The fact that a liquid surface contracts spontaneously shows that there is free energy associated with it, that work must be done to extend the surface. The origin of this work, in terms of the molecules, is that when the surface is extended molecules must be brought from then interior to the surface against the inward attractive forces. Work must be done against these inward attractive forces for each molecule that is brought to the surface. Since the molecules have a definite size, there will always be a definite number of them in the surface. Provided the surface is of the same nature and structure everywhere, the work done in extending it will be definite.

This free energy in the surface is of fundamental importance. A vast number of problems relating to the equilibrium of the surface can be solved without knowing more

than the magnitude of this free energy. In the solution of such problems, a mathematical device is almost invariably employed to simplify the calculations; it is to substitute for the surface free energy a hypothetical tension, acting in all directions parallel to the surface, equal to the free surface energy. This is what is generally known as the *surface tension.* It is always mathematically possible to replace a free energy per unit area of surface by a tension acting parallel to the surface. Such a surface tension has the same dimension as a surface energy (mass/time^2) and it must have the same numerical magnitude.

This substitution of a tension for a free energy per unit area is the converse of the mathematical method of 'virtual work' often used in statics. There the calculations are often simplified by considering the energy changes involved in a slight displacement of the system, adding all together, and finally equating of the energy changes to zero, to obtain the condition of equilibrium. In systems involving liquid surfaces, the equilibrium could be obtained by adding up the changes in surface energy in the various surfaces whose area is altered during displacement. It is, however, simpler to pay no attention to these changes in area directly, but to consider the surfaces which depend solely on the existence of this free surface energy. Surface free energy, due to the inward pull on the molecules on the surface, is the fundamental property of surfaces. Surface tension can be simply taken as its equivalent.

Surface tension values are influenced by two important factors. These two factors are fluid temperature and presence of contaminants.

A.1.1 Influence of Temperature on Surface Tension

The kinetic agitation of the molecules and the tendency of the molecules to fly outwards increases as the temperature rises; consequently the net inward pull may be expected to become less, even if the real cohesion remains unchanged by the temperature. In fact, the surface tension almost invariably decreases with rising temperature, the only known exceptions being with a few substances over a restricted range of temperature. As temperature rises towards the critical, the restraining force on the surface molecules diminishes and vapor pressure increases: when the critical temperature is met the surface tension vanishes all together. "Negative surface tension" is impossible for a liquid: it would only occur when the liquid temperature rises above its critical temperature, where the liquid can not exist.

The temperature dependency of surface tension is often the basis for interpolation schemes and curve-fit equations used to predict the variation of surface tension with temperature. For example, the surface tension of water can be computed from the correlation:

$$\sigma = 235.8(1-T_{sat}/T_c)^{1.256}[1-0.625(1- T_{sat}/T_c)] \qquad (A.2)$$

where both T_{sat} and T_c are in Kelvin and σ is in millinewtons per meter.

In the case of most liquids the relationship between surface tension and temperature is nearly linear. Jasper (1972) fit a linear relationship of the form

$$\sigma = C_0 - C_1T \qquad (A.3)$$

to surface tension data for a wide variety of pure liquids over a given temperature range, where T is in degree Celsius. Table 1 (Carey 1992) lists the constants C_0 and C_1 for a

variety of different liquids. Figure A.1 shows the variation of surface tension with temperature based on equations (A.2) and (A.3) in the temperature range of 0-100°C.

Substance	Constants for Eq. (2.57) C_0 (mN/m)	C_1 (mN/m °C)	Temperature range (°C)	Reidel parameter
Acetone	26.26	0.112	25 to 50	7.30
Acetylene	3.42	0.1935	−90 to −50	
Argon	−34.28	0.2493	−189 to −181	
Butane	14.87	0.1206	−70 to 20	
n-Butyl alcohol	27.18	0.08983	10 to 100	8.91
Carbon tetrachloride	29.49	0.1224	15 to 105	6.75
Chlorine	19.87	0.1897	−80 to −30	
Ethyl alcohol	24.05	0.0832	10 to 70	8.98
Ethylene glycol	50.21	0.089	20 to 140	
Flourine	−16.10	0.1646	−202 to −188	
Heptane	22.10	0.0980	10 to 90	
Hydrazine	72.41	0.2407	15 to 40	
Hydrogen				4.74
Hydrogen peroxide	78.97	0.1549	2 to 20	
Isopropyl alcohol	22.90	0.0789	10 to 80	
Mercury	490.6	0.2049	5 to 200	
Methyl alcohol	24.00	0.0773	10 to 60	8.48
Nitrogen	−26.42	0.2265	−195 to −183	5.98
Octane	23.52	0.09509	10 to 120	
Oxygen	−33.72	0.2561	−202 to −184	5.92
Propane	9.22	0.0874	−90 to 10	
Sulfur dioxide	26.58	0.1948	−50 to 10	
Water	75.83	0.1477	10 to 100	7.39

Table A1. Constants for the linear surface tension relation proposed by Jasper and the values of the Reidel parameter for various substances (Carey 1992)

Based on the principles of corresponding states, Brock and Bird (1955) developed the following relation for estimating the surface tension of non polar liquids:

$$\sigma = P_c^{2/3} T_c^{1/3} (0.133 R_c - 0.281)[1 - T/T_c)]^{11/9} \qquad (A.4)$$

where R_c is the Reidel (1954) parameter, defined as:

$$R_c = \{d[\ln P_{sat}(T)]/d(\ln T)\}_{T=Tc} \qquad (A.5)$$

Values of R_c for various substances have been tabulated by Miller (1963) and some are listed in Table A.1. Miller also proposed the following relationship for R_c:

$$R_c = 0.9076[1+(T_b/T_c)\ln P_c]/[1-(T_b/T_c)] \quad (A.6)$$

where T_b is the normal boiling temperature of the liquid (at atmospheric pressure).

Using Eqs. A.4 and A.6 together, it is possible to estimate the variation of surface tension with temperature from critical data and the normal boiling point. This method works good for a wide variety of simple organic compounds, but is not intended for light molecules, highly polar inorganic substances, or associated substances such as alcohols and liquid metals.

A.1.2 Effects of Contamination on Surface Tension

The second major factor affecting surface tension is the presence of one or more substances dissolved in the fluid. From thermodynamic analysis of the liquid-vapor interfacial region for a binary mixture, in which A is a solute exhibiting ideal mixture behavior in solvent B, it can be shown that the surface excess mass of species A is related to the variation of σ with concentration as

$$\Gamma_A = - (x_A/RT)(\partial\sigma/\partial x_A)_T \quad (A.7)$$

In this equation, x_A is the concentration of the solute species A.

Some surface-active materials are so highly enriched at the interface that they are termed surface agent or surfactants. Since they concentrate so highly at the interface, the presence of material of this type even in very low concentrations may significantly alter the interfacial tension.

Equation A.7 may also be interpreted in a converse manner, such that A accumulates at the interface, so that $\Gamma_A > 0$; then $(\partial\sigma/\partial x_A)$ is negative and the presence of

the surface-active material decreases the surface tension. This is the case with a typical soap solution added to water. Because water is highly polar, polar molecules are readily accepted into its structure and nonpolar compound such as hydrocarbon chains, are not.

With this observation, at least quantitatively, the effects of soap molecules on the surface tension of water can be interpreted. Typical soap molecules have both a hydrocarbon chain as well as polar group, as indicated in Figure A.2. Since water attracts polar groups and repels hydrocarbon chains, the system would clearly prefer the situation where the polar group is in contact with the water and the hydrocarbon end is facing away from the water as depicted in Figure A.2. The preferred configuration shown in Figure A.2 can be achieved if the soap molecules form a monolayer at the water and vapor interface. The soap molecules will generally concentrate at the interface. In this case Eq. A.7 would imply that the interfacial tension will be decreased.

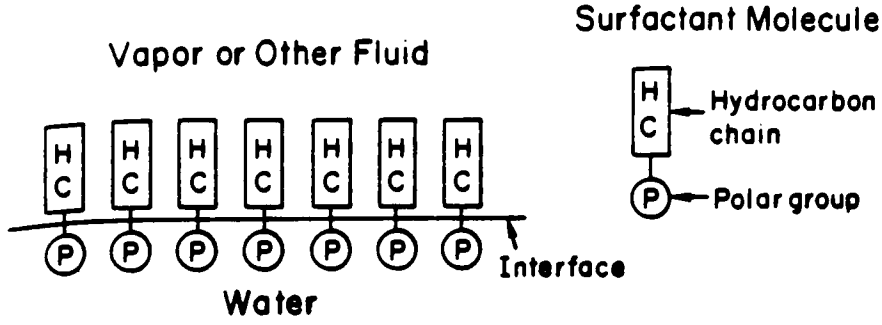

Figure A.2. Orientation of surface molecules at the interface between water and another non-polar fluid

Because so many substances can act as surfactant in water, and because only a minute amount of them can form a monolayer at the interface, it is very easy for the surface tension of water to be altered by only small traces of contaminants.

A.1.3 Classification of the methods of measuring surface tension:

Surface tension measurement techniques can be classified into two categories: static and dynamic methods. The static method measures the tension of practically stationary surfaces which have been formed for an appreciable time, and depend on one of two principles. The most accurate depend on pressure difference set up on the two sides of a curved surface possessing surface tension; these include the capillary height method with its many variations, the maximum bubble pressure method, the drop-volume method, and the method of sessile drop.

A.1.3.1 Static Methods -Capillary height Method

Capillarity occurs when a free surface of liquid in a small tubes or porous media will rise or fall satisfying the Young-Laplace equation:

$$P_{II} = P_{inside} - P_{outside} = 2\sigma/r \qquad (A.8)$$

Consider a small tube of radius r_i shown in Figure A.3. The tube contains liquid with a free surface, and is in contact with an extensive pool of liquid. The liquid is assumed to meet the wall at an angle $\theta < 90°$. When $r_i << L_c$, where L_c is defined as follows,

$$[2\sigma(1 - \sin\theta)/((\rho_l - \rho_v)g)]^{1/2} \qquad (A.9)$$

and the radius of curvature of For small radius of curvature in the meniscus, the Young-Laplace equation requires large jumps in pressure across the interface. This difference supports a large column of liquid against gravity.

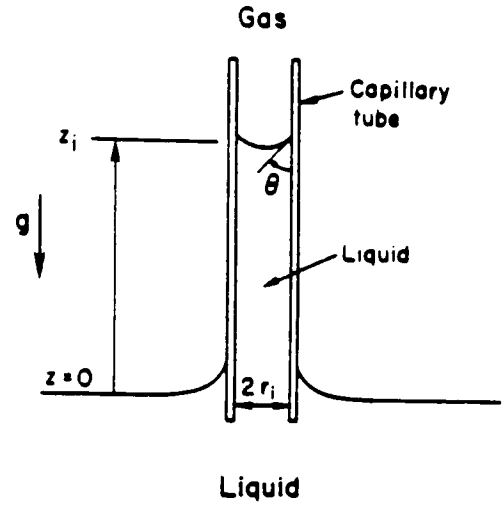

Figure A.3. Rise of a wetting liquid in a capillary tube

Combining the Young -Laplace equation with the hydrostatic pressure variance in the fluid, the condition for equilibrium is:

$$P_I - P_{II} = (\rho_l - \rho_v)gz_i = 2\sigma \cos\theta/r_i \qquad (A.10)$$

This equation can be solved for the equilibrium height of the liquid column, z_i:

$$z_i = 2\sigma \cos\theta/(\rho_l - \rho_v)gr_i \qquad (A.11)$$

or the surface tension, σ :

$$\sigma = r_i z_i(\rho_l - \rho_v)g/2 \cos\theta \qquad (A.12)$$

Knowing this, the surface tension of a liquid can be easily determined using basic experimental methods. In this case a piece of glass tube, container of water and an accurate measurement scale is all that was needed to make accurate readings of the surface tension. Depending on the accuracy of the measurements, the value for surface tension can be found within 1 to 5% of the actual value.

- Apparatus and Procedure

The equipment used to perform this method was quite simple and consisted of a 3.810 mm diameter glass tube, an accurate scale, and a water container. A constant temperature bath was used to increase the water temperature up to 70°C. The height of the meniscus in the tube, and the angle of contact were measured and using equation (A.12) the surface temperature of the water was determined.

- Results

The obtained surface tension values corresponding to the respective temperatures were plotted on Figure A.1. A very good fit with the actual correlation was obtained, with the majority of the points falling in the +/- 5% accuracy bend.

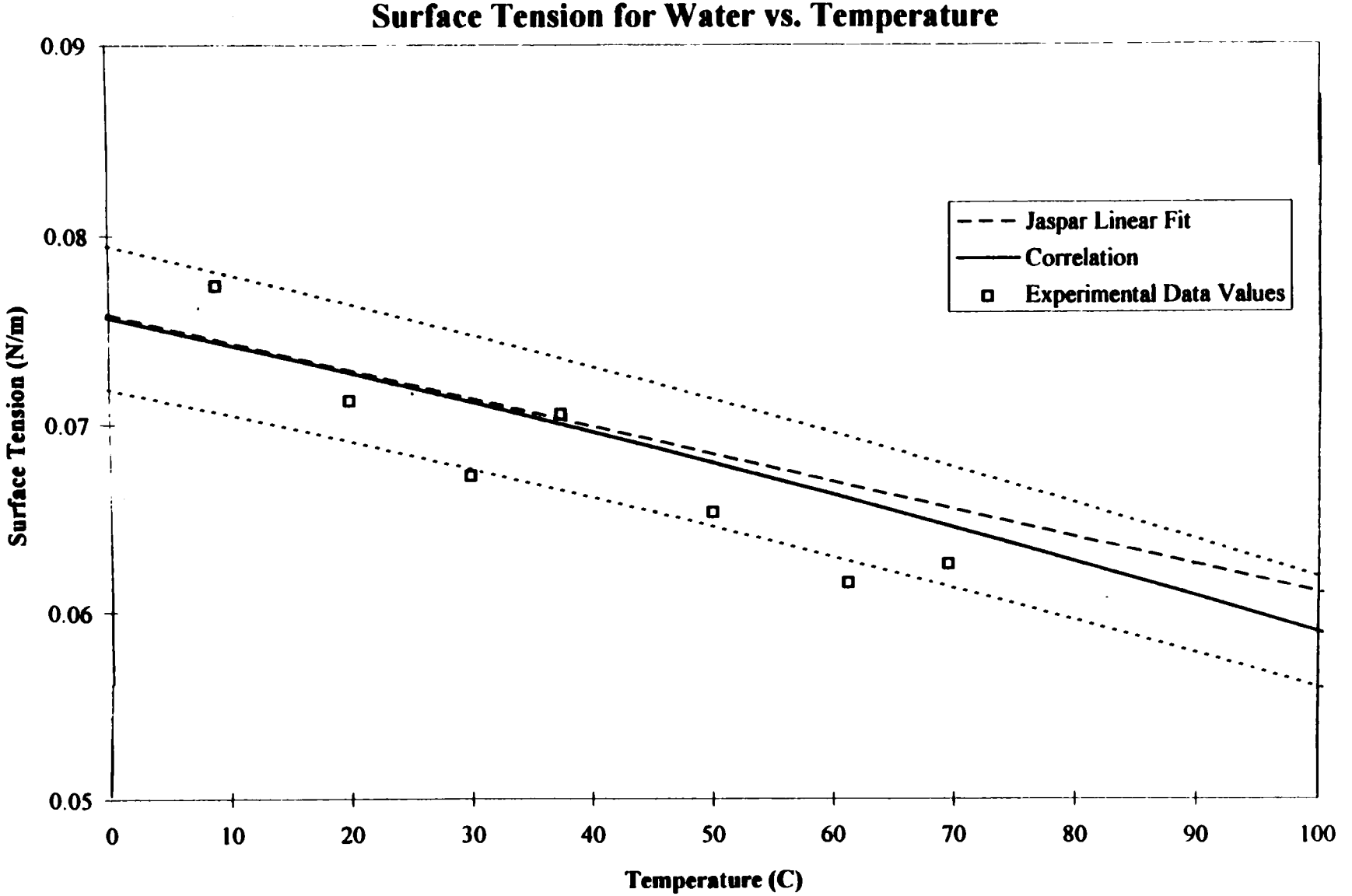

Figure A.1 Surface Tension Experimental Data Results

APPENDIX B
Fortran Input File

```
34.427e-6
.211
55
55
955
1.5e-3
'pow'
29.535
0.378
0
0
33.27e-6
.211
55
55
955
1.677e-3
'pow'
23.473
0.7049
0
0
43.38e-6
.211
55
55
955
5e-3
'pow'
35.496
0.1258
0
0
38.76e-6
.211
55
55
985
21e-3
'pow'
12.091
```

0.384
0
0
105e-6
0.211
55
55
955
47.99e-3
'pow'
7.9655
0.3838
0
0
66.45e-6
0.211
55
55
955
156e-3
'pow'
10.513
0.366
0
0
64.608e-6
0.211
55
55
955
247e-3
'pow'
8.5947
0.3687
0
0
90.7e-6
0.211
55
55
955
200e-3
'pow'
18.567
0.2983

0
0
74.8e-6
0.211
55
55
955
200e-3
'pow'
19.199
0.2572
0
0
23.997e-6
0.844
55
55
955
15e-3
'pow'
14.634
0.1818
0
0
17.54e-6
0.644
55
55
955
9e-3
'pow'
9.2039
0.2972
0
0
11.998e-6
0.844
55
55
955
13e-3
'pow'
3.1115
0.5338
0

0
11.998e-6
0.844
55
55
955
13e-3
'pow'
2.5265
0.6028
0
0
39e-6
0.211
55
55
955
350e-3
'pow'
6.4328
0.3595
0
0
27.69e-6
0.3798
55
55
955
57e-3
'pow'
10.493
0.2249
0
0
88.6e-6
0.7596
55
55
955
200e-3
'pow'
18.135
0.2983
0
0

14.77e-6
0.7596
55
55
955
27e-3
'pow'
6.2628
0.2661
0
0

Temperature Distribution
Actual Data vs. Thermonet Model

APPENDIX C
Temperature Distribution
Actual Data vs. ThermoNet Model

Velocity	10%
Temperature	70C

	Position UP Along Heater (mm)	Actual Data (C)	T-Net (C)	Difference
T7	0.00	144.40	144.40	0.00
T8	15.20	130.20	130.25	0.04
T9	30.40	115.90	115.91	0.01
T10	40.60	106.40	106.40	0.00
Tsurf *	45.20	103.30	102.44	0.84

* ⟶ Tsurf for "Actual" is a predicted value from the original 9-node T-Net model. Therefore, the new T-Net value is more accurate.

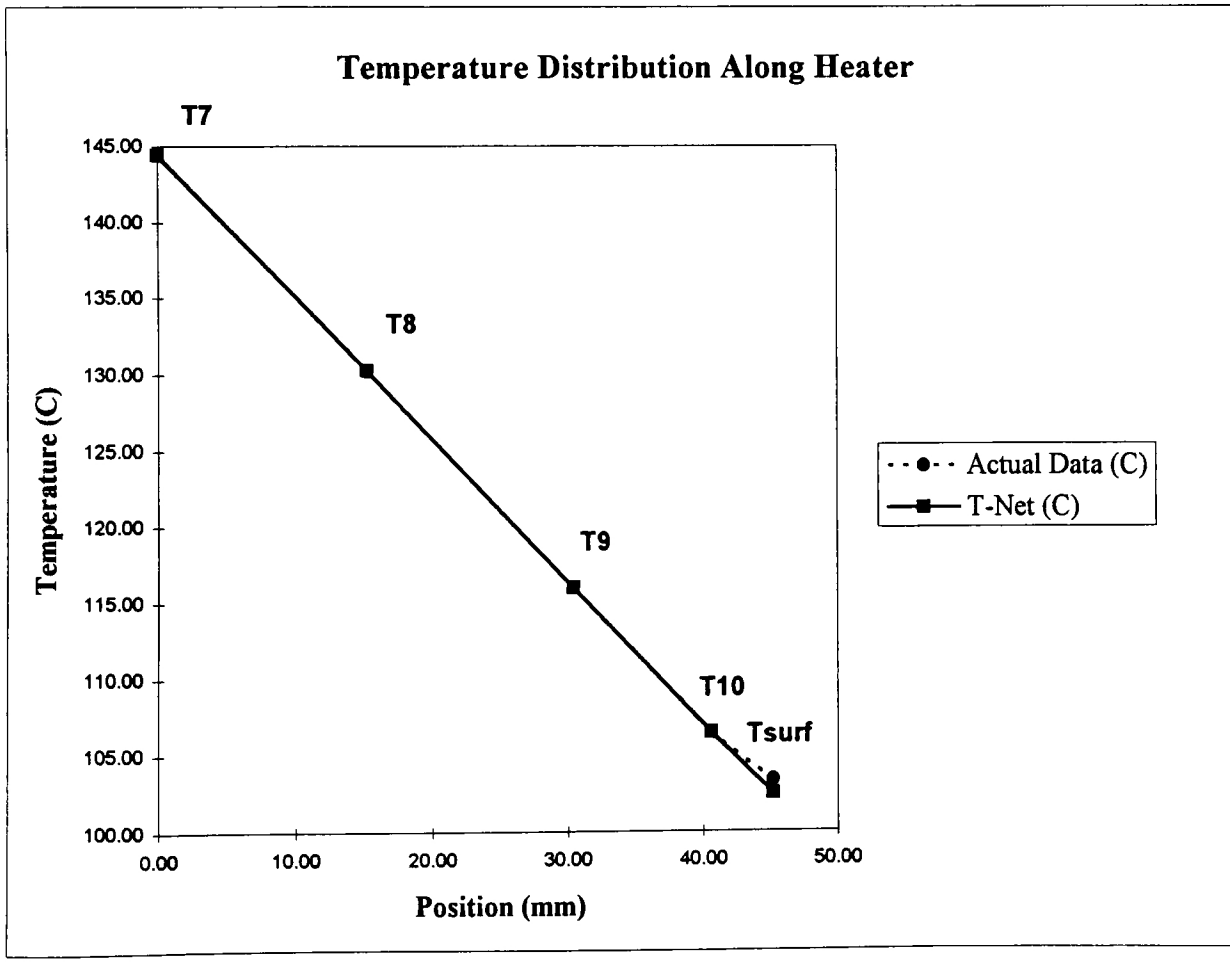

Temperature Distribution
Actual Data vs. Thermonet Model

Velocity	30%
Temperature	60C

	Position UP Along Heater (mm)	Actual Data (C)	T-Net (C)	Difference
T7	0.00	185.20	185.20	0.00
T8	15.20	157.20	157.05	0.15
T9	30.40	128.40	128.41	0.01
T10	40.60	109.20	109.20	0.00
Tsurf *	45.20	101.84	100.94	0.90

* ⟶ Tsurf for "Actual" is a predicted value from the original 9-node T-Net model. Therefore, the new T-Net value is more accurate.

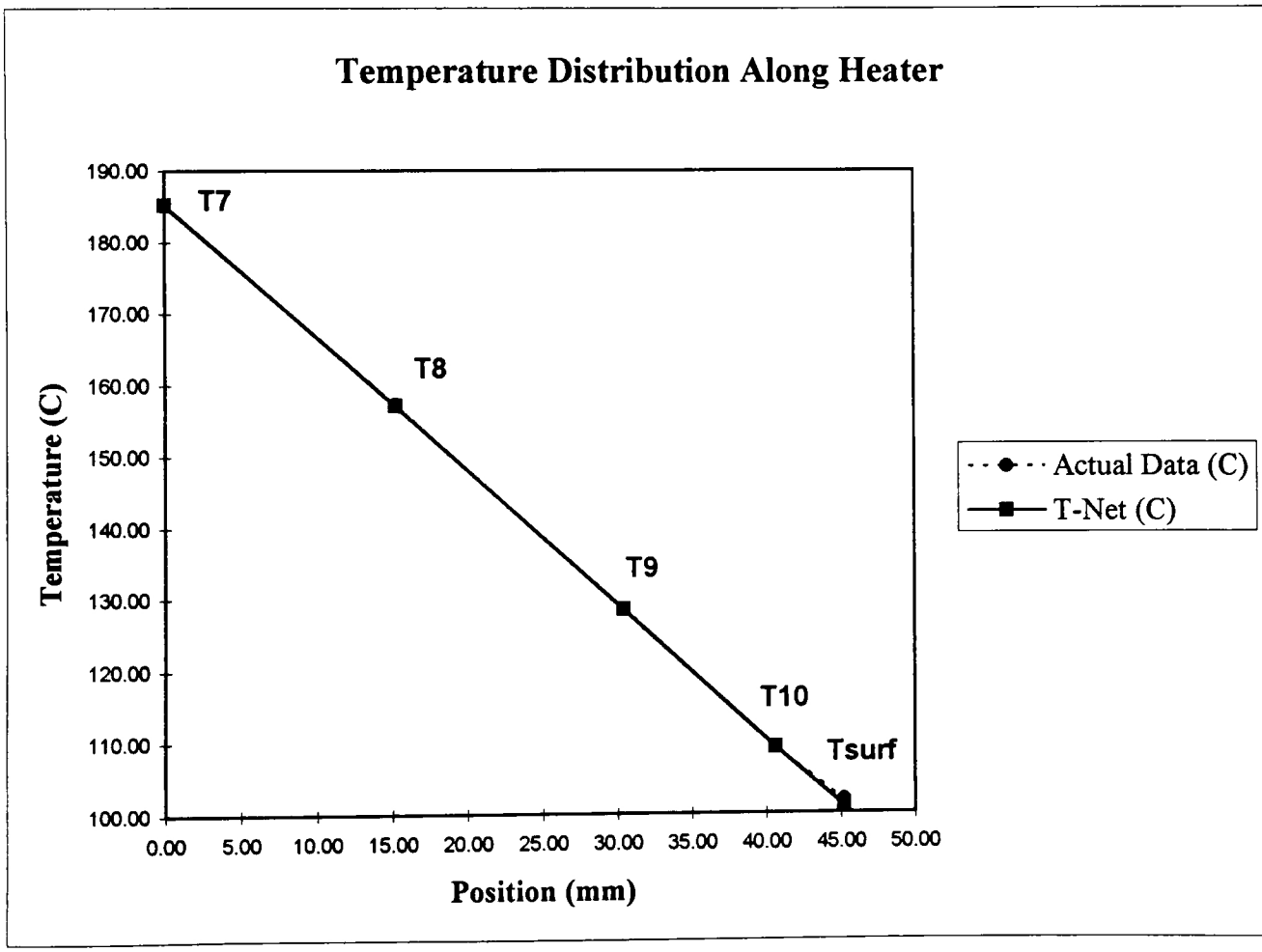

Appendix D
Fortran Code

```
c
c       Modified by Viktor Mizo
c
c       Date:May 1995
c
c       Purpose: To numerically calculate the force balance on a departing bubble
c                in flow boiling.
c


        Program Main
        real intopz,inbotz,nety,netz,netz2,nety2,tempy,tempz,tempz2,tempy2
        real rb,win,adv,rec,deptime,dens
        real con1, con2, con3, con4
        character*3 eqtype
        open(8,file='data1.dat',status='old')
        open(7,file='dpA.dat',status='new')
        open(9,file='graph1.dat',status='old')
        open(10,file='graph2.dat',status='old')
        open(11,file='dp2A.dat',status='new')
        open(12,file='graph3.dat',status='old')
        open(13,file='graph4.dat',status='old')
        open(14,file='net1A.dat',status='unknown')
        open(15,file='mikeA.dat',status='new')
        open(16,file='peteA.dat',status='new')
c
c       Start Main loop
c
        write(7,*) 'Front Control Volume'
        write(7,*)
        write(11,*) 'Back Control Volume'
        write(11,*)
c
c       To use single bubble mode comment out the next two lines
c       and un-comment out the lines following
c
        do 300 i=1,50
        read(8,*,end=320) rb,win,adv,rec,dens,deptime,eqtype,
     +  con1,con2,con3,con4

c       write(6,*) 'Enter in Bubble Radius'
c       read(5,*) rb
c       write(6,*) 'Enter in Velocity'
c       read(5,*) win
c       write(6,*) 'Enter in Adv Contact Angle'
```

```
c       read(5,*) adv
c       write(6,*) 'Enter in Receding Contact Angle'
c       read(5,*) rec

        r=rb

c       define bot,pi
        tempy=0
        tempz=0
        tempz2=0
        tempy2=0
        pi=3.1415

c       Average contact angle
        bm=(adv+rec)/2

c       Bottom bubble radius
        bot=rb*cosd(bm)
        sigma=5.81e-2
        sc=2*pi*rb*(180-bm)/180
        rs=rb*sind(bm)

c       begin function calls
c
c       Call momentum equations for Top portion of bubble
c
c       Momentum in (Z dir)
        topinz=intopz(r,win)

c       Momentum out (Z dir)
        topoutz=outtopz(r,win)

c       Momentum out (Y dir)
        topouty=outtopy(r,win)
c
c       Call momentum functions for bottom portion of bubble
c
c       Momentum in (Z dir)
        botinz=inbotz(r,win)

c       Momentum out (Z dir)
        botoutz=outbotz(r,win)

c       Calculate the net momentum in Z and Y dir
c
```

```
c       Net momentum (Z dir)
        netz=((topinz+botinz)-(topoutz+botoutz))

c       Net momentum (Y dir)
        nety=-topouty

c       Calculation of other forces acting on the bubble
c       Surface Tension force
c
c       Surface Tension along the edge separating the two control volumes
        fs1=-sigma*sc

c       Surface Tension along the edge of the bubble (Z and Y dir)
        fs2z=-surftenz(rb,adv,rec)
        fs2y=-surfteny(rb,adv,rec)

c       Bouyancy Force (Y dir)
        t=rb-bot
        fby=(2.0/3.0*pi*rb**3)
        fby=fby+((1.0/6.0)*pi*bot*(3*rb**2+3*bot**2+rs**2))
        fby=fby*(955.0*9.81)

c       Area Calcualtions
        az=0.5*pi*rb**2 + bot*sqrt(rb**2-bot**2)+rb**2*(bm*pi/180.0)
        as=0.5*pi*(rs)**2

c       Call Inertia Force Subroutine
        call finertia(rb,bm,dens,deptime,eqtype,con1,con2,con3,con4,
     +  finer1z,finer1y)

c       Inertia Forces acting on front and rear control volumes in Y dir
c       are equal
        finer2y=finer1y

c       Inertia Forces acting in Z dir are of equal magnitude and
c       opposite direction
        finer2z=-finer1z
c
c       Calcualtion of Delta P (Excess pressures in Z and Y dir)
        dpz=(netz-(fs1+fs2z+finer1z))/az
        dpy=(nety+(-fs2y-fby-finer1y))/(as)

        write(7,5) rb,win,adv,rec,dpz,dpy,fs1,fs2z,fby,fs2y,netz,nety,
     +  finer1z,finer1y
```

```
      tempz=fs1+fs2z+netz
      tempy=fby+fs2y+nety

      write(9,*) rb,dpz
      write(10,*) rb,dpy

 5    format(' Radius=',e9.3,' Velocity=',f5.3,' Adv=',f5.1,' Rec=',
     +  f5.1,/,' DPz=',e11.3,' DPy=',e11.3,' Fs1=',e11.3,' Fs2z=',e11.3
     +  ,/,' Fby=',e11.3,' Fs2y=',e11.3,' Momz=',e11.3,' Momy=',e11.3,/,
     +  ' Inrtiaz=',e11.3,' Inertiay=',e11.3,//)

c     Back Control Volume Calculations
c
c     Calculate Net Momentum in Y and Z dir
      Netz2=-(topinz+botinz)-(-topoutz-botoutz)
      Nety2=-topouty

c     Surface Tension Force
c
c     Surface tension along the edge separating the two control volumes
      fs12=-fs1

c     Surface tension in Z and Y dir along the edge of the bubble
      fs2z2=-surftenz2(rb,adv,rec)
      fs2y2=-surfteny2(rb,adv,rec)

c     Buoyancy Force (Y dir)
      fby2=fby

c     Calculation of Delta P (excess pressure in Y and Z dir)
      dpz2=(-Netz2+fs12+fs2z2+finer2z)/az
      dpy2=(Nety2-fs2y2-fby2-finer2y)/as

      write(11,6) rb,win,adv,rec,dpz2,dpy2,fs12,fs2z2,fby2,fs2y2,
     +  netz2,nety2,finer2z,finer2y

      tempz2=fs12+fs2z2+netz2
      tempy2=fby2+fs2y2+nety2

      write(14,11) rb,win,tempz,tempy,tempz2,tempy2
 11   format(' Radius= ',e9.3,' Velocity= ',f5.3,/,' CV1 Net Z= ',
     +  e9.3,' CV1 Net Y= ',e9.3,/,' CV2 Net Z= ',e9.3,' CV2 Net Y= ',
     +  e9.3,/)

      write(12,*) rb,-dpz2
```

```
      write(13,*) rb,dpy2

  6   format(' Radius=',e9.3,' Velocity=',f5.3,' Adv=',f5.1,' Rec=',
     +  f5.1,/,' DPz=',e11.3,' DPy=',e11.3,' Fs1=',e11.3,' Fs2z=',e11.
     +  3,/,' Fby=',e11.3,' Fs2y=',e11.3,' Momz=',e11.3,' Momy=',e11.3,/,
     +  ' Inertiaz=',e11.3,' Inertiay=',e11.3,//)

300   enddo

320   stop
      end


c     Subroutine for calculating the inertia force on FCV in the y and z dir

      subroutine finertia(rb,bm,dens,deptime,eqtype,con1,con2,con3,con4,
     +  finer1z,finer1y)

      real rb,bm,dens,deptime,pi,acc,h
      real con1,con2,con3,con4,finer1y,finer1z
      character*3 eqtype
      pi = 3.1415

      if (eqtype .eq. 'pow') then
            acc = con1*con2*(con2-1)*deptime**(con2-2)
      elseif (eqtype .eq. 'log') then
            acc = -con1*deptime**(-2)
      elseif (eqtype .eq. 'pol') then
            acc = 20*con1*deptime**3 + 12*con2*deptime**2 +
     +            6*con3*deptime + 2*con4
      endif
      h = rb*(1+cosd(bm))
      finer1z = -pi*h**2*(rb-h/3)*dens*acc/2
      finer1y = -(pi*((4*rb**3)/3-h**2*(rb-h/3)))*dens*acc/2
      write(15,*) acc,h,finer1z,finer1y
      return
      end
```

```
c       Written by:     Viktor Mizo
c
c       Date: May 1995
c
c       Purpose:  To calculate a double integral for the inlet momentum for the bottom
c                 portion of the bubble

        real function inbotz(r,win)
        real a,b,h,j1,j2,j3,k1,k2,k3,x,hy
        real d,c,f,y,q,l,win
        integer m,n,i,j,temp

c       open(unit=7, file='inbotz.out', status='old')
c       open(unit=8, file='data.dat', status='old')

c       do 150 p=1,100
c       write(6,*) 'Enter in the values of m & n'
c       read(8,*,end=200) m,n
c       write(6,*) 'Enter in the Velocity'
c       read(8,*) win
c       write(6,*) 'Enter in the bubble radius'
c       read(8,*) r
        m=20
        n=20
        b=0
        a=-r*cosd(55.0)
        k1=0
        k2=0
        k3=0
        y=0
        l=0
        h=(b-a)/(2*n)
        j1=0
        j2=0
        j3=0

        do 100 i=1,2*n-1

        y=a+i*h
        hy=(d(y,r)-c(y,r))/(2*m)
        k1=f5(y,c(y,r),win,r)
        k1=k1+f5(y,d(y,r),win,r)
        k2=0
        k3=0
```

```
      do 50 j=1,2*m
      x=c(y,r) +j*hx
      q=f5(y,x,win,r)
      temp=(j+1)/2
      if (j/2 .eq. temp) then
      k2=k2+q
      else
      k3=k3+q
      end
50    enddo
      l=(k1+2*k2+4*k3)*hy/3
      temp=(i+1)/2
      if ((i .eq.0) .or. (i .eq. 2*n)) then
      j1=j1+l
      elseif (temp .eq. i/2) then
      j2=j2+l
      else
      j3=j3+l
      endif
100   enddo
      answ=(j1+2*j2+4*j3)*h/3
c     write(6,*) 'The bottom momentum in equals ',answ
c     write(7,*) 'The bottom momentum in equals ',answ
c     write(7,*) 'For a bubble of radius',r
c     write(6,*) 'For a bubble of radius',r
c     write(6,*) 'At a velocity of ',win
c     write(7,*) 'At a velocity of ',win
      inbotz=answ
      return
c 150 enddo
 200  stop
      end

c     real function d(y,r)
c     real y,r
c     d=sqrt(r**2-y**2)
c     return
c     end

c     real function c(x,r)
c     real x,r
c     c=0
c     return
c     end
```

```
c       real function w(y,win,r)
c       real y,bot,win,l,r
c       l=0.003
c       bot=r*cosd(55.0)
c       w=-1.5*win*(1.0-(((l/2-y-bot)**2)/((l/2)**2)))
c       return
c       end

        real function ux5(x1,y1,b1)
        real x1,y1,z,b1
        zz=b1**2-x1**2-y1**2
        if (zz.le.1e-20) zz=1e-20
        z=zz**0.5
        ux5=x/sqrt(x**2+z**2)
        return
        end

        real function uy5(x1,y1,b1)
        real x1,y1,z,b1
        zz=(b1**2 -x1**2 - y1**2)
        if (zz.le.1e-20) zz=1e-20
        z=zz**0.5
        uy5=(y1*z)/(sqrt(x1**2*z**2 + y1**2*z**2 +(x1**2+y1**2)**2))
        return
        end

        real function uz5(x1,y1,b1)
        real x1,y1,z,b1
        zz=(b1**2 -x1**2 - y1**2)
        if (zz.le.1e-20) zz=1e-20
        z=zz**0.5
        uz5=z/sqrt(x**2+z**2)
        return
        end

        real function f5(y,x,win,r)
        real x,temp,y,r,w,win,ux,uy,temp2,uz
        real rho
        rho=955
        temp=2*rho*w(y,win,r)**2
        f5=temp
        return
        end
```

```
c   Written by:      Viktor Mizo
c
c   Date:            May 1995
c
c       Purpose:  To calculate a double integral for the inlet momentum for the top
c
        real function intopz(b,win)
        real a,b,h,j1,j2,j3,k1,k2,k3,x,hy
        real d,c,f,y,q,l,win
        integer m,n,i,j,temp

c       open(unit=7, file='intopz.out', status='old')
c       open(unit=8, file='data.dat', status='old')

c       do 150 p=1,100

        m=20
        n=20
        a=0
        k1=0
        k2=0
        k3=0
        y=0
        l=0
        h=(b-a)/(2*n)
        j1=0
        j2=0
        j3=0
        do 100 i=1,2*n-1
        y=a+i*h
        hy=(d(y,b)-c(y,b))/(2*m)
        k1=f1(y,c(y,b),win,b)
        k1=k1+f1(y,d(y,b),win,b)
        k2=0
        k3=0
        do 50 j=1,2*m
        x=c(y,b) +j*hy
        q=f1(y,x,win,b)
        temp=(j+1)/2
        if (j/2 .eq. temp) then
        k2=k2+q
        else
        k3=k3+q
        endif
  50    enddo
```

```
      l=(k1+2*k2+4*k3)*hy/3.0
      temp=(i+1)/2
      if ((i .eq.0) .or. (i .eq. 2*n)) then
      j1=j1+l
      elseif (temp .eq. i/2) then
      j2=j2+l
      else
      j3=j3+l
      endif
 100  enddo
      answ=(j1+2*j2+4*j3)*h/3.0
c     write(6,*) 'The momentum in equals ',answ
      intopz=answ
c     write(7,*) 'The momentum in equals ',answ
c      write(7,*) 'For a bubble of radius',b
c     write(6,*) 'For a bubble of radius',b
c     write(6,*) 'At a velocity of ',win
c     write(7,*) 'At a velocity of ',win

      return
c 150 enddo
 200  stop
      end

      real function d(y,b)
      real y,b,z
      d=sqrt(b**2-y**2)
      return
      end

      real function c(y,b)
      real y,b
      c=0
      return
      end

      real function w(y,win,b)
      real y,bot,win,l,b
      l=0.003
      bot=b*cosd(55.0)
      w=-1.5*win*(1.0-(((l/2.0-y-bot)**2)/((l/2.0)**2)))
      return
      end

      real function ux1(x1,y1,b1)
```

```
real x1,y1,z,b1
zz=b1**2-x1**2-y1**2
if (zz.le.1e-20) zz=1e-20
z=zz**0.5
ux1=(x1*z)/(sqrt(x1**2*z**2 + y1**2*z**2 +(x1**2+y1**2)**2))
return
end

real function uy1(x1,y1,b1)
real x1,y1,z,b1
zz=(b1**2 -x1**2 - y1**2)
if (zz.le.1e-20) zz=1e-20
z=zz**0.5
uy1=(y1*z)/(sqrt(x1**2*z**2 + y1**2*z**2 +(x1**2+y1**2)**2))
return

end

real function uz1(x1,y1,b1)
real x1,y1,z,b1
zz=(b1**2 -x1**2 - y1**2)
if (zz.le.1e-20) zz=1e-20
z=zz**0.5
uz1=(x1**2+y1**2)/(sqrt(x1**2*z**2+y1**2*z**2 +(x1**2+y1**2)**2))
return
end

real function f1(y,x,win,b)
real x,temp,y,b,w,win,ux1,uy1,temp2,uz1
real rho
rho=955.0
temp=2.0*rho*w(y,win,b)**2
f1=temp
return
end
```

```
c    Written by:Viktor Mizo
c
c    Date:          May 1995
c
c    Purpose:  To calculate a double integral that calculates the outlet momentum for the c
c              bottom in the Z dir

      function outbotz(r,win)
      real a,b,h,j1,j2,j3,k1,k2,k3,x,hy
      real d,c,f,y,q,l,win
      integer m,n,i,j,temp

c     open(unit=7, file='outbotz.out', status='old')
c     open(unit=8, file='data.dat', status='old')

c     do 150 p=1,100

c     write(6,*) 'Enter in the values of m & n'
c     read(8,*,end=200) m,n
c     write(6,*) 'Enter in the Velocity'
c     read(8,*) win
c     write(6,*) 'Enter in the bubble radius'
c     read(8,*) r
      m=20
      n=20
      b=0
      a=-r*cosd(55.0)
      k1=0
      k2=0
      k3=0
      y=0
      l=0
      h=(b-a)/(2*n)
      j1=0
      j2=0
      j3=0
      do 100 i=1,2*n-1
      y=a+i*h
      hy=(d(y,r)-c(y,r))/(2*m)
      k1=f6(y,c(y,r),win,r)
      k1=k1+f6(y,d(y,r),win,r)
      k2=0
      k3=0
      do 50 j=1,2*m
      x=c(y,r) +j*hy
```

```
        q=f6(y,x,win,r)
        temp=(j+1)/2
        if (j/2 .eq. temp) then
        k2=k2+q
        else
        k3=k3+q
        endif
 50     enddo
        l=(k1+2*k2+4*k3)*hy/3.0
        temp=(i+1)/2
        if ((i .eq.0) .or. (i .eq. 2*n)) then
        j1=j1+l
        elseif (temp .eq. i/2) then
        j2=j2+l
        else
        j3=j3+l
        endif
 100    enddo
        answ=(j1+2*j2+4*j3)*h/3.0
c       write(6,*) 'The bottom momentum out in Z equals ',answ
c       write(7,*) 'The bottom momentum out in Z equals ',answ
c       write(7,*) 'For a bubble of radius',r
c       write(6,*) 'For a bubble of radius',r
c       write(6,*) 'At a velocity of ',win
c       write(7,*) 'At a velocity of ',win
        outbotz=answ
        return

c 150  enddo
 200    stop
        end

c       real function d(y,r)
c       real y,r
c       d=sqrt(r**2-y**2)
c       return
c       end

c       real function c(x,r)
c       real x,r
c       c=0
c       return
c       end

c       real function w(y,win,r)
```

```
c       real y,bot,win,l,r
c       l=0.003
c       bot=r*cosd(55.0)
c       w=-1.5*win*(1.0-(((l/2.0-y-bot)**2)/((l/2.0)**2)))
c       return
c       end

        real function ux6(x1,y1,b1)
        real x1,y1,z,b1
        z=b1**2-y1**2-x1**2
        if (z .le. 1e-20) z=1e-20
        ux6=sqrt(z)/sqrt(b1**2-y1**2)
        return
        end

        real function uz6(x1,y1,b1)
        real x1,y1,z,b1
        uz6=x1/sqrt(b1**2-y1**2)
        return
        end


        real function f6(y,x,win,r)
        real x,temp,y,r,w,win,ux6,uy6,temp2,uz6
        real rho
        rho=955.0
        temp=2*rho*w(y,win,r)**2*((uz6(x,y,r))**3.0)
        temp2=((ux6(x,y,r))**2+(uz6(x,y,r))**2)**(3.0/2.0)
        f6=temp/temp2
        return
        end
```

```
c    Written by:Viktor Mizo
c
c    Date: May 1995
c
c    Purpose:  To calculate a double integral for the mometum leaving  in the top in the Yc
c        direction
c


      function outtopy(b,win)
      real a,b,h,j1,j2,j3,k1,k2,k3,x,hy
      real d,c,f,y,q,l,win
      integer m,n,i,j,temp

c     open(unit=7, file='outtopy.out', status='old')
c     open(unit=8, file='data.dat', status='old')

c     do 150 p=1,100

c     write(6,*) 'Enter in the values of m & n'
c     read(8,*,end=200) m,n
c     write(6,*) 'Enter in the Velocity'
c     read(8,*) win
c     write(6,*) 'Enter in the bubble radius'
c     read(8,*) b

      m=20
      n=20
      a=0
      k1=0
      k2=0
      k3=0
      y=0
      l=0
      h=(b-a)/(2*n)
      j1=0
      j2=0
      j3=0
      do 100 i=1,2*n-1
      y=a+i*h
      hy=(d(y,b)-c(y,b))/(2*m)
      k1=f3(y,c(y,b),win,b)
      k1=k1+f3(y,d(y,b),win,b)
      k2=0
```

```
      k3=0
      do 50 j=1,2*m
      x=c(y,b) +j*hy
      q=f3(y,x,win,b)
      temp=(j+1)/2
      if (j/2 .eq. temp) then
        k2=k2+q
      else
        k3=k3+q
      endif
50    enddo
      l=(k1+2*k2+4*k3)*hy/3
      temp=(i+1)/2
      if ((i .eq.0) .or. (i .eq. 2*n)) then
        j1=j1+l
      elseif (temp .eq. i/2) then
        j2=j2+l
      else
        j3=j3+l
      endif
100   enddo
      answ=(j1+2*j2+4*j3)*h/3
c     write(6,*) 'The top momentum out in Y equals ',answ
c     write(7,*) 'The top momentum out in Y equals ',answ
c     write(7,*) 'For a bubble of radius',b
c     write(6,*) 'For a bubble of radius',b
c     write(6,*) 'At a velocity of ',win
c     write(7,*) 'At a velocity of ',win
      outtopy=answ
      return
c 150 enddo
200   stop
      end

c     real function d(y,b)
c     real y,b
c     d=sqrt(b**2-y**2)
c     return
c     end

c     real function c(x,b)
c     real x,b
c     c=0
c     return
c     end
```

```
c     real function w(y,win,b)
c     real y,bot,win,l,b
c     l=0.003
c     bot=b*cosd(55.0)
c     w=-1.5*win*(1.0-(((l/2-y-bot)**2)/((l/2)**2)))
c     return
c     end

      real function ux3(x1,y1,b1)
      real x1,y1,z,b1
      zz=b1**2-x1**2-y1**2
      if (zz.le.1e-20) zz=1e-20
      z=zz**0.5
      ux3=(x1*z)/(sqrt(x1**2*z**2 + y1**2*z**2 +(x1**2+y1**2)**2))
      return
      end

      real function uy3(x1,y1,b1)
      real x1,y1,z,b1
      zz=(b1**2 -x1**2 - y1**2)
      if (zz.le.1e-20) zz=1e-20
      z=zz**0.5
      uy3=(y1*z)/(sqrt(x1**2*z**2 + y1**2*z**2 +(x1**2+y1**2)**2))
      return
      end

      real function uz3(x1,y1,b1)
      real x1,y1,z,b1
      zz=(b1**2 -x1**2 - y1**2)
      if (zz.le.1e-20) zz=1e-20
      z=zz**0.5
      uz3=(x1**2+y1**2)/(sqrt(x1**2*z**2+y1**2*z**2 +(x1**2+y1**2)**2))
      return
      end

      real function f3(y,x,win,b)
      real x,temp,y,b,w,win,ux3,uy3,temp2,uz3
      real rho
      rho=955
      temp=2*rho*w(y,win,b)**2*((uy3(x,y,b))**3)
      temp2=((ux3(x,y,b))**2+(uy3(x,y,b))**2+(uz3(x,y,b))**2)**1.5
      f3=temp/temp2
      return
      end
```

```
c   Written by:      Viktor Mizo
c
c   Date: May 1995
c
c   Purpose:  To calculate a double integral for the outlet momentum for the top in the Z
c             direction

      function outtopz(b,win)
      real a,b,h,j1,j2,j3,k1,k2,k3,x,hy
      real d,c,f,y,q,l,win
      integer m,n,i,j,temp

c     open(unit=7, file='outtopz.out', status='old')
c     open(unit=8, file='data.dat', status='old')

c     do 150 p=1,100

c     write(6,*) 'Enter in the values of m & n'
c     read(8,*,end=200) m,n
c     write(6,*) 'Enter in the Velocity'
c     read(8,*) win
c     write(6,*) 'Enter in the bubble radius'
c     read(8,*) b
      m=20
      n=20
      a=0
      k1=0
      k2=0
      k3=0
      y=0
      l=0
      h=(b-a)/(2*n)
      j1=0
      j2=0
      j3=0
      do 100 i=1,2*n-1
      y=a+i*h
      hy=(d(y,b)-c(y,b))/(2*m)
      k1=f2(y,c(y,b),win,b)
      k1=k1+f2(y,d(y,b),win,b)
      k2=0
      k3=0
      do 50 j=1,2*m
      x=c(y,b) +j*hy
      q=f2(y,x,win,b)
```

```
      temp=(j+1)/2
      if (j/2 .eq. temp) then
        k2=k2+q
      else
        k3=k3+q
      endif
50    enddo
      l=(k1+2*k2+4*k3)*hy/3
      temp=(i+1)/2
      if ((i .eq.0) .or. (i .eq. 2*n)) then
        j1=j1+l
      elseif (temp .eq. i/2) then
        j2=j2+l
      else
        j3=j3+l
      endif
100   enddo
      answ=(j1+2*j2+4*j3)*h/3
c     write(6,*) 'The top momentum out in Z equals ',answ
c     write(7,*) 'The top momentum out in Z equals ',answ
c     write(7,*) 'For a bubble of radius',b
c     write(6,*) 'For a bubble of radius',b
c     write(6,*) 'At a velocity of ',win
c     write(7,*) 'At a velocity of ',win
      outtopz=answ
      return
c 150  enddo
200   stop
      end

c     real function d(y,b)
c     real y,b
c     d=sqrt(b**2-y**2)
c     return
c     end

c     real function c(x,b)
c     real x,b
c     c=0
c     return
c     end

c     real function w(y,win,b)
c     real y,bot,win,l,b
c     l=0.003
```

```
c     bot=b*cosd(55.0)
c     w=-1.5*win*(1.0-(((l/2-y-bot)**2)/((l/2)**2)))
c     return
c     end

      real function ux2(x1,y1,b1)
      real x1,y1,z,b1
      zz=b1**2-x1**2-y1**2
      if (zz.le.1e-20) zz=1e-20
      z=zz**0.5
      ux2=(x1*z)/(sqrt(x1**2*z**2 + y1**2*z**2 +(x1**2+y1**2)**2))
      return
      end

      real function uy2(x1,y1,b1)
      real x1,y1,z,b1
      zz=(b1**2 -x1**2 - y1**2)
      if (zz.le.1e-20) zz=1e-20
      z=zz**0.5
      uy2=(y1*z)/(sqrt(x1**2*z**2 + y1**2*z**2 +(x1**2+y1**2)**2))
      return
      end

      real function uz2(x1,y1,b1)
      real x1,y1,z,b1
      zz=(b1**2 -x1**2 - y1**2)
      if (zz.le.1e-20) zz=1e-20
      z=zz**0.5
      uz2=(x1**2+y1**2)/(sqrt(x1**2*z**2+y1**2*z**2 +(x1**2+y1**2)**2))
      return
      end

      real function f2(y,x,win,b)
      real x,temp,y,b,w,win,ux2,uy2,temp2,uz2
      real rho
      rho=955
      temp=2*rho*w(y,win,b)**2*((uz2(x,y,b))**3)
      temp2=((ux2(x,y,b))**2+(uy2(x,y,b))**2+(uz2(x,y,b))**2)**1.5
      f2=temp/temp2
      return
      end
```

```
c     Written by: Viktor Mizo
c
c     Date: May 1995
c
c     Purpose: To calculte a single integral for the surface tension force
c
      real function surfteny(rb,adv,rec)
      real h
      pi=3.1415
      n=10
      a=0
      b=pi/2
      xi=0
      h=(b-a)/n
      xi0=g2(a,rb,adv,rec)+g2(b,rb,adv,rec)
      xi1=0
      xi2=0
      do 100 i=1,n-1
      x=a+i*h
      itemp=(i+1)/2
      if (i/2 .eq. itemp) then
        xi1=xi1+g2(x,rb,adv,rec)
      else
        xi2=xi2+g2(x,rb,adv,rec)
      endif
  100 enddo

      xi=h*(xi0+2*xi2+4*xi1)/2
      surfteny=xi
      write(16,*) surfteny
      return
      end

      real function g2(x,rb,adv,rec)
      sigma=5.81e-2
      pi=3.1415
      bf=adv*pi/180.0
      bb=rec*pi/180.0
      bm=(bf+bb)/2.0
      rs=rb*sin(bm)
      b1=bf-(bf-bm)*(x/(pi/2))
      g2=2*sigma*sin(b1)*rs
      write(16,*) g2
      return
      end
```

```
c     Written by: Viktor Mizo
c
c     Date: May 1995
c
c     Purpose: To calculte a single integral for the surface tension force
c
      real function surfteny2(rb,adv,rec)
      real h
      pi=3.1415
      n=10
      a=pi/2
      b=pi
      xi=0
      h=(b-a)/n
      xi0=g3(a,rb,adv,rec)+g3(b,rb,adv,rec)
      xi1=0
      xi2=0
      do 100 i=1,n-1
      x=a+i*h
      itemp=(i+1)/2
      if (i/2 .eq. itemp) then
        xi1=xi1+g3(x,rb,adv,rec)
      else
        xi2=xi2+g3(x,rb,adv,rec)
      endif
  100 enddo

      xi=h*(xi0+2*xi2+4*xi1)/2
      surfteny2=xi
      write(16,*) surfteny2
      return
      end

      real function g3(x,rb,adv,rec)
      sigma=5.81e-2
      pi=3.1415
      bf=adv*pi/180.0
      bb=rec*pi/180.0
      bm=(bf+bb)/2.0
      rs=rb*sin(bm)
      b1=bf-(bf-bm)*(x/(pi/2))
      g3=2*sigma*sin(b1)*rs
      return
      end
```

```
c    Written by: Viktor Mizo
c
c    Date: May 1995
c
c    Purpose: To calculte a single integral for the surface tension force (Z component)

     real function surftenz(rb,adv,rec)
     real h
     pi=3.1415
     n=10
     a=0
     b=pi/2
     xi=0
     h=(b-a)/n
     xi0=g(a,rb,adv,rec)+g(b,rb,adv,rec)
     xi1=0
     xi2=0
     do 100 i=1,n-1
     x=a+i*h
     itemp=(i+1)/2
     if (i/2 .eq. itemp) then
       xi1=xi1+g(x,rb,adv,rec)
     else
       xi2=xi2+g(x,rb,adv,rec)
     endif
 100  enddo

     xi=h*(xi0+2*xi2+4*xi1)/2
     surftenz=xi
     return
     end

     real function g(x,rb,adv,rec)
     sigma=5.81e-2
     pi=3.1415
     bf=adv*pi/180
     bb=rec*pi/180
     bm=(bf+bb)/2
     rs=rb*sin(bm)
     b1=bf-(bf-bm)*(x/(pi/2))
     g=2*sigma*cos(b1)*cos(x)*rs
     return
     end
```

```
c    Written By Viktor Mizo
c
c    April 1993
c
c    Purpose: To calculte a single integral for the surface tension force (Z direction CV2)
c

     real function surftenz2(rb,adv,rec)
     real h
     pi=3.1415
     n=10
     a=pi/2
     b=pi
     xi=0
     h=(b-a)/n
     xi0=g4(a,rb,adv,rec)+g4(b,rb,adv,rec)
     xi1=0
     xi2=0
     do 100 i=1,n-1
     x=a+i*h
     itemp=(i+1)/2
     if (i/2 .eq. itemp) then
       xi1=xi1+g4(x,rb,adv,rec)
     else
       xi2=xi2+g4(x,rb,adv,rec)
     endif
 100  enddo

     xi=h*(xi0+2*xi2+4*xi1)/2
     surftenz2=xi
     return
     end

     real function g4(x,rb,adv,rec)
     sigma=5.81e-2
     pi=3.1415
     bf=adv*pi/180
     bb=rec*pi/180
     bm=(bf+bb)/2
     rs=rb*sin(bm)
     b1=bf-(bf-bm)*(x/(pi/2))
     g4=2*sigma*cos(b1)*cos(x)*rs
     return
     end
```

APPENDIX E
Fortran Code Output

Front Control Volume

Radius=0.344E-04 Velocity=0.211 Adv= 55.0 Rec= 55.0
DPz= -0.215E+04 DPy= 0.270E+04 Fs1= -0.873E-05 Fs2z= -0.266E-05
Fby= 0.134E-08 Fs2y= -0.590E-05 Momz= 0.221E-09 Momy= -0.655E-10
Inrtiaz= 0.190E-04 Inertiay= 0.252E-05

Radius=0.333E-04 Velocity=0.211 Adv= 55.0 Rec= 55.0
DPz= 0.475E+04 DPy= 0.294E+04 Fs1= -0.843E-05 Fs2z= -0.257E-05
Fby= 0.121E-08 Fs2y= -0.570E-05 Momz= 0.193E-09 Momy= -0.572E-10
Inrtiaz= 0.125E-05 Inertiay= 0.165E-06

Radius=0.434E-04 Velocity=0.211 Adv= 55.0 Rec= 55.0
DPz= 0.494E+03 DPy= 0.298E+04 Fs1= -0.110E-04 Fs2z= -0.335E-05
Fby= 0.267E-08 Fs2y= -0.744E-05 Momz= 0.554E-09 Momy= -0.164E-09
Inrtiaz= 0.116E-04 Inertiay= 0.153E-05

Radius=0.388E-04 Velocity=0.211 Adv= 55.0 Rec= 55.0
DPz= 0.281E+04 DPy= 0.418E+04 Fs1= -0.983E-05 Fs2z= -0.300E-05
Fby= 0.191E-08 Fs2y= -0.665E-05 Momz= 0.354E-09 Momy= -0.105E-09
Inrtiaz= 0.156E-06 Inertiay= 0.207E-07

Radius=0.105E-03 Velocity=0.211 Adv= 55.0 Rec= 55.0
DPz= 0.103E+04 DPy= 0.154E+04 Fs1= -0.266E-04 Fs2z= -0.811E-05
Fby= 0.379E-07 Fs2y= -0.180E-04 Momz= 0.183E-07 Momy= -0.538E-08
Inrtiaz= 0.521E-06 Inertiay= 0.691E-07

Radius=0.664E-04 Velocity=0.211 Adv= 55.0 Rec= 55.0
DPz= 0.166E+04 DPy= 0.245E+04 Fs1= -0.168E-04 Fs2z= -0.513E-05
Fby= 0.960E-08 Fs2y= -0.114E-04 Momz= 0.300E-08 Momy= -0.889E-09
Inrtiaz= 0.263E-07 Inertiay= 0.349E-08

Radius=0.646E-04 Velocity=0.211 Adv= 55.0 Rec= 55.0
DPz= 0.171E+04 DPy= 0.252E+04 Fs1= -0.164E-04 Fs2z= -0.499E-05
Fby= 0.883E-08 Fs2y= -0.111E-04 Momz= 0.269E-08 Momy= -0.795E-09
Inrtiaz= 0.933E-08 Inertiay= 0.124E-08

Radius=0.907E-04 Velocity=0.211 Adv= 55.0 Rec= 55.0
DPz= 0.121E+04 DPy= 0.179E+04 Fs1= -0.230E-04 Fs2z= -0.701E-05
Fby= 0.244E-07 Fs2y= -0.156E-04 Momz= 0.103E-07 Momy= -0.303E-08
Inrtiaz= 0.792E-07 Inertiay= 0.105E-07

Radius=0.748E-04 Velocity=0.211 Adv= 55.0 Rec= 55.0
DPz= 0.147E+04 DPy= 0.217E+04 Fs1= -0.190E-04 Fs2z= -0.578E-05
Fby= 0.137E-07 Fs2y= -0.128E-04 Momz= 0.480E-08 Momy= -0.142E-08
Inrtiaz= 0.448E-07 Inertiay= 0.594E-08

Radius=0.240E-04 Velocity=0.844 Adv= 55.0 Rec= 55.0
DPz= 0.453E+04 DPy= 0.675E+04 Fs1= -0.608E-05 Fs2z= -0.185E-05
Fby= 0.452E-09 Fs2y= -0.411E-05 Momz= 0.841E-09 Momy= -0.249E-09
Inrtiaz= 0.110E-06 Inertiay= 0.146E-07

Radius=0.175E-04 Velocity=0.644 Adv= 55.0 Rec= 55.0
DPz= 0.622E+04 DPy= 0.925E+04 Fs1= -0.445E-05 Fs2z= -0.136E-05
Fby= 0.177E-09 Fs2y= -0.301E-05 Momz= 0.140E-09 Momy= -0.417E-10
Inrtiaz= 0.558E-07 Inertiay= 0.739E-08

Radius=0.120E-04 Velocity=0.844 Adv= 55.0 Rec= 55.0
DPz= 0.919E+04 DPy= 0.136E+05 Fs1= -0.304E-05 Fs2z= -0.927E-06
Fby= 0.565E-10 Fs2y= -0.206E-05 Momz= 0.530E-10 Momy= -0.157E-10
Inrtiaz= 0.138E-08 Inertiay= 0.182E-09

Radius=0.120E-04 Velocity=0.844 Adv= 55.0 Rec= 55.0
DPz= 0.919E+04 DPy= 0.136E+05 Fs1= -0.304E-05 Fs2z= -0.927E-06
Fby= 0.565E-10 Fs2y= -0.206E-05 Momz= 0.530E-10 Momy= -0.157E-10
Inrtiaz= 0.797E-09 Inertiay= 0.106E-09

Radius=0.390E-04 Velocity=0.211 Adv= 55.0 Rec= 55.0
DPz= 0.283E+04 DPy= 0.417E+04 Fs1= -0.989E-05 Fs2z= -0.301E-05
Fby= 0.194E-08 Fs2y= -0.669E-05 Momz= 0.363E-09 Momy= -0.108E-09
Inrtiaz= 0.869E-09 Inertiay= 0.115E-09

Radius=0.277E-04 Velocity=0.380 Adv= 55.0 Rec= 55.0

DPz= 0.398E+04 DPy= 0.587E+04 Fs1= -0.702E-05 Fs2z= -0.214E-05
Fby= 0.695E-09 Fs2y= -0.475E-05 Momz= 0.301E-09 Momy= -0.893E-10
Inrtiaz= 0.111E-07 Inertiay= 0.147E-08

Radius=0.886E-04 Velocity=0.760 Adv= 55.0 Rec= 55.0
DPz= 0.125E+04 DPy= 0.183E+04 Fs1= -0.225E-04 Fs2z= -0.685E-05
Fby= 0.228E-07 Fs2y= -0.152E-04 Momz= 0.121E-06 Momy= -0.358E-07
Inrtiaz= 0.721E-07 Inertiay= 0.956E-08

Radius=0.148E-04 Velocity=0.760 Adv= 55.0 Rec= 55.0
DPz= 0.746E+04 DPy= 0.110E+05 Fs1= -0.374E-05 Fs2z= -0.114E-05
Fby= 0.105E-09 Fs2y= -0.253E-05 Momz= 0.984E-10 Momy= -0.292E-10
Inrtiaz= 0.365E-08 Inertiay= 0.484E-09

Back Control Volume

Radius=0.344E-04 Velocity=0.211 Adv= 55.0 Rec= 55.0
DPz= -0.215E+04 DPy= 0.270E+04 Fs1= 0.873E-05 Fs2z= 0.266E-05
Fby= 0.134E-08 Fs2y= -0.590E-05 Momz= -0.221E-09 Momy= -0.655E-10
Inertiaz= -0.190E-04 Inertiay= 0.252E-05

Radius=0.333E-04 Velocity=0.211 Adv= 55.0 Rec= 55.0
DPz= 0.475E+04 DPy= 0.294E+04 Fs1= 0.843E-05 Fs2z= 0.257E-05
Fby= 0.121E-08 Fs2y= -0.570E-05 Momz= -0.193E-09 Momy= -0.572E-10
Inertiaz= -0.125E-05 Inertiay= 0.165E-06

Radius=0.434E-04 Velocity=0.211 Adv= 55.0 Rec= 55.0
DPz= 0.494E+03 DPy= 0.298E+04 Fs1= 0.110E-04 Fs2z= 0.335E-05
Fby= 0.267E-08 Fs2y= -0.744E-05 Momz= -0.554E-09 Momy= -0.164E-09
Inertiaz= -0.116E-04 Inertiay= 0.153E-05

Radius=0.388E-04 Velocity=0.211 Adv= 55.0 Rec= 55.0
DPz= 0.281E+04 DPy= 0.418E+04 Fs1= 0.983E-05 Fs2z= 0.299E-05
Fby= 0.191E-08 Fs2y= -0.665E-05 Momz= -0.354E-09 Momy= -0.105E-09
Inertiaz= -0.156E-06 Inertiay= 0.207E-07

Radius=0.105E-03 Velocity=0.211 Adv= 55.0 Rec= 55.0
DPz= 0.103E+04 DPy= 0.154E+04 Fs1= 0.266E-04 Fs2z= 0.811E-05
Fby= 0.379E-07 Fs2y= -0.180E-04 Momz= -0.183E-07 Momy= -0.538E-08
Inertiaz= -0.521E-06 Inertiay= 0.691E-07

Radius=0.664E-04 Velocity=0.211 Adv= 55.0 Rec= 55.0
DPz= 0.166E+04 DPy= 0.245E+04 Fs1= 0.168E-04 Fs2z= 0.513E-05
Fby= 0.960E-08 Fs2y= -0.114E-04 Momz= -0.300E-08 Momy= -0.889E-09
Inertiaz= -0.263E-07 Inertiay= 0.349E-08

Radius=0.646E-04 Velocity=0.211 Adv= 55.0 Rec= 55.0
DPz= 0.171E+04 DPy= 0.252E+04 Fs1= 0.164E-04 Fs2z= 0.499E-05
Fby= 0.883E-08 Fs2y= -0.111E-04 Momz= -0.269E-08 Momy= -0.795E-09
Inertiaz= -0.933E-08 Inertiay= 0.124E-08

Radius=0.907E-04 Velocity=0.211 Adv= 55.0 Rec= 55.0
DPz= 0.121E+04 DPy= 0.179E+04 Fs1= 0.230E-04 Fs2z= 0.701E-05
Fby= 0.244E-07 Fs2y= -0.156E-04 Momz= -0.103E-07 Momy= -0.303E-08
Inertiaz= -0.792E-07 Inertiay= 0.105E-07

Radius=0.748E-04 Velocity=0.211 Adv= 55.0 Rec= 55.0
DPz= 0.147E+04 DPy= 0.217E+04 Fs1= 0.190E-04 Fs2z= 0.578E-05
Fby= 0.137E-07 Fs2y= -0.128E-04 Momz= -0.480E-08 Momy= -0.142E-08
Inertiaz= -0.448E-07 Inertiay= 0.594E-08

Radius=0.240E-04 Velocity=0.844 Adv= 55.0 Rec= 55.0
DPz= 0.453E+04 DPy= 0.675E+04 Fs1= 0.608E-05 Fs2z= 0.185E-05
Fby= 0.452E-09 Fs2y= -0.411E-05 Momz= -0.841E-09 Momy= -0.249E-09
Inertiaz= -0.110E-06 Inertiay= 0.146E-07

Radius=0.175E-04 Velocity=0.644 Adv= 55.0 Rec= 55.0
DPz= 0.622E+04 DPy= 0.925E+04 Fs1= 0.445E-05 Fs2z= 0.136E-05
Fby= 0.177E-09 Fs2y= -0.301E-05 Momz= -0.140E-09 Momy= -0.417E-10
Inertiaz= -0.558E-07 Inertiay= 0.739E-08

Radius=0.120E-04 Velocity=0.844 Adv= 55.0 Rec= 55.0
DPz= 0.918E+04 DPy= 0.136E+05 Fs1= 0.304E-05 Fs2z= 0.927E-06
Fby= 0.565E-10 Fs2y= -0.206E-05 Momz= -0.530E-10 Momy= -0.157E-10
Inertiaz= -0.138E-08 Inertiay= 0.182E-09

Radius=0.120E-04 Velocity=0.844 Adv= 55.0 Rec= 55.0
DPz= 0.919E+04 DPy= 0.136E+05 Fs1= 0.304E-05 Fs2z= 0.927E-06
Fby= 0.565E-10 Fs2y= -0.206E-05 Momz= -0.530E-10 Momy= -0.157E-10
Inertiaz= -0.797E-09 Inertiay= 0.106E-09

Radius=0.390E-04 Velocity=0.211 Adv= 55.0 Rec= 55.0
DPz= 0.283E+04 DPy= 0.417E+04 Fs1= 0.989E-05 Fs2z= 0.301E-05
Fby= 0.194E-08 Fs2y= -0.669E-05 Momz= -0.363E-09 Momy= -0.108E-09
Inertiaz= -0.869E-09 Inertiay= 0.115E-09

Radius=0.277E-04 Velocity=0.380 Adv= 55.0 Rec= 55.0
DPz= 0.398E+04 DPy= 0.587E+04 Fs1= 0.702E-05 Fs2z= 0.214E-05
Fby= 0.695E-09 Fs2y= -0.475E-05 Momz= -0.301E-09 Momy= -0.893E-10

Inertiaz= -0.111E-07 Inertiay= 0.147E-08

Radius=0.886E-04 Velocity=0.760 Adv= 55.0 Rec= 55.0
DPz= 0.125E+04 DPy= 0.183E+04 Fs1= 0.225E-04 Fs2z= 0.685E-05
Fby= 0.228E-07 Fs2y= -0.152E-04 Momz= -0.121E-06 Momy= -0.358E-07
Inertiaz= -0.721E-07 Inertiay= 0.956E-08

Radius=0.148E-04 Velocity=0.760 Adv= 55.0 Rec= 55.0
DPz= 0.746E+04 DPy= 0.110E+05 Fs1= 0.374E-05 Fs2z= 0.114E-05
Fby= 0.105E-09 Fs2y= -0.253E-05 Momz= -0.984E-10 Momy= -0.292E-10
Inertiaz= -0.365E-08 Inertiay= 0.484E-09